Supporting Information for

Supported Au Nanoparticles with N-Heterocyclic Carbene Ligands as Active and Stable Heterogeneous Catalysts for Lactonization

Rong Ye,[†, ‡, ⊥, ¶, #] Aleksandr V. Zhukhovitskiy,[†, #] Roman V. Kazantsev, [†, $] Sirine C. Fakra, [&] Brent B. Wickemeyer,[†] F. Dean Toste,[*,†,‡] and Gabor A. Somorjai[*, †, ‡, ⊥]

[†]Department of Chemistry, [⊥]Kavli Energy NanoScience Institute, University of California, Berkeley, California 94720, United States

[‡]Chemical Science Division, [$]Joint Center for Artificial Photosynthesis, [&]Advanced Light Source, Lawrence Berkeley National Laboratory, 1 Cyclotron Road, Berkeley, California 94720, United States

* fdtoste@berkeley.edu (F.D.T.)

* somorjai@berkeley.edu (G.A.S.)

Table of Contents

Supplementary Figures and Tables

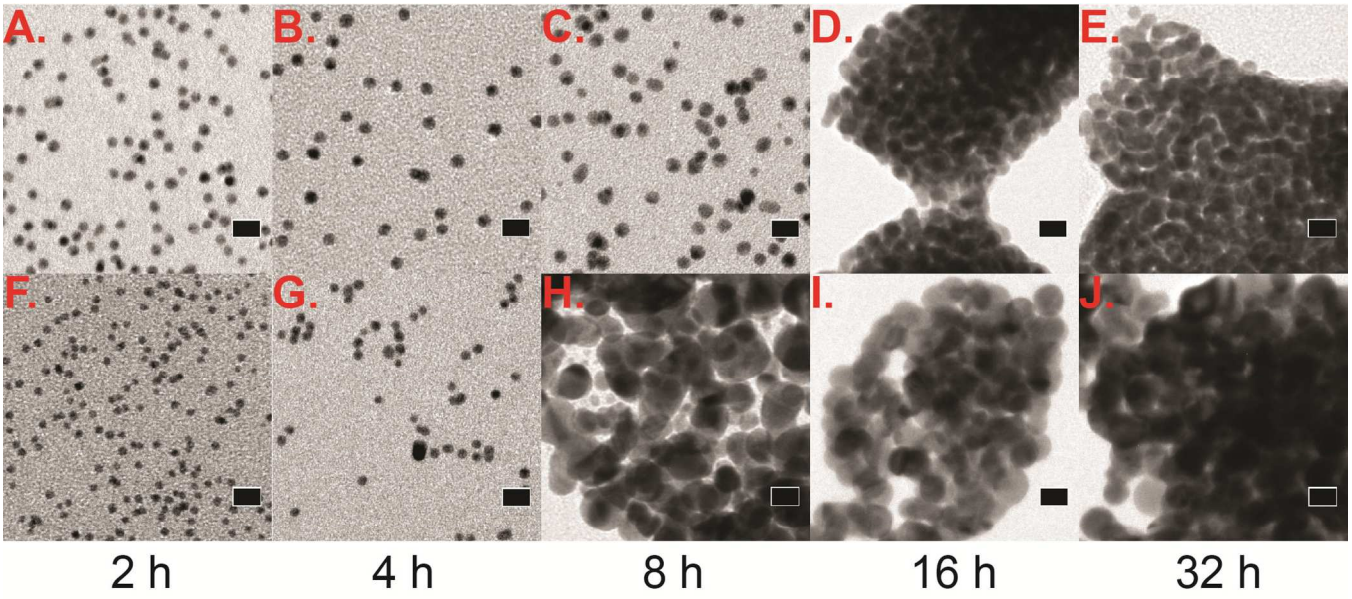

Figure S1. TEM images showing evolvements of morphology of (A-E) **Au/G4OH-NP-1** and (F-J) **AuNP-1** in the same synthetic conditions (other than whether dendrimers were used) A./F. 2 h, B./G. 4 h, C./H. 8 h, D./I. 16 h, and E./J. 32 h after the addition of the reducing agent. The scale bar is 10 nm.

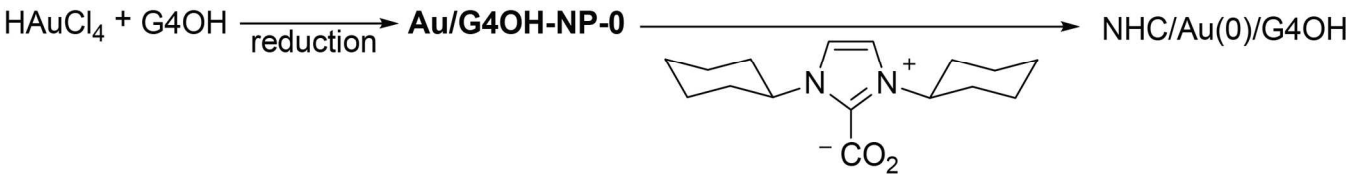

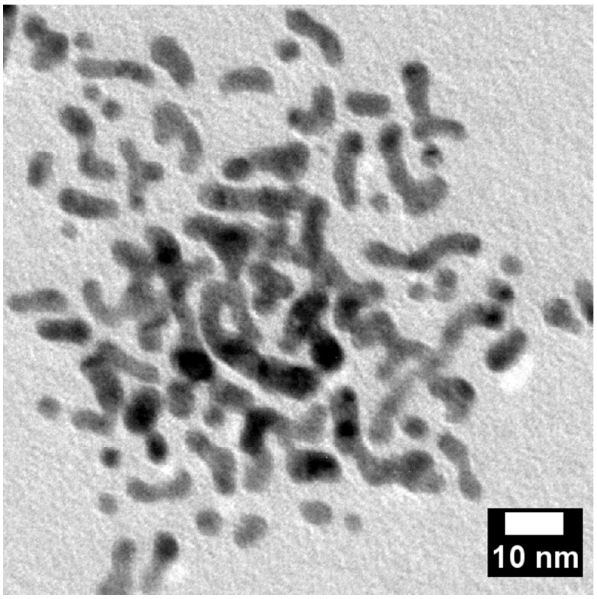

Figure S2. Another synthetic route for NHC attachment on the surface of **Au/G4OH-NP-0**, i.e., via stirring the CO_2 adducts of the NHC (NHC-CO_2) with **Au/G4OH-NP-0** at room temperature in water (top). However, this method led to the aggregation of Au particles under the conditions, as shown in the TEM image (bottom).

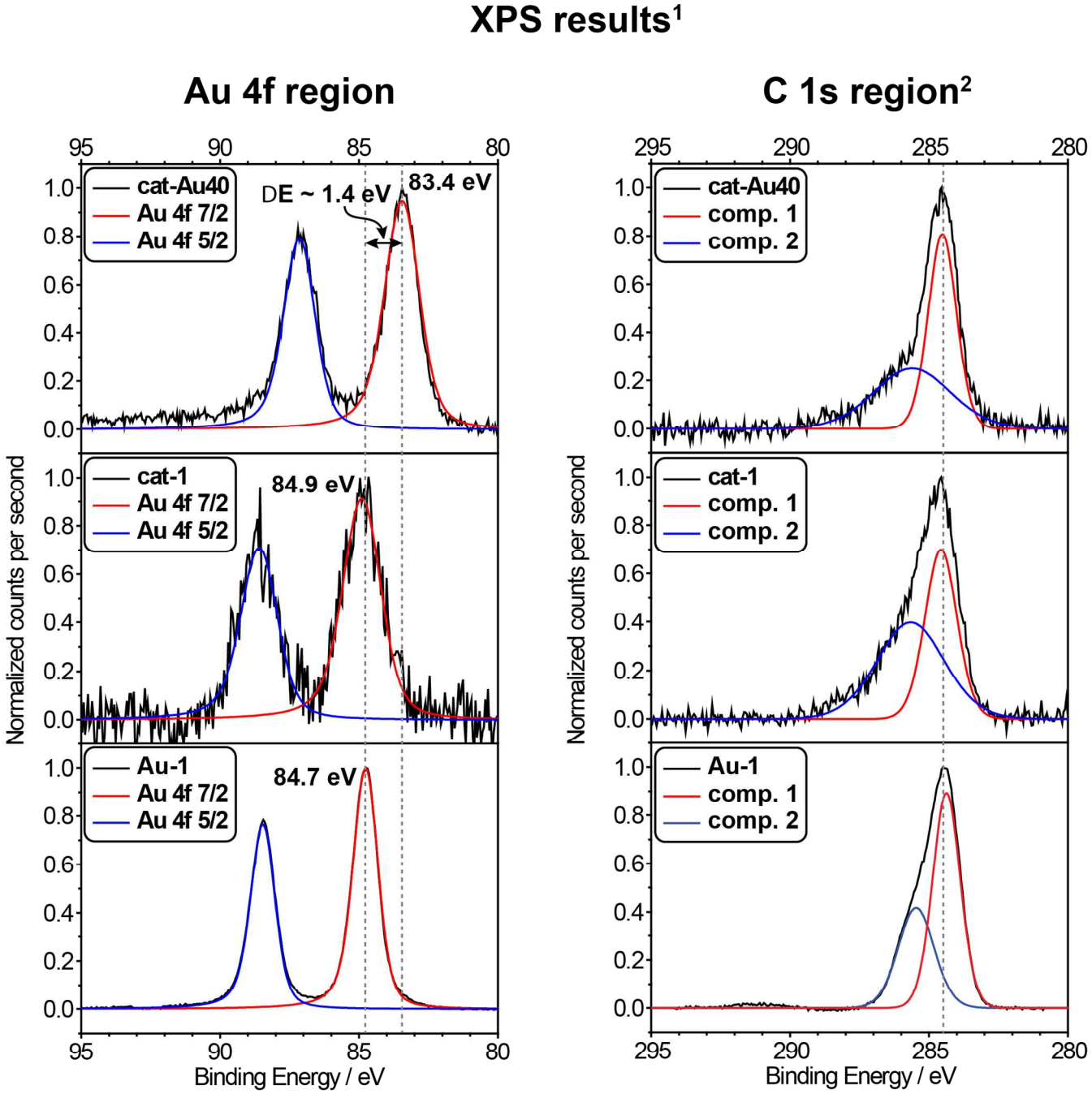

[1]*Binding energy axis calibrated to SiO_2 Si 2p = 103.4 eV*

[2]*C 1s comp. 2 is likely a superposition of multiple components.*

Figure S3. Normalized Au 4f XPS spectra of (a) **Cat-0**, (b) **Cat-1**, and (c) **1**, along with the corresponding C 1s spectra.

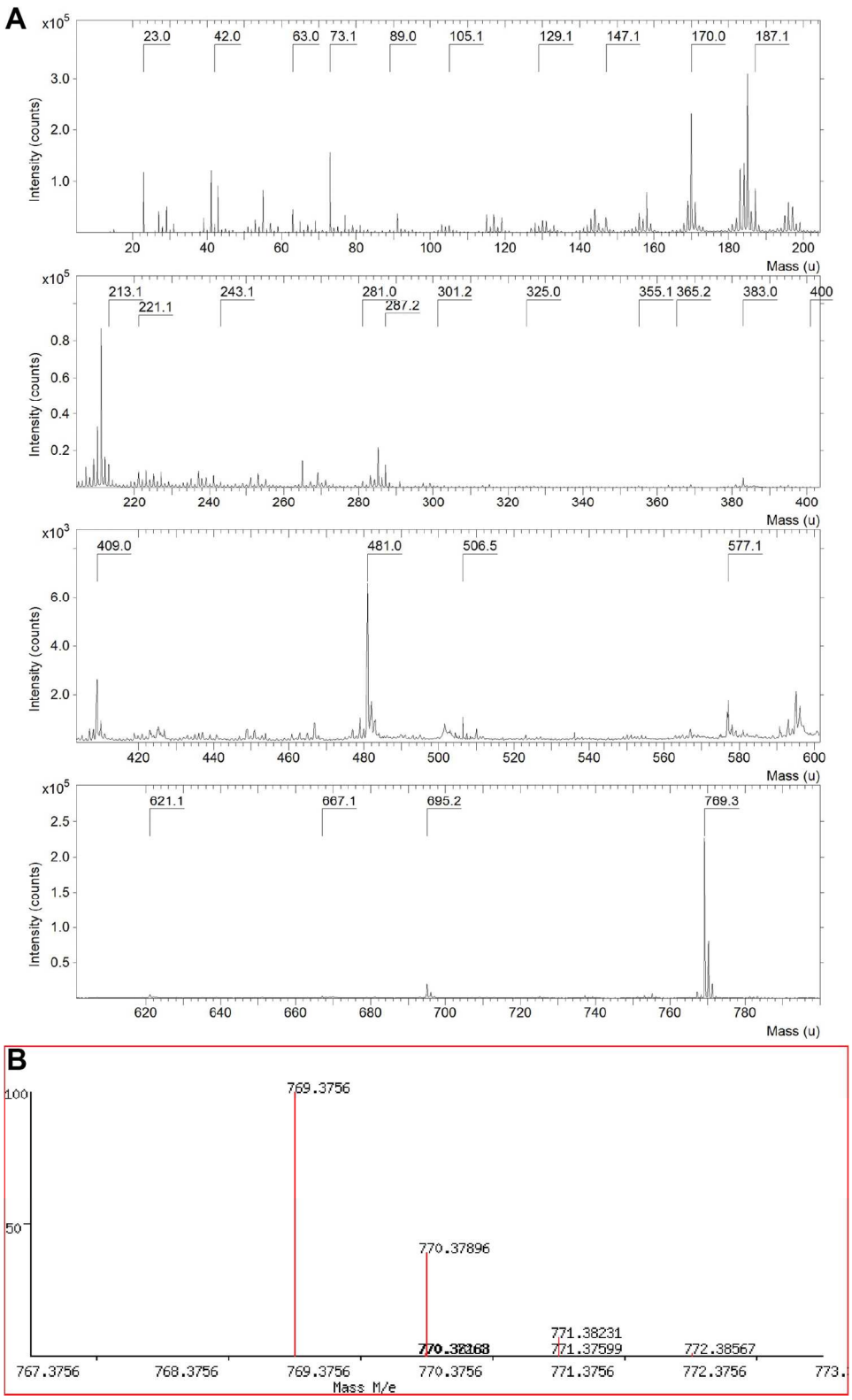

Figure S4. A. Representative positive ion spectrum from **AuNP-1**, with the m/z = 769.3 peak at the bottom panel. B. Simulated mass spectrum of $C_{36}H_{52}AuN_4O_2^+$, i.e., the corresponding $(NHC)_2Au^+$ ion.

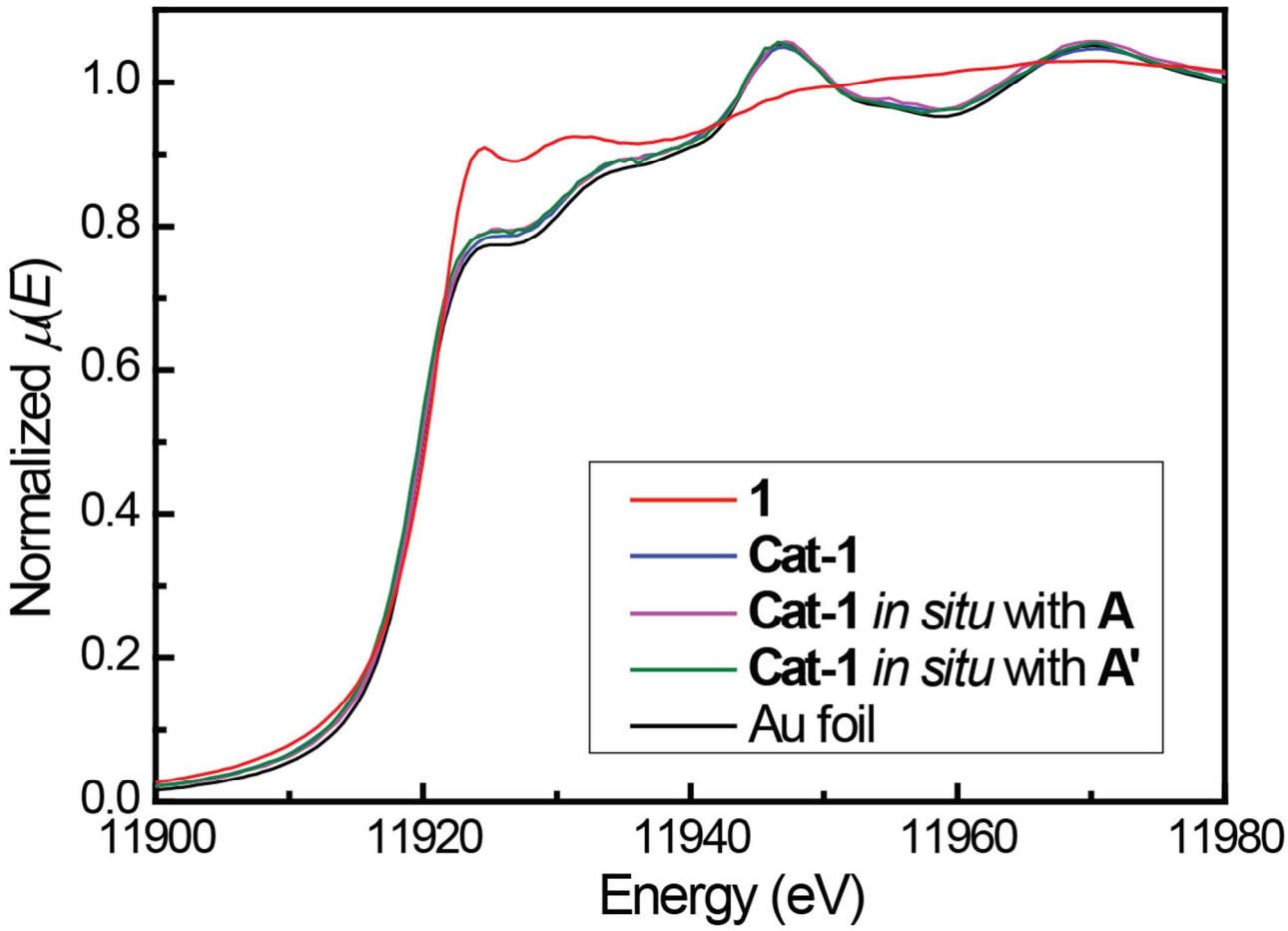

Figure S5. XANES spectra of **Cat-1** under reaction conditions.

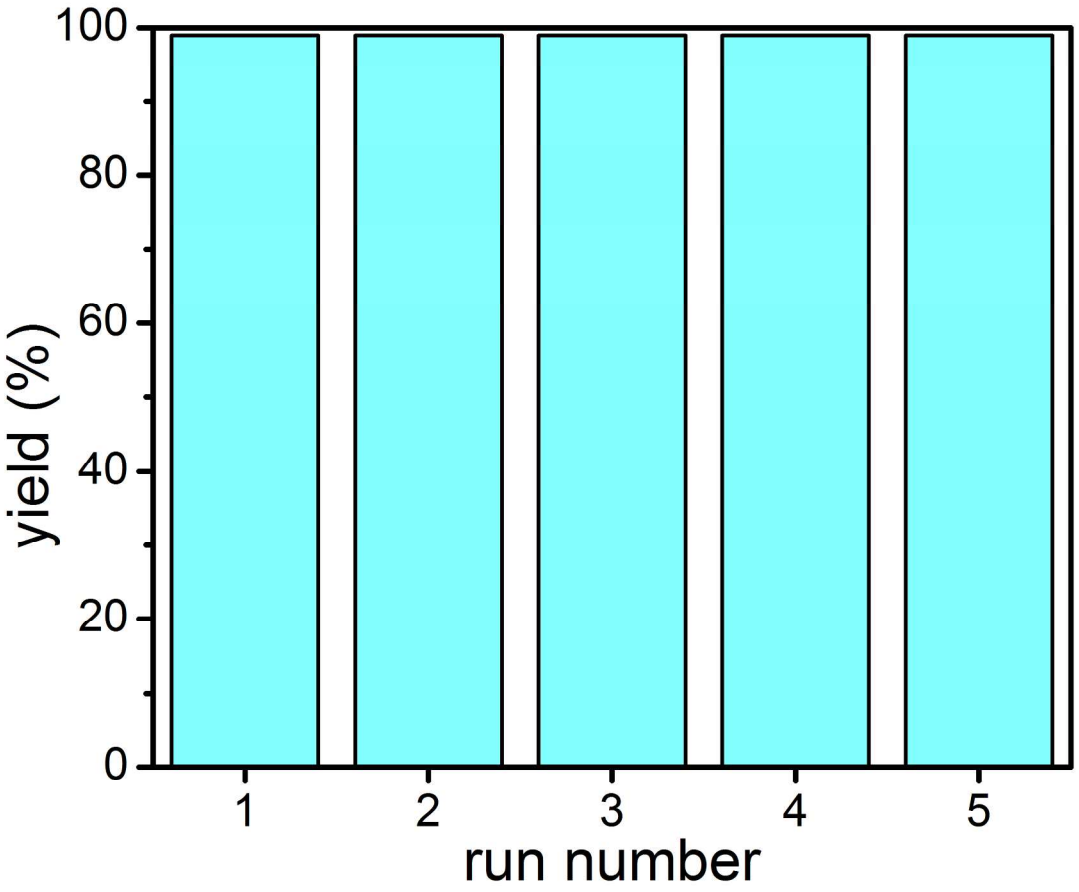

Figure S6. Recycling tests of the lactonization reaction catalyzed by **Cat-1**. Each run was performed with reactant **A** with **Cat-1** containing 2.2 mol % Au in CD_2Cl_2 for 22 h with stirring at 20 °C. The yield was determined by ^1H NMR using 1,1,2,2-tetrachloroethane as an internal standard.

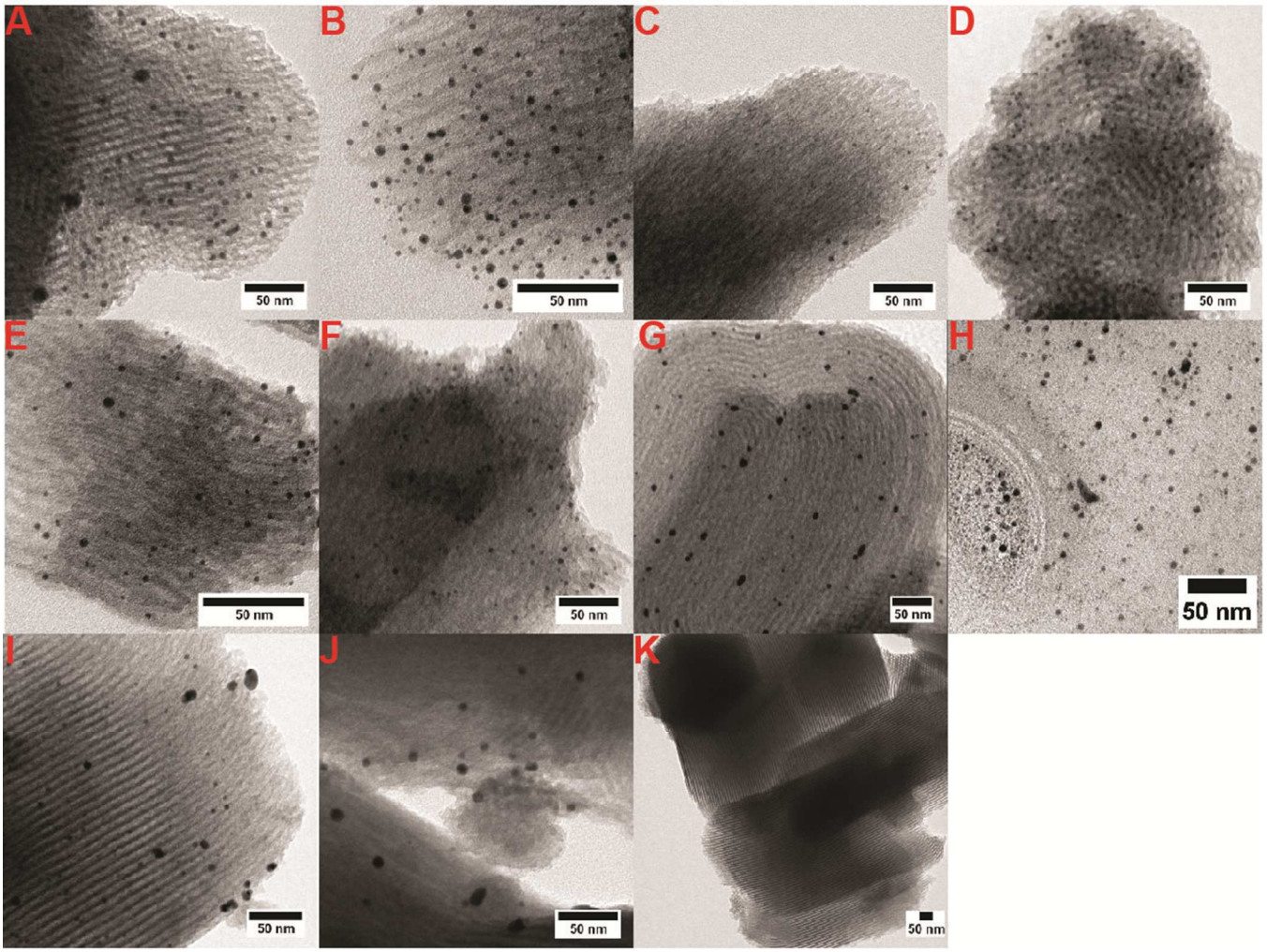

Figure S7. Representative TEM images of A. **Cat-2**, B. **Cat-3**, C. **Cat-4**, D. **Cat-5**, E. **Cat-6**, F. **Cat-7**, G. **Cat-8**, H. **Cat-9**, I. **Cat-10**, J. **Cat-11**, K. **AuNP-1**/SBA-15. The corresponding statistics analyses are summarized in Table S2.

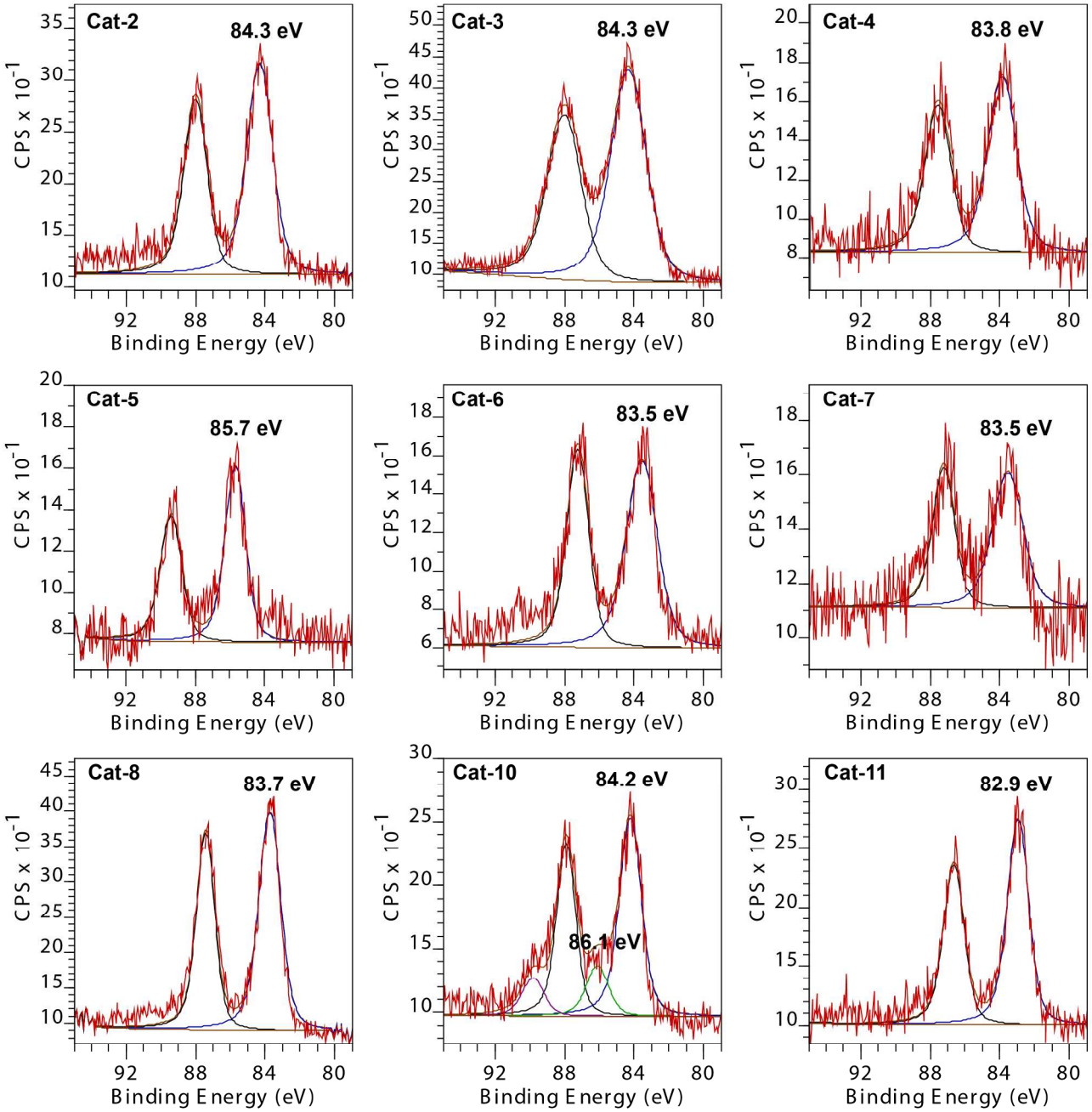

Figure S8. Au 4f XPS spectra of **Cat-2** – **Cat-11**.

Table S1. Dependence of ee on Reaction Conditions and Catalysts.

entry	catalyst	Au mol %	solvent	temperature (°C)	time (h)	yield (%)	ee (%)
1	**Cat-1**	2.2	CD_2Cl_2	20	22	100	16[h]
2	**1**[a]	2.0	CD_2Cl_2	20	22	0	N/A
3	**1**(cation)[b]	2.0	CD_2Cl_2	20	22	100	2[i]
4	**1**(cation)/SBA-15[c]	6.7	CD_2Cl_2	20	22	100	<-1
5	**AuNP-1**/SBA-15[d]	0.58	CD_2Cl_2	20	22	81.5	<1
6	**Cat-1'**[e]	5.2	CD_2Cl_2	20	22	100	2
7	**Cat-1**	3.4	CD_2Cl_2	0	22	49	15
8	**Cat-1**	3.4	CD_2Cl_2	40	22	100	14
9	**Cat-1**	3.4	CD_2Cl_2	60	22	100	13
10	**Cat-1**	3.4	C_6F_6	20	22	100	3
11	**Cat-1**	3.4	C_6D_6	20	22	100	9
12	**Cat-1**	3.4	Tol-d_8	20	22	100	9
13	**Cat-1**	3.4	cyclohexane	20	22	100	5
14	**1**/G2OH/SBA-15[f]	0.54	CD_2Cl_2	20	22	100	13
15	**1**/G5OH/SBA-15[f]	0.63	CD_2Cl_2	20	22	100	15
16	**1**/G6OH/SBA-15[f]	0.73	CD_2Cl_2	20	22	100	13
17	$(\mathbf{1})_{40}$/G4OH/SBA-15[g]	0.88	CD_2Cl_2	20	22	100	7
18	$(\mathbf{1})_{60}$/G4OH/SBA-15[g]	0.92	CD_2Cl_2	20	22	68.7	6
19	**Cat-2**	4.3	CD_2Cl_2	20	22	100	1
20	**Cat-3**	3.5	CD_2Cl_2	20	22	100	<-1
21	**Cat-4**	4.3	CD_2Cl_2	20	22	100	5
22	**Cat-5**	4.9	CD_2Cl_2	20	22	100	<1
23	**Cat-6**	4.4	CD_2Cl_2	20	22	100	<-1
24	**Cat-7**	3.5	CD_2Cl_2	20	22	100	1

25	**Cat-8**	4.1	CD_2Cl_2	20	22	64.9	1
26	**Cat-9**	1.9	CD_2Cl_2	20	22	4.8	0
27	**Cat-10**	1.5	CD_2Cl_2	20	22	0	N/A
28	**Cat-11**	1.0	CD_2Cl_2	20	22	0	N/A

[a]Potential Au(0) particles were removed by a filter. [b]The cation of **1** was obtained by mixing 6 μmol of **1** with 6.6 μmol of $AgBF_4$ in 0.6 mL CD_2Cl_2, sonicated for 10 min, and then filtered through a syringe filter. The filtrate turned black within a few minutes, but after mixing 2 mol % of Au from the filtrate with the reactant **A**, internal standard (1,1,2,2-tetrachloroethane), the reaction solution maintained clear and colorless over time. [c]**1**@SBA-15 was prepared by mixing 10 μmol of **1** with 11 μmol of $AgBF_4$ in 1 mL CH_2Cl_2, stirred for 1.5 h, and filtering the mixture through a pad of celite with twice of CH_2Cl_2 washing (2 × 1.5 mL), and stirring the resultant liquid with SBA-15 for 4 h. The solid was dried at 100 °C overnight before use. [d]Everything was the same as **Cat-1** except that no dendrimer was used in the synthesis. [e]The synthesis of **Cat-1'** was the same as that of **Cat-1** except that the Au particles were loaded into SBA-15 through sonication for **Cat-1** but through stirring for **Cat-1'**. [f]Everything is the same as **Cat-1**, except that G2OH, G5OH, or G6OH was used instead of G4OH. [g]Everything is the same as **Cat-1**, except that the ratio of **1** and G4OH used for the reduction was 5:1, 10:1, 40:1, or 60:1 instead of 20:1. [h]See Figure S44. [i]See Figure S70.

Table S2. Statistics of Au NPs in Catalysts Calculated from over 100 NPs in TEM Images.

entry	catalyst	average size (nm)	standard deviation (nm)
1	**Cat-0**	3.0	0.8
2	**Cat-1**	4.7	0.9
3	**Cat-2**	5.3	1.7
4	**Cat-3**	3.1	0.7
5	**Cat-4**	3.1	0.6
6	**Cat-5**	3.4	0.8
7	**Cat-6**	2.4	0.8
8	**Cat-7**	3.2	0.8
9	**Cat-8**	4.9	1.4
10	**Cat-9**	5.2	1.1
11	**Cat-10**	6	2
12	**Cat-11**	11	7

Materials

Purchased: The PAMAM dendrimer G4OH was purchased from Dendritech Inc. as water or methanol solutions. Dimethylsulfide, 37 wt.% aqueous formaldehyde solution, 40 wt.% glyoxal solution were purchased from Sigma-Aldrich. Acetic acid was purchased from EMD-Millipore Corp. 2,4,6-trimethylaniline was purchased from Acros Organics. Al of the aminoalcohols utilized for imidazolium salt synthesis were purchased from Combi-Blocks, Inc. 1-(2,4,6-Trimethylphenyl)-3-[(2S)-4-methyl-1-pentanol]imidazolium chloride (**IS1**) and chloro[1,3-bis(cyclohexyl)2H-imidazol-2-ylidene]gold(I) (complex **9**) were purchased from Strem Chemical. Gold(III) chloride was purchased from Strem and Alfa Aesar. Deuterated solvents were purchased from Cambridge Isotope Laboratories, Inc. and used as received. All other solvents and reagents were purchased from Sigma-Aldrich, Fisher Chemical, VWR, or Acros Organics. Deuterated solvents were purchased from Cambridge Isotope Laboratories, Inc. and used as received. All other solvents were purchased from Sigma-Aldrich and Fisher Scientific. Solvents utilized in air-sensitive experiments were sparged with argon and passed through solvent purification columns prior to use.[1] Silica gel for column chromatography (Grade 60, 230-400 mesh, 40–63 micron particle size) was purchased from Fisher Scientific. 20 x 20 cm^2 "TLC Silica gel 60 F_{254}" plates were purchased from the EMD Millipore Corporation and utilized for analytical thin-layer chromatography (TLC).

Prepared following reported procedures: (Dimethylsulfide)gold chloride ((DMS)AuCl),[2] substrate **A** (2,2,6-trimethylhepta-4,5-dienoic acid),[3] 1,3-bis((*R*)-1-(naphthalen-1-yl)ethyl)-1*H*-imidazol-3-ium tetrafluoroborate,[4] (*R*)-1-(1-phenylethyl)-1*H*-imidazole,[5] and N,N-dicyclohexylimidazolium carboxylate (ICy-CO_2 adduct[6]) were prepared according to the cited references. We thank Patrick Bohan for generously donating 1,3-bis((*R*)-1-(naphthalen-1-yl)ethyl)-1*H*-imidazol-3-ium tetrafluoroborate.

Methods

General synthetic protocol

All air-sensitive reactions were carried out in flame- or oven-dried glassware using standard Schlenk techniques. Inhomogeneous reaction mixtures were stirred with Teflon-coated magnetic stir bars. Reactions were monitored via nuclear magnetic resonance (NMR) spectroscopy and thin-layer chromatography (TLC), and the TLC plates were visualized under UV irradiation or via standard staining procedures. Unless otherwise indicated, filtration was carried out using medium-porosity fritted glass-funnels. Removal of solvents *in vacuo* was achieved using a Büchi rotary evaporator and a Schlenk line (~60-120 mTorr, dynamic vacuum). Purification via flash chromatography was carried out following standard procedures,[7] or, scaled down to pipettes.

Solution NMR spectroscopy

^{1}H and ^{13}C (^{1}H-decoupled) NMR spectra were recorded on Bruker NMR spectrometers operating at 400, 500, 600, and 900 MHz for ^{1}H (100, 125, 150, and 225 MHz for ^{13}C, respectively). These instrument models are listed here with the corresponding supporting federal grants: AVQ400 (*NSF grants HE79-26291-A02 and CHE-0130862*), AVB400 (*NSF grants CHE-0130862 and CHE-8703048, and NIH grant S10 RR 03353-01*), DRX500 (*NSF grants CHE 9633007 and CHE 82-08992, and NIH grant RR 02424A-01*), AV500 (*NIH grant 1S10RR016634-01*), AV600 (*NIH grant SRR023679A*), and μS2900 (900 MHz, NIH grant GM68933). Chemical shifts are expressed in parts per million (ppm), and splitting patterns are designated as s (singlet), d (doublet), t (triplet), q (quartet), p (pentet), sext (sextet), sept (septet), oct (octet), m (multiplet), b (broad), and combinations thereof. Scalar coupling constants *J* are reported in Hertz (Hz). MestReNova v10.0.2-15465 software (Mestrelab Research S.L.) was used to analyze the NMR spectra. ^{1}H and ^{13}C NMR spectra were referenced to residual monoproteo-solvent peaks as reported in literature.[8]

Mass spectrometry (MS)

High-resolution mass spectrometry (HRMS) was performed on the following instruments: (1) Thermo LTQ-FT-ICE (7T, ESI); (2) Thermo Fusion Lumos mass spectrometer; both (1) and (2) were at the QB3/Chemistry Mass Spectrometry Facility at the University of California, Berkeley. Unless state otherwise, the analysis was carried out in positive ion mode.

X-ray photoelectron spectroscopy (XPS)

1. Sample preparation for XPS. Solutions/dispersions/suspensions of the samples were drop-cast onto silicon wafers (covered with a film of native oxide) and allowed to dry. These samples were then affixed onto carbon tape for XPS.

2. XPS parameters. X-ray photoelectron spectroscopy (XPS) was carried out on a Kratos Axis Ultra X-ray Photoelectron Spectrometer, at the Joint Center for Artificial Photosynthesis, a DOE Energy Innovation Hub, supported through the Office of Science of the U.S. Department of Energy under Award Number DE-SC0004993. Main chamber pressure during XPS analysis was in the range of ~$5 \bullet 10^{-8}$ Torr. Charge neutralization was accomplished through both conductive contacts through the holder as well as flooding the experiment chamber with electrons. The X-ray source had 225 W power and 15 kV potential applied to it. Monochromatized Al−Kα source (hν = 1486.69 eV) source was used. The take-off angle was 0°. For all samples, prior to collection of the narrow-region data, automatic z-alignment was performed, and three cycles of a survey scan at a pass energy of 160 eV were collected and averaged (data not shown). Narrow region scans were then carried out under the following conditions. A pass energy of 20 eV with a step size of 0.05 eV were used; the number of sweeps for each probed orbital was set as follows (in order these orbitals were actually measured): Au 4f – 5-8 sweeps, C 1s – 5 sweeps, Si 2p – 5 sweeps. CasaXPS Version 2.3.17PR1.1 software was used to process and analyze the XPS data as follows. Notably, the transmission correction was virtually identical for all regions, and did not affect the computations.

3. Binding energy (B.E.) calibration for XPS spectra. The B.E. scale was calibrated to the Si 2p of SiO2 (either native oxide on silicon wafer or SBA-15 mesoporous silica) with the peak at 103.4 eV.[9]

4. Baseline selection for XPS regions. Linear baselines were chosen for C 1s regions; Tougaard baselines[10] baselines were used for Au 4f, and Shirley for Si 2p regions.

5. Lineshape selection and fitting of XPS spectra. N 1s and C 1s peaks were fitted using GL(30) lineshapes[10a] through the application of the Downhill Simplex approximation provided in the CasaXPS software[10a]; standard deviation of the residual was typically between 0.5 and 3 Au 4f peaks were fitted using LF(0.95,1.1,255,280) lineshapes through the application of the Downhill Simplex approximation

provided in the CasaXPS software; standard deviation of the residual was generally between 0.8 and 2 (1 being an indicator of an excellent fit); the effective RSF calculated from the fit was also within ~10% of actual RSF, which also affirmed that good fits were obtained. The relationship between the Au 4f 7/2 and 5/2 components was constrained to be as follows: area of Au 4f 5/2 = 0.75 x area of Au 4f 7/2; position of Au 4f 5/2 (in eV) = 3.70 + position of Au 4f 7/2 component.[11]

Chiral phase high-performance liquid chromatography (chiral HPLC)

Chiral HPLC was performed on the Shimadzu Prominence series instrument using the Chiralpak® AD-H column (5μm, 4.6 mm x 250 mm). Racemic traces were obtained by using **Cat-0**. Samples were prepared by dissolving the products in 92:8 hexane/isopropanol at a concentration of ~10 μmol/mL. The following conditions were used for product **B**: 99.6:0.4 hexane/isopropanol eluent, 0.5 mL/min flow rate, temperature = 40 °C, with enantiomers of **B** eluting at ~40 min (first enantiomer) and ~43.5 min (second enantiomer) (Note: these retention times varied typically by ±1 min, and in some cases were reduced by 10 min, and this difference was ascribed to variation in solvent composition, given the low concentration of isopropanol that was used). The following conditions were used for product **B′**: 95:5 hexane/isopropanol eluent, 1 mL/min flow rate, temperature = 40 °C, with enantiomers of **B′** eluting at ~12.3 min (first enantiomer) and ~15.0 min (second enantiomer). The enantiomers were detected with a UV detector at 211 nm. The % enantiomeric excess (% ee) was determined by subtracting the % area of the first enantiomer from the % area of the second.

Time-of-flight secondary ion mass spectrometry (ToF-SIMS)

Spectra of Time-of-flight secondary ion mass spectrometry (ToF-SIMS) were acquired on a Iontof ToF-SIMS 5 spectrometer using a 25 keV Bi^{3+} cluster ion source in the pulsed mode. Spectra were acquired for both positive and negative secondary ions over a mass range of m/z = 0 to 800. The ion source was operated with at a current of 0.088 pA. Secondary ions of a given polarity were extracted and detected using a reflectron time-of-flight mass analyzer. Spectra were acquired using an analysis area of 100 micron x 100 micron. Positive ion spectra were calibrated using the CH_3^+, $C_2H_3^+$, $C_3H_5^+$, $C_4H_7^+$ and $C_5H_7^+$ peaks. The negative ion spectra were calibrated using the CH^-, OH^-, C_2H^-, C_4H^-, and C_5H^- peaks. Calibration errors were kept below 25 ppm. Mass resolution (m/Δm) for a typical spectrum was between 5000 to 5600 for m/z = 27 (pos) and between 5000 to 5700 for m/z = 25 (neg).

X-ray absorption fine structure (XAFS)

The XAS measurements in this work were performed at beamline 10.3.2 at Advanced Light Source (ALS) at Lawrence Berkeley National laboratory (Berkeley, CA). The data were collected in fluorescence mode at the Au L3 edge (11919.7 eV). A bulk Au foil was measured in transmission mode every 24 hours for calibration purposes. All spectra were taken at room temperature (22 °C). The QuickXAS mode at beamline 10.3.2 at ALS was utilized to collect multiple scans for each sample. A quartz capillary tube was used for both *ex situ* and *in situ* measurements. Only the solid samples were loaded into the capillary tube in the ex situ tests, while the catalyst, the reactant, and the solvent were loaded for the *in situ* measurements.

For EXAFS analysis, the software at the beamline was used to perform dead time correction, energy calibration, glitch removal, pre-edge subtraction, postedge normalization, and conversion to *k*-space. All spectra were aligned using metallic gold spectra as reference prior to analysis.

Transmission electron microscopy (TEM)

Samples were prepared by drop-casting a solution or a suspension of a powder sample in ethanol onto Cu TEM grids (Lacey Formvar/Carbon, Copper for nanoparticles in a solution and Formvar, 400 mesh, copper for powder samples). The grids were dried at ambient conditions before analysis. The TEM images were taken with a FEI Tecnai TEM at an accelerating voltage of 200 kV. The software ImageJ was used to analyze the TEM images.

Attenuated total reflectance Fourier transform infrared (ATR-FTIR)

ATR-FTIR spectra were recorded on a Bruker Vertex80 model with a Bruker Platinum ATR cell. 32 scans were collected from 4000 to 400 cm^{-1} with a resolution of 4 cm^{-1} for each spectrum.

Optima 7000 DV Inductively coupled plasma optical emission spectroscopy (ICP-OES)

Catalyst loading was analyzed by Optima 7000 DV ICP-OES after digesting 10 mg of the solid catalysts in 0.6 mL of concentrated hydrochloric acid, 0.2 mL of concentrated HNO_3, and 0.2 mL of HF, and diluting the resultant solution to 10 mL. This technique was also used to determine whether Au was leached into the filtrate after a catalytic reaction, as a means of checking whether the catalysis is truly heterogeneous. For this purpose, after removing the solid catalyst at the end of a catalytic reaction run via syringe filtration, the filtrate was dried by rotary evaporation, then mixed with 0.6 mL of concentrated hydrochloric acid, 0.2 mL of concentrated HNO_3, and 0.2 mL of HF, and diluting the resultant solution to 10 mL for ICP-OES.

Synthetic Procedures

Modified Syntheses of Previously Reported Compounds

Substrate **A′** (6-methyl-2,2-diphenylhepta-4,5-dienoic acid) was prepared analogously to substrate **A** (*vide supra*), beginning with 1-bromo-4-methylpenta-2,3-diene, an intermediate generated in the synthesis of **A**. Enolate alkylation of methyl 2,2-diphenylacetate (instead of ethyl isobutyrate for **A**) with 1-bromo-4-methylpenta-2,3-diene, followed by alkaline hydrolysis of the product ester and workup (identically to **A**[3]) afforded **A′** as a powdery white solid (942 mg, 57% yield over two steps). ^{1}H NMR spectrum of **A′** matched reported.[3]

Au(I) complexes **1**[12] and **8** were prepared following the general procedure for new Au(I) complex synthesis (*vide infra*), and their ^{1}H NMR spectra matched the reported, with the following caveat: in fact, only the opposite (bis(S)) enantiomer of **8** has been reported in prior literature,[13] so for the sake of completeness, the characterization of **8** is provided below.

Imidazolium salt **IS6** was previously observed to form during the synthesis of **IS1**.[12] We have prepared it here directly, as described below. The isolated **IS6** (% purity assessed by ^{1}H NMR) was taken forward without full characterization, because it was an intermediate in a linear two-step sequences *en route* to Au(I) complex **6**.

1,3-bis((S)-1-hydroxy-4-methylpentan-2-yl)-1H-imidazol-3-ium chloride IS6. (S)-2-amino-4-methylpentan-1-ol (2.6 mL, 20. mmol), 40 wt.% glyoxal$_{(aq.)}$ (1.14 mL, 10.0 mmol), 37 wt.% formaldehyde$_{(aq.)}$ (0.74 mL, 10.0 mmol), and acetic acid (5.1 mL, 90 mmol) were mixed in a 40-mL scintillation vial equipped with a teflon-coated magnetic stir bar. The sealed vial was heated at 80 °C overnight. The resulting mixture was cooled to room temperature, extracted with dichloromethane (30 mL), and the organic phase was washed with brine (3 x 30 mL). The combined organic phase was dried over magnesium sulfate, filtered, and concentrated by rotary evaporation to afford the crude product. The crude product was washed with hot ethyl acetate (3 x 20 mL). Drying *in vacuo* at 60 °C afforded the title product as an orange highly viscous liquid (1.1261 g, 37% yield, ~80% purity by ^{1}H NMR). ^{1}H NMR (500 MHz, $CDCl_3$, 23 °C): δ 9.09–8.97 (m, 1H, imidazolium C–H), 7.32 (d, J = 1.9 Hz, 2H),

5.71–5.43 (bs, 2H), 4.47–4.38 (m, 2H), 3.92 (d, J = 12.4 Hz, 2H), 3.77 (dd, J = 12.5, 7.5 Hz, 2H), 1.86–1.78 (m, 2H), 1.78–1.58 (m, 4H), 1.57–1.46 (m, 2H), 0.95 ppm (d, J = 6.6 Hz, 12H).

Syntheses and Characterization of New Compounds

Imidazolium salts:

The imidazolium salt precursors of Au(I) complexes **2**–**5** and **7** (**IS2**–**IS5** and **IS7**) were prepared following a previously reported procedure for the synthesis of the **IS1**,[12] except the reactions were carried out at 80 °C for 10 min or overnight, and with alternative purification procedures. The imidazolium salt precursors of Au(I) complexes of **10**–**11** were prepared by alkylation of (*R*)-1-(1-phenylethyl)-1*H*-imidazole,[5] as described below. All of the isolated imidazolium salts (% purity assessed by ^{1}H NMR) were taken forward without full characterization, because they were intermediates in linear two-step sequences en route to the Au(I) complexes.

3-((2*S*,3*S*)-1-hydroxy-3-methylpentan-2-yl)-1-mesityl-1*H*-imidazol-3-ium chloride IS2. (1R,2S)-1-amino-2-methylbutan-1-ol (1.23 mL, 10.0 mmol), 2,4,6-trimethylaniline (1.41 mL, 10.0 mmol), 40 wt.% glyoxal$_{(aq.)}$ (1.14 mL, 10.0 mmol), 37 wt.% formaldehyde$_{(aq.)}$ (0.74 mL, 10.0 mmol), and acetic acid (5.1 mL, 90 mmol) were mixed in a 40-mL scintillation vial equipped with a teflon-coated magnetic stir bar. The sealed vial was heated at 80 °C for 10 min. The resulting mixture was cooled to room temperature, extracted with dichloromethane (30 mL), and the organic phase was washed with brine (3 x 30 mL). The combined organic phase was dried over magnesium sulfate, filtered, and concentrated by rotary evaporation to afford the crude product Addition of 40 mL ethyl acetate and gentle heating below reflux led to formation of a precipitate, which was filtered and washed with ethyl acetate (3 x 20 mL). Drying this solid *in vacuo* at 60 °C afforded the title product as a beige powdery solid (1.519 g, 47% yield, ~95% purity by ^{1}H NMR). ^{1}H NMR (400 MHz, $CDCl_3$, 23 °C): δ 9.84 (t, J = 1.6 Hz, 1H, imidazolium C–H), 7.50 (t, J = 1.7 Hz, 1H), 7.17 (t, J = 1.9 Hz, 1H), 7.01 (s, 2H), 5.58 (bd, J = 9.0 Hz, 1H), 5.04 (td, J = 9.7, 4.1 Hz, 1H), 4.24 (dd, J = 12.2, 4.1 Hz, 1H), 3.78 (q, J = 10.0 Hz, 1H), 2.35 (s, 3H), 2.12 (s, 3H), 2.08 (s, 3H), 2.03–1.92 (m, 1H), 1.42–1.30 (m, 1H), 1.25–1.12 (m, 1H), 1.09 (d, J = 6.7 Hz, 3H), 0.94 ppm (t, J = 7.4 Hz, 3H).

(S)-3-(2-hydroxy-1-phenylethyl)-1-mesityl-1H-imidazol-3-ium chloride IS3. (S)-2-amino-2-phenylethan-1-ol (1.372 g, 10.0 mmol), 2,4,6-trimethylaniline (1.41 mL, 10.0 mmol), 40 wt.%

glyoxal$_{(aq.)}$ (1.14 mL, 10.0 mmol), 37 wt.% formaldehyde$_{(aq.)}$ (0.74 mL, 10.0 mmol), and acetic acid (5.1 mL, 90 mmol) were mixed in a 40-mL scintillation vial equipped with a teflon-coated magnetic stir bar. The sealed vial was heated at 80 °C for 10 min. The resulting mixture was cooled to room temperature, extracted with dichloromethane (30 mL), and the organic phase was washed with brine (3 x 30 mL). The combined organic phase was dried over magnesium sulfate, filtered, and concentrated by rotary evaporation to afford the crude product. The crude product was washed with hot ethyl acetate (3 x 20 mL), and then excess acetone (product is insoluble). Drying the resulting solid *in vacuo* afforded the title product as a beige powdery solid (0.829 g, 24% yield, ~95% purity by ^{1}H NMR). ^{1}H NMR (500 MHz, $CDCl_3$, 23 °C): δ 10.24 (bs, 1H, imidazolium C–H), 7.50–7.44 (m, 3H), 7.40–7.35 (m, 2H), 7.28–7.26 (b, 1H, overlaps with $CHCl_3$ resonance), 7.10 (t, J = 1.7 Hz, 1H), 7.02 (s, 2H), 6.42 (dd, J = 10.8, 3.9 Hz, 1H), 6.18 (m, 1H), 4.38 (bd, J = 12.6 Hz, 1H), 4.24 (q, J = 11.1 Hz, 1H), 2.35 (s, 3H), 2.13 (s, 3H), 2.10 ppm (s, 3H).

(S)-3-(1-hydroxy-3-phenylpropan-2-yl)-1-mesityl-1H-imidazol-3-ium chloride IS4. (S)-2-amino-3-phenylpropan-1-ol (1.512 g, 10.0 mmol), 2,4,6-trimethylaniline (1.41 mL, 10.0 mmol), 40 wt.% glyoxal$_{(aq.)}$ (1.14 mL, 10.0 mmol), 37 wt.% formaldehyde$_{(aq.)}$ (0.74 mL, 10.0 mmol), and acetic acid (5.1 mL, 90 mmol) were mixed in a 40-mL scintillation vial equipped with a teflon-coated magnetic stir bar. The sealed vial was heated at 80 °C for 10 min. The resulting mixture was cooled to room temperature, extracted with dichloromethane (30 mL), and the organic phase was washed with brine (3 x 30 mL). The combined organic phase was dried over magnesium sulfate, filtered, and concentrated by rotary evaporation to afford the crude product. The crude product was dissolved in dichlromethane (~5 mL), precipitated into ethyl acetate (75 mL), decanting off the supernatant; repeated, but with addition of ethyl acetate to the solution of crude product in dichloromethane. Drying this material *in vacuo* afforded the title product as a brown/beige solid foam that was ground with a spatula to powder (1.7669 g, 50% yield, ~75% purity by ^{1}H NMR). ^{1}H NMR (500 MHz, $CDCl_3$, 23 °C): δ 9.38 (s, 1H, imidazolium C–H), 7.70 (bs, 1H), 6.95 (s, 1H), 6.91 (s, 1H), 5.76 (bs, 1H), 5.64–5.55 (m, 1H), 4.25 (dd, J = 12.3, 3.8 Hz, 1H), 3.97 (d, J = 11.6 Hz, 1H), 3.32 (dd, J = 14.6, 4.7 Hz, 1H), 3.17–3.09 (m, 1H), 2.30 (s, 3H), 2.01 (s, 3H), 1.72 (s, 3H); remaining aromatic ^{1}H resonances were not assigned due to the presence of overlapping resonances from the symmetric (i.e., bis-alcohol and bis(mesityl)) imidazolium salts.

(S)-3-(1-hydroxy-4-(methylthio)butan-2-yl)-1-mesityl-1H-imidazol-3-ium chloride IS5. (S)-2-amino-4-(methylthio)butan-1-ol (1.3523 g, 10.0 mmol), 2,4,6-trimethylaniline (1.41 mL, 10.0 mmol), 40 wt.% glyoxal$_{(aq.)}$ (1.14 mL, 10.0 mmol), 37 wt.% formaldehyde$_{(aq.)}$ (0.74 mL, 10.0 mmol), and acetic

acid (5.1 mL, 90 mmol) were mixed in a 40-mL scintillation vial equipped with a teflon-coated magnetic stir bar. The sealed vial was heated at 80 °C overnight. The resulting mixture was cooled to room temperature, extracted with dichloromethane (30 mL), and the organic phase was washed with brine (3 x 30 mL). The combined organic phase was dried over magnesium sulfate, filtered, and concentrated by rotary evaporation to afford the crude product. The crude product was washed with hot ethyl acetate (2 x 50 mL), then precipitated from acetone (50 mL) by addition of ethyl acetate (150 mL), and then precipitated again from dichloromethane (~30 mL) by addition of diethyl ether (150 mL). Supernatants were removed by decantation, and the remaining product was dried *in vacuo*, affording the title product as a brown powdery solid (0.8028 g, 47% yield, ~90% purity by ^{1}H NMR). ^{1}H NMR (500 MHz, $CDCl_3$, 23 °C): δ 9.82 (t, J = 1.6 Hz, 1H, imidazolium C–H), 7.62 (t, J = 1.5 Hz, 1H), 7.18 (t, J = 1.6 Hz, 1H), 7.01 (s, 2H), 5.74 (bs, 1H), 5.48–5.39 (m, 1H), 4.14 (dd, J = 12.0, 3.8 Hz, 1H), 3.77–3.66 (m, 1H), 2.63–2.50 (m, 2H), 2.35 (s, 3H), 2.27–2.21 (m, 2H), 2.11 (s, 6H), 2.08 ppm (s, 3H).

1,3-bis((S)-1-hydroxy-3-phenylpropan-2-yl)-1H-imidazol-3-ium chloride IS7. (S)-2-amino-3-phenylpropan-1-ol (3.024 g, 20.0 mmol), 40 wt.% $glyoxal_{(aq.)}$ (1.14 mL, 10.0 mmol), 37 wt.% $formaldehyde_{(aq.)}$ (0.74 mL, 10.0 mmol), and acetic acid (5 mL, 90 mmol) were mixed in a 40-mL scintillation vial equipped with a teflon-coated magnetic stir bar. The sealed vial was heated at 80 °C overnight. The resulting mixture was cooled to room temperature, extracted with dichloromethane (30 mL), and the organic phase was washed with brine (3 x 30 mL). The combined organic phase was dried over magnesium sulfate, filtered, and concentrated by rotary evaporation to afford the crude product. The crude product was dissolved in dichlromethane (~5 mL), precipitated into ethyl acetate (75 mL), and the supernatant was decanted off; repeated, but with addition of ethyl acetate to the solution of crude product in dichloromethane. Drying this material *in vacuo* afforded the title product as a tacky brown solid (2.379 g, 64% yield, ~88% purity by ^{1}H NMR). ^{1}H NMR (500 MHz, $CDCl_3$, 23 °C): δ 9.34 (s, 1H, imidazolium C–H), 7.23–7.20 (m, 6H), 7.10 (s, 2H), 7.05–7.00 (m, 4H), 5.52 (bs, 2H), 4.70–4.60 (m, 2H), 3.99 (d, J = 12.3 Hz, 2H), 3.91 (dd, J = 12.4, 7.0 Hz, 2H), 3.18 (dd, J = 14.3, 5.8 Hz, 2H), 3.03 ppm (dd, J = 14.3, 9.4 Hz, 2H).

(R)-3-dodecyl-1-(1-phenylethyl)-1H-imidazol-3-ium chloride IS10. (*R*)-1-(1-phenylethyl)-1*H*-imidazole[5] (0.1722 g, 1.00 mmol) and 1-bromododecane (0.72 mL, 3.00 mmol) were mixed in toluene (1 mL) in a sealed microwave vial equipped with a Teflon-coated magnetic stir-bar. The sealed vial was heated at 120 °C for 4.5 h. The resulting phase-separated mixture was subjected to column chromatography on silica gel, eluting first with dichloromethane, and then with 9:1

dichloromethane/methanol. Drying the collected product *in vacuo* afforded the title product as a light-brown viscous liquid that slowly crystallized (0.3186 g, 76% yield, >95% purity by ^{1}H NMR). ^{1}H NMR (600 MHz, $CDCl_3$, 23 °C): δ 11.00 (t, J = 1.6 Hz, 1H, imidazolium C–H), 7.47–7.42 (m, 2H), 7.42–7.34 (m, 3H), 7.22 (t, J = 1.8 Hz, 1H), 7.15 (t, J = 1.9 Hz, 1H), 6.00 (q, J = 7.0 Hz, 1H), 4.42–4.32 (m, 2H), 2.04 (d, J = 7.0 Hz, 3H), 1.91 (m ≈ p, J = 7.5 Hz, 2H), 1.38–1.17 (m, 18H), 0.87 ppm (t, J = 7.0 Hz, 3H).

(R)-3-octadecyl-1-(1-phenylethyl)-1H-imidazol-3-ium chloride IS11. (*R*)-1-(1-phenylethyl)-1*H*-imidazole[5] (0.1722 g, 1.00 mmol) and 1-bromooctadecane (1.000 g, 3.00 mmol) were mixed in toluene (1 mL) in a sealed microwave vial equipped with a Teflon-coated magnetic stir-bar. The sealed vial was heated at 120 °C for 4.5 h. The resulting phase-separated mixture was subjected to column chromatography on silica gel, eluting first with dichloromethane, and then with 5:1 dichloromethane/methanol. Drying the collected product *in vacuo* afforded the title product as a light-brown waxy solid (0.3849 g, 76% yield, >95% purity by ^{1}H NMR). ^{1}H NMR (400 MHz, $CDCl_3$, 23 °C): δ 11.19 (s, 1H, imidazolium C–H), 7.47–7.36 (m, 5H), 7.09 (t, J = 1.9 Hz, 1H), 7.03 (t, J = 1.8 Hz, 1H), 6.00 (q, J = 7.1 Hz, 1H), 4.43–4.33 (m, 2H), 2.06 (d, J = 7.0 Hz, 3H), 1.93 (m ≈ p, J = 7.5 Hz, 2H), 1.43–1.18 (m, 30H), 0.88 ppm (t, J = 6.8 Hz, 3H).

Au(I) complexes:

New Au(I) complexes **2**–**7** and **10**–**11** were synthesized from the corresponding imidazolium salts (*vide supra*) following the procedure developed by Nolan *et al.*,[14] with the following specific conditions utilized in all cases: 3 equiv of potassium carbonate, 1 equiv of (DMS)AuCl, and 1 equiv of the imidazolium salt, were mixed in acetone, and the reaction mixtures (0.25 M in (DMS)AuCl) were heated for 4 h at 60 °C. Products were purified by column chromatography, and afterward, if trace Au^0 particles were observed, they were removed by filtration of DCM solutions through glass microfibre filters (691, VWR) packed in glass Pasteur pipettes. Column chromatography conditions, absolute and % yields (based on (DMS)AuCl), appearance, and characterization of all compounds are reported below. All complexes were >95% pure unless stated otherwise.

(1-((2*S*,3*S*)-1-hydroxy-3-methylpentan-2-yl)-3-mesityl-1,3-dihydro-2*H*-imidazol-2-ylidene)gold(I) chloride 2. Purified via flash column chromatography on silica gel using 1:1 HXN/EtOAc as the eluent (R_f = 0.17) to afford **2** as a crystalline white solid (20.1 mg, 78% yield). ^{1}H NMR (500 MHz, CD_2Cl_2, 23 °C): δ 7.38 (d, J = 2.0 Hz, 1H), 7.03 (bs, 2H), 6.95 (d, J = 1.9 Hz, 1H), 4.74–4.67 (m, 1H), 4.13 (dt, J = 11.5, 5.7 Hz, 1H), 4.03 (ddd, J = 11.8, 5.1, 2.9 Hz, 1H), 2.36 (s, 3H),

2.23–2.14 (m, 1H), 2.04 (s, 3H), 2.02 (s, 3H), 1.67 (-OH, t, J = 5.2 Hz, 1H), 1.33–1.22 (m, 1H), 1.20–1.13 (m, 1H), 1.11 (d, J = 6.7 Hz, 3H), 0.92 ppm (t, J = 7.4 Hz, 3H). ^{13}C NMR (225 MHz, CD_2Cl_2, 23 °C): δ 172.0, 140.1, 135.42, 135.40, 135.38, 129.59, 129.58, 122.7, 119.8, 67.8, 63.4, 35.5, 25.8, 21.3, 17.9, 17.8, 15.7, 10.8 ppm. HRMS (ESI): calcd. for $C_{18}H_{26}AuClN_2O$ [M-Cl+MeCN]$^+$, most abundant *m/z* = 524.1976; found, 524.1980.

(*S*)-(1-(2-hydroxy-1-phenylethyl)-3-mesityl-1,3-dihydro-2*H*-imidazol-2-ylidene)gold(I) chloride 3. Purified via flash column chromatography on silica gel using 1:1 HXN/EtOAc as the eluent (R_f = 0.2) to afford **3** as a powdery white solid (99.9 mg, 74% yield). ^{1}H NMR (500 MHz, $CDCl_3$, 23 °C): δ 7.47–7.37 (m, 4H), 7.37–7.33 (m, 2H), 7.04 (bs, 1H), 7.03 (bs, 1H), 6.97 (d, J = 2.0 Hz, 1H), 6.20 (dd, J = 6.8, 4.5 Hz, 1H), 4.49–4.35 (m, 2H), 2.36 (s, 3H), 2.07 (s, 3H), 2.01 (s, 3H), 1.92 ppm (-OH, t, J = 6.0 Hz, 1H). ^{13}C NMR (225 MHz, CD_2Cl_2, 23 °C): δ 172.9, 140.2, 136.8, 135.4, 135.32, 135.29, 129.63, 129.61, 129.5, 129.0, 127.4, 122.8, 120.1, 66.0, 64.3, 21.3, 18.0, 17.9 ppm. HRMS (ESI): calcd. for $C_{20}H_{22}AuClN_2O$ [M-Cl+MeCN]$^+$, most abundant *m/z* = 544.1663; found, 544.1662.

(*S*)-(1-(1-hydroxy-3-phenylpropan-2-yl)-3-mesityl-1,3-dihydro-2*H*-imidazol-2-ylidene)gold(I) chloride 4. Purified via flash column chromatography on silica gel using 1:2 HXN/EtOAc as the eluent (R_f = 0.26) to afford **4** as a brown powdery solid (40.6 mg, ~95% pure by ^{1}H NMR, 24% yield). ^{1}H NMR (500 MHz, CD_2Cl_2, 23 °C): δ 7.38 (d, J = 2.1 Hz, 1H), 7.29–7.23 (m, 2H), 7.23–7.17 (m, 3H), 6.98 (bs, 1H), 6.95 (bs, 1H), 6.85 (d, J = 1.9 Hz, 1H), 5.27–5.19 (m, 1H), 4.18–4.02 (m, 2H), 3.31 (dd, J = 14.1, 5.6 Hz, 1H), 3.23 (dd, J = 14.1, 10.3 Hz, 1H), 2.33 (s, 3H), 2.04 (-OH, t, J = 5.3 Hz, 1H), 1.98 (s, 3H), 1.70 ppm (s, 3H). ^{13}C NMR (225 MHz, CD_2Cl_2, 23 °C): δ 171.9, 140.1, 136.6, 135.4, 135.3, 135.2, 129.6, 129.49, 129.47, 129.0, 127.3, 122.6, 119.6, 64.9, 64.8, 38.0, 21.3, 17.9, 17.8 ppm. HRMS (ESI): calcd. for $C_{21}H_{24}AuClN_2O$ [M-Cl+MeCN]$^+$, most abundant *m/z* = 558.1820; found, 558.1810.

(*S*)-(1-(1-hydroxy-4-(methylthio)butan-2-yl)-3-mesityl-1,3-dihydro-2*H*-imidazol-2-ylidene)gold(I) chloride 5. Purified via flash column chromatography on silica gel using 3:7 HXN/EtOAc as the eluent (R_f = 0.23) to afford **5** as a crystalline beige solid (115.3 mg, 43% yield). ^{1}H NMR (500 MHz, CD_2Cl_2, 23 °C): δ 7.39 (d, J = 2.0 Hz, 1H), 7.03 (bs, 2H), 6.97 (d, J = 2.0 Hz, 1H), 5.15–5.07 (m, 1H), 4.12–3.98 (m, 1H), 2.55–2.42 (m, 1H), 2.36 (s, 3H), 2.35–2.27 (m, 1H), 2.24–2.15 (m, 1H), 2.12 (s, 3H), 2.03 (s, 3H), 2.02 (s, 3H), 1.87 ppm (-OH, t, J = 5.4 Hz, 1H). ^{13}C NMR (225 MHz, CD_2Cl_2, 23 °C): δ 172.1, 140.3, 135.41, 135.36, 135.3, 129.64, 129.63, 123.0, 119.6, 65.1, 62.6,

30.9, 21.3, 17.94, 17.93 ppm. HRMS (ESI): calcd. for $C_{17}H_{24}AuClN_2OS$ $[M+Na]^+$, most abundant *m/z* = 559.0856; found, 559.0852.

(1,3-bis((*S*)-1-hydroxy-4-methylpentan-2-yl)-1,3-dihydro-2*H*-imidazol-2-ylidene)gold(I) chloride 6. Purified via flash column chromatography on silica gel using 2:8 HXN/EtOAc as the eluent (R_f = 0.23, streaks) to afford **6** as a light-yellow film (20.1 mg, 78% yield). ^{1}H NMR (500 MHz, CD_2Cl_2, 23 °C): δ 7.13 (s, 2H), 4.88 (ddt, J = 10.7, 6.5, 4.4 Hz, 2H), 3.95–3.83 (m, 4H), 1.95–1.84 (m, 4H), 1.59 (ddd, J = 14.0, 9.0, 4.7 Hz, 2H), 1.46–1.35 (m, 2H), 1.01 (d, J = 6.5 Hz, 6H), 0.90 ppm (d, J = 6.6 Hz, 6H). ^{13}C NMR (225 MHz, CD_2Cl_2, 23 °C): δ 170.3, 119.5, 65.9, 62.7, 40.1, 24.9, 23.2, 22.2 ppm. HRMS (ESI): calcd. for $C_{15}H_{28}AuClN_2O_2$ $[M-Cl+MeCN]^+$, most abundant *m/z* = 506.2082; found, 506.2081.

(1,3-bis((*S*)-1-hydroxy-3-phenylpropan-2-yl)-1,3-dihydro-2*H*-imidazol-2-ylidene)gold(I) chloride 7. Purified via flash column chromatography on silica gel using 2:8 HXN/EtOAc as the eluent (R_f = 0.21) to afford **7** as a powdery beige solid (108.2 mg, 27% yield). ^{1}H NMR (500 MHz, CD_2Cl_2, 23 °C): δ 7.28–7.18 (m, 6H), 7.14–7.06 (m, 6H), 4.97 (dtd, J = 10.0, 6.4, 3.7 Hz, 2H), 3.98 (dt, J = 11.6, 5.7 Hz, 2H), 3.89 (ddd, J = 11.7, 5.6, 3.8 Hz, 2H), 3.20 (dd, J = 14.0, 6.6 Hz, 2H), 3.13 (dd, J = 14.0, 8.8 Hz, 2H), 1.77 ppm (-O<u>H</u>, t, J = 5.5 Hz, 2H). ^{13}C NMR (225 MHz, CD_2Cl_2, 23 °C): δ 169.5, 136.3, 129.0, 128.6, 126.8, 119.5, 65.3, 64.1, 37.5 ppm. HRMS (ESI): calcd. for $C_{21}H_{24}AuClN_2O_2$ $[M-Cl+MeCN]^+$, most abundant *m/z* = 574.1757; found, 574.1769.

(1,3-bis((*R*)-1-(naphthalen-1-yl)ethyl)-1,3-dihydro-2*H*-imidazol-2-ylidene)gold(I) chloride 8. 1,3-bis((*R*)-1-(naphthalen-1-yl)ethyl)-1*H*-imidazol-3-ium tetrafluoroborate was converted to the corresponding chloride salt by dissolving the former in dichloromethane (5 mL) and washing with brine (3 x 5 mL), and then drying the organic phase over sodium sulfate, filtration and solvent evaporation. The formation of the Au(I) complex **8** was carried out following the general procedure, and the product was purified via flash column chromatography on silica gel using 1:1 HXN/EtOAc as the eluent (R_f = 0.45) to afford **8** as a crystalline beige solid (103.6 mg, 55% yield). ^{1}H NMR (500 MHz, CD_2Cl_2, 23 °C): δ 8.20 (bd, J = 8.4 Hz, 2H), 7.94–7.89 (m, 4H), 7.65 (dt, J = 7.2, 0.99 Hz, 2H), 7.59–7.50 (m, 6H), 6.80 (q, J = 6.9 Hz, 2H), 6.44 (s, 2H), 1.99 ppm (d, J = 6.9 Hz, 6H). ^{13}C NMR (225 MHz, CD_2Cl_2, 23 °C): δ 171.2, 134.4, 134.2, 131.6, 130.2, 129.3, 127.6, 126.6, 125.5, 125.0, 123.5, 118.5, 57.1, 21.9 ppm. HRMS (ESI): calcd. for $C_{27}H_{24}AuClN_2$ $[M+Na]^+$, most abundant *m/z* = 631.1186; found, 631.1171.

(*R*)-(1-dodecyl-3-(1-phenylethyl)-1,3-dihydro-2*H*-imidazol-2-ylidene)gold(I) bromide 10. Purified via flash column chromatography on silica gel using 8:2 HXN/EtOAc as the eluent (R_f = 0.24) to afford **10** as a light-beige viscous liquid that slowly crystallized (27.7 mg, 90% yield). ^{1}H NMR (600 MHz, CD_2Cl_2, 23 °C): δ 7.41–7.29 (m, 5H), 6.96 (d, J = 2.0 Hz, 1H), 6.92 (d, J = 2.0 Hz, 1H), 6.14 (q, J = 7.1 Hz, 1H), 4.21–4.10 (m, 2H), 1.90–1.79 (m, 5H), 1.39–1.19 (m, 18H), 0.88 ppm (t, J = 7.0 Hz, 3H). ^{13}C NMR (150 MHz, CD_2Cl_2, 23 °C): δ 174.1, 140.3, 129.2, 128.7, 127.0, 121.2, 118.0, 60.2, 51.9, 32.3, 31.4, 30.04, 30.03, 29.9, 29.84, 29.75, 29.5, 26.8, 23.1, 21.0, 14.3 ppm. HRMS (ESI): calcd. for $C_{23}H_{36}AuBrN_2$ $[M+Na]^+$, most abundant *m/z* = 639.1620; found, 639.1625.

(*R*)-(1-octadecyl-3-(1-phenylethyl)-1,3-dihydro-2*H*-imidazol-2-ylidene)gold(I) bromide 11. Purified via flash column chromatography on silica gel using 8:2 HXN/EtOAc as the eluent (R_f = 0.17) to afford a crystalline white solid (30.4 mg, 87% yield). ^{1}H NMR (600 MHz, CD_2Cl_2, 23 °C): δ 7.41–7.31 (m, 5H), 6.96 (d, J = 2.0 Hz, 1H), 6.92 (d, J = 2.0 Hz, 1H), 6.14 (q, J = 7.1 Hz, 1H), 4.21–4.11 (m, 2H), 1.90–1.79 (m, 5H), 1.40–1.19 (m, 30H), 0.88 ppm (t, J = 7.0 Hz, 3H). ^{13}C NMR (150 MHz, CD_2Cl_2, 23 °C): δ 174.1, 140.3, 129.2, 128.7, 127.0, 121.2, 118.0, 60.2, 51.9, 32.3, 31.4, 30.12, 30.09, 30.07, 30.05, 30.0, 29.9, 29.8, 29.5, 26.8, 23.1, 21.0, 14.3 ppm. HRMS (ESI): calcd. for $C_{29}H_{48}AuBrN_2$ $[M+Na]^+$, most abundant *m/z* = 723.2559; found, 723.2563.

Spectroscopy Data.

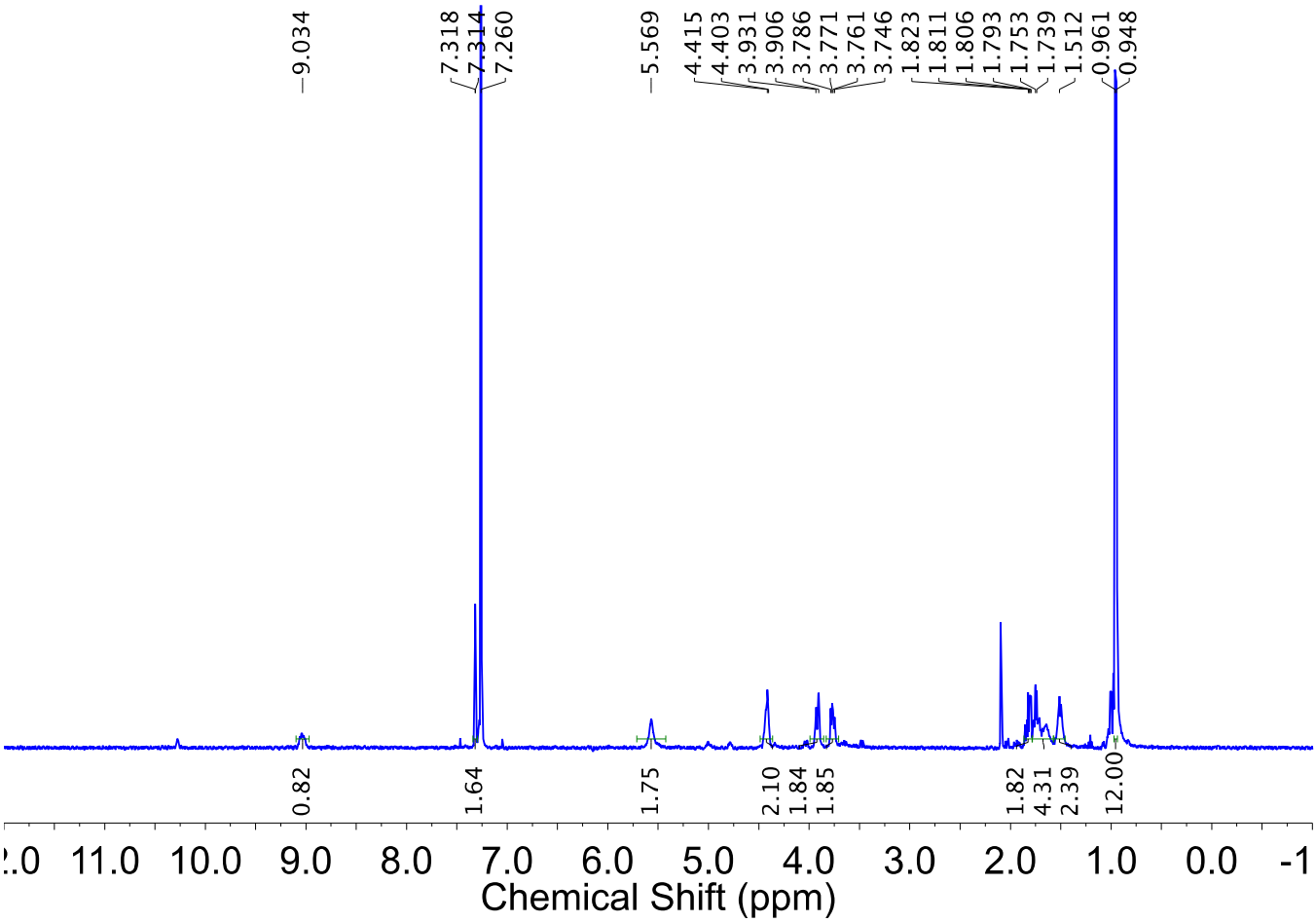

Figure S9. ^{1}H NMR (500 MHz, $CDCl_3$, 23 °C) spectrum of partially purified 1,3-bis((S)-1-hydroxy-4-methylpentan-2-yl)-1H-imidazol-3-ium chloride **IS6.**[12] Resonances attributable to **IS6** are labeled and integrated.

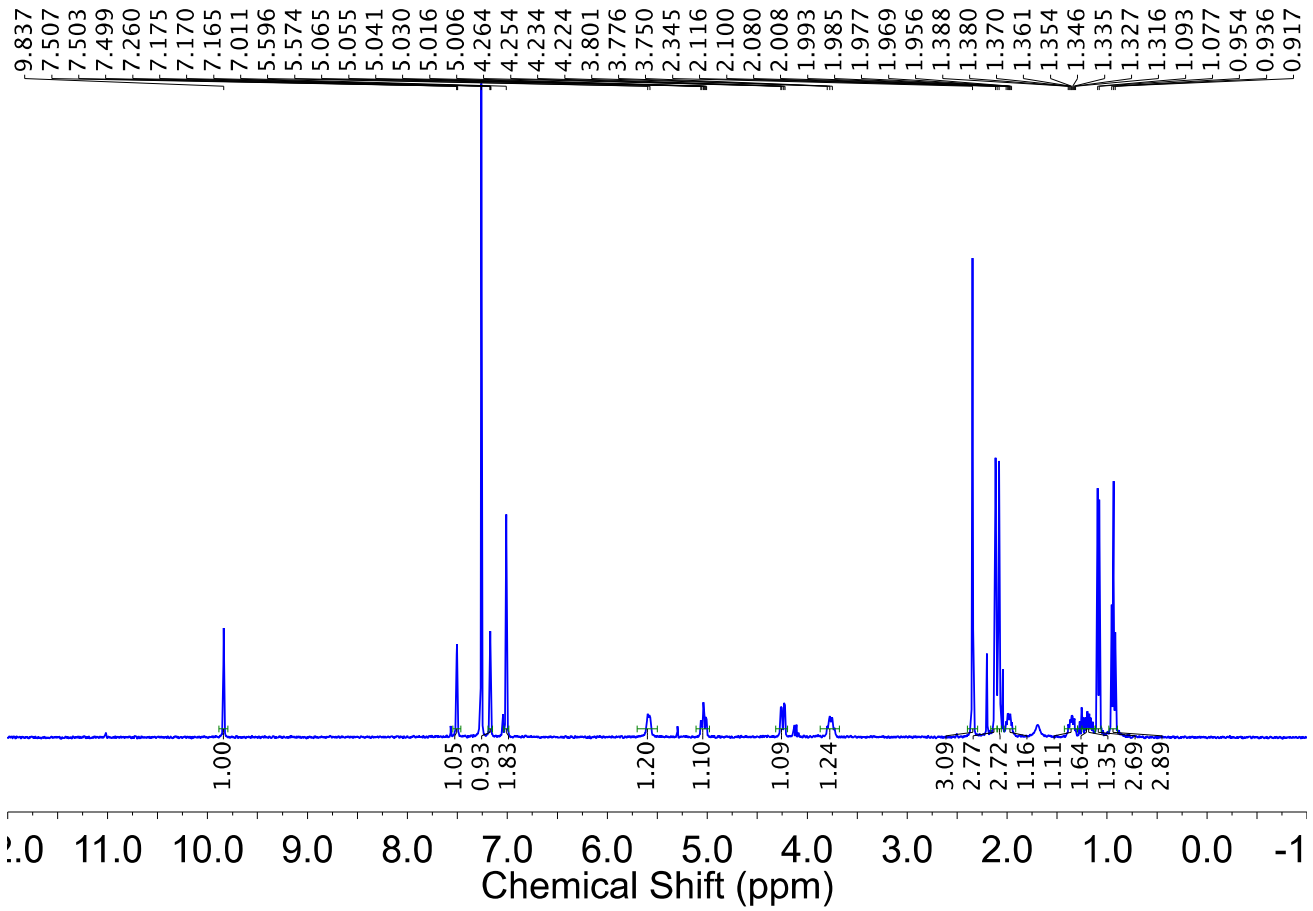

Figure S10. ^{1}H NMR (500 MHz, $CDCl_3$, 23 °C) spectrum of partially purified 3-((2S,3S)-1-hydroxy-3-methylpentan-2-yl)-1-mesityl-1H-imidazol-3-ium chloride **IS2**. Resonances attributable to **IS2** are labeled and integrated.

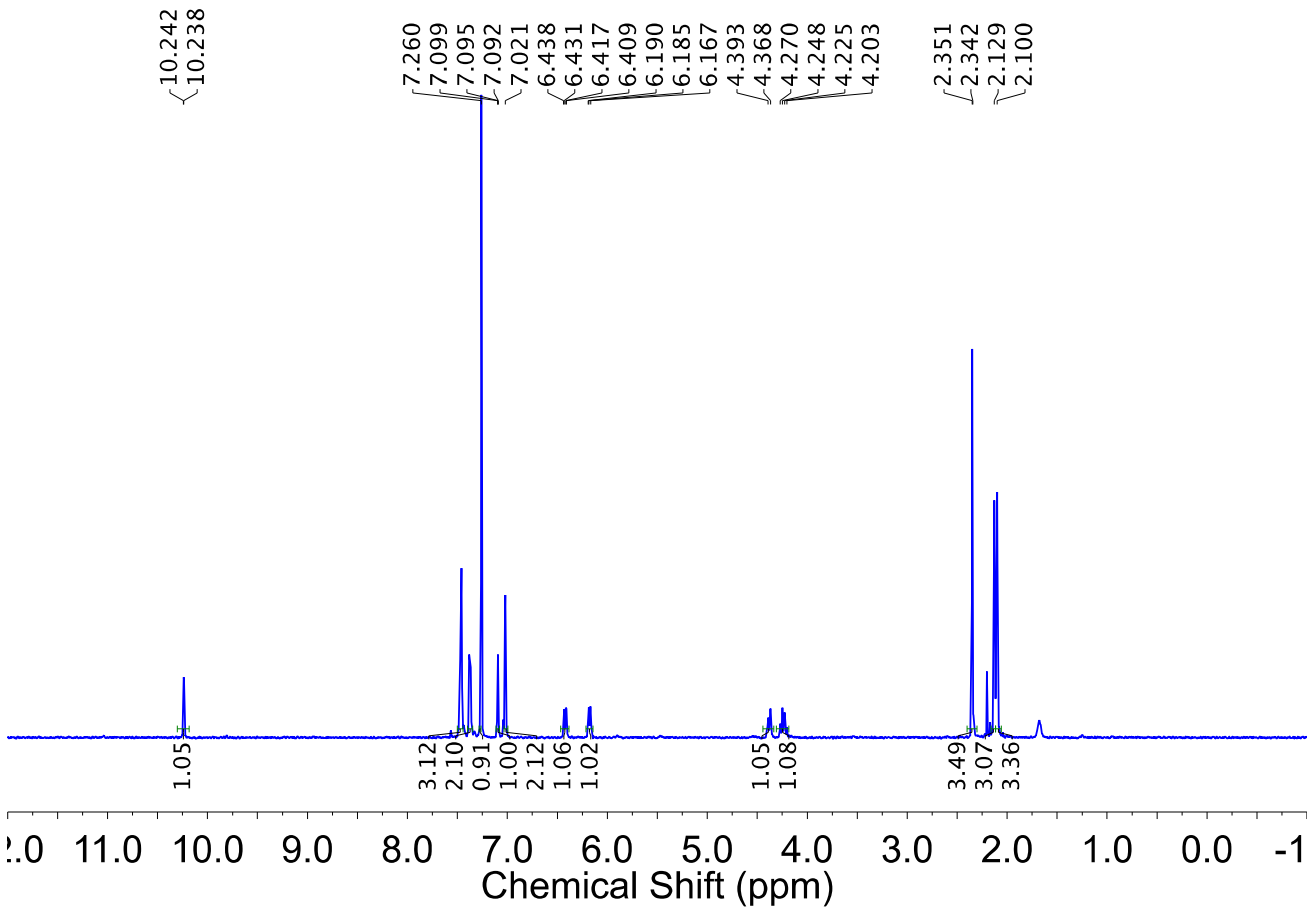

Figure S11. ^{1}H NMR (500 MHz, $CDCl_3$, 23 °C) spectrum of (S)-3-(2-hydroxy-1-phenylethyl)-1-mesityl-1H-imidazol-3-ium chloride **IS3**.

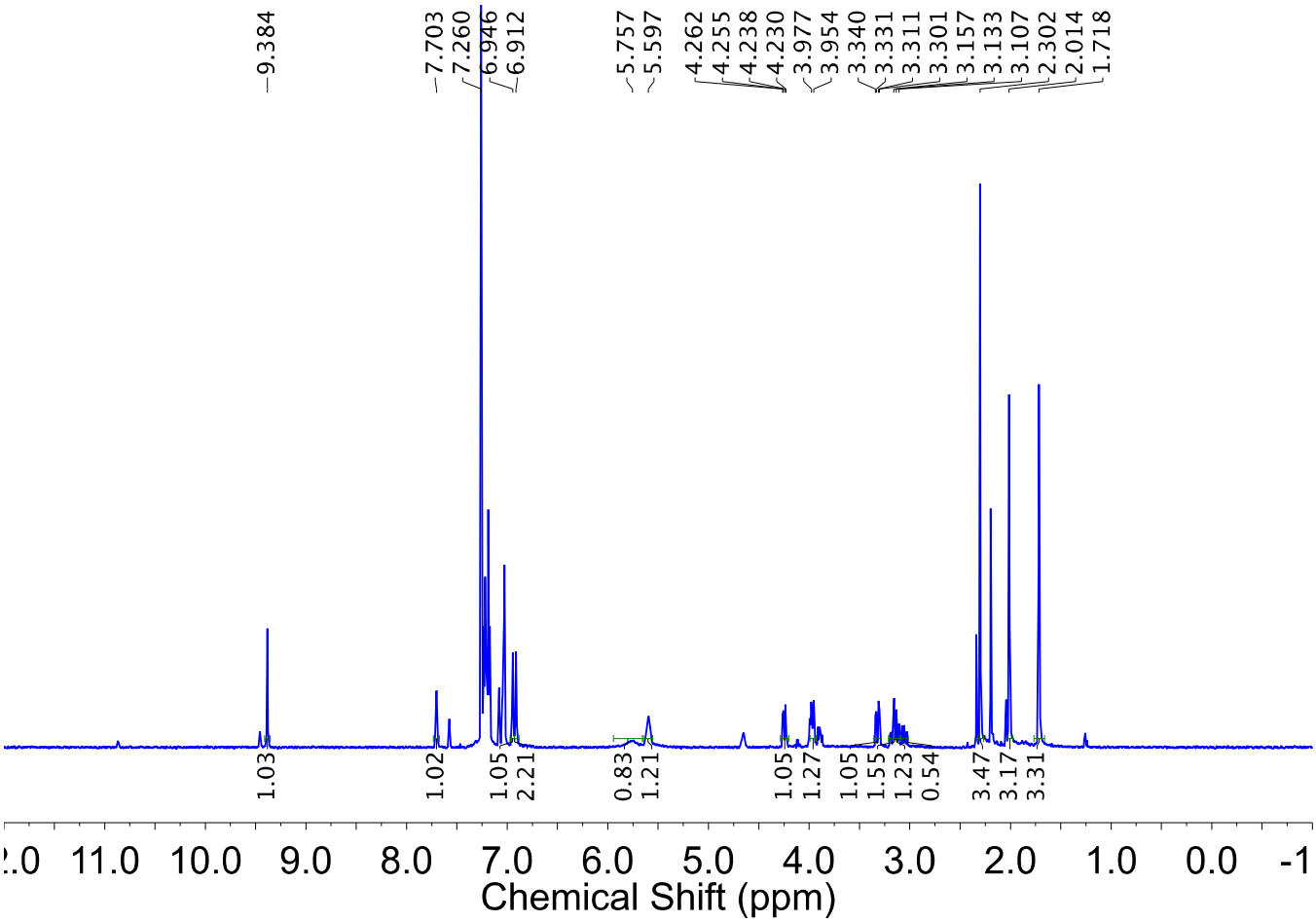

Figure S12. ^{1}H NMR (500 MHz, $CDCl_3$, 23 °C) spectrum of partially purified (S)-3-(1-hydroxy-3-phenylpropan-2-yl)-1-mesityl-1H-imidazol-3-ium chloride **IS4**. Resonances attributable to **IS4** are labeled and integrated were the assignment is unambiguous.

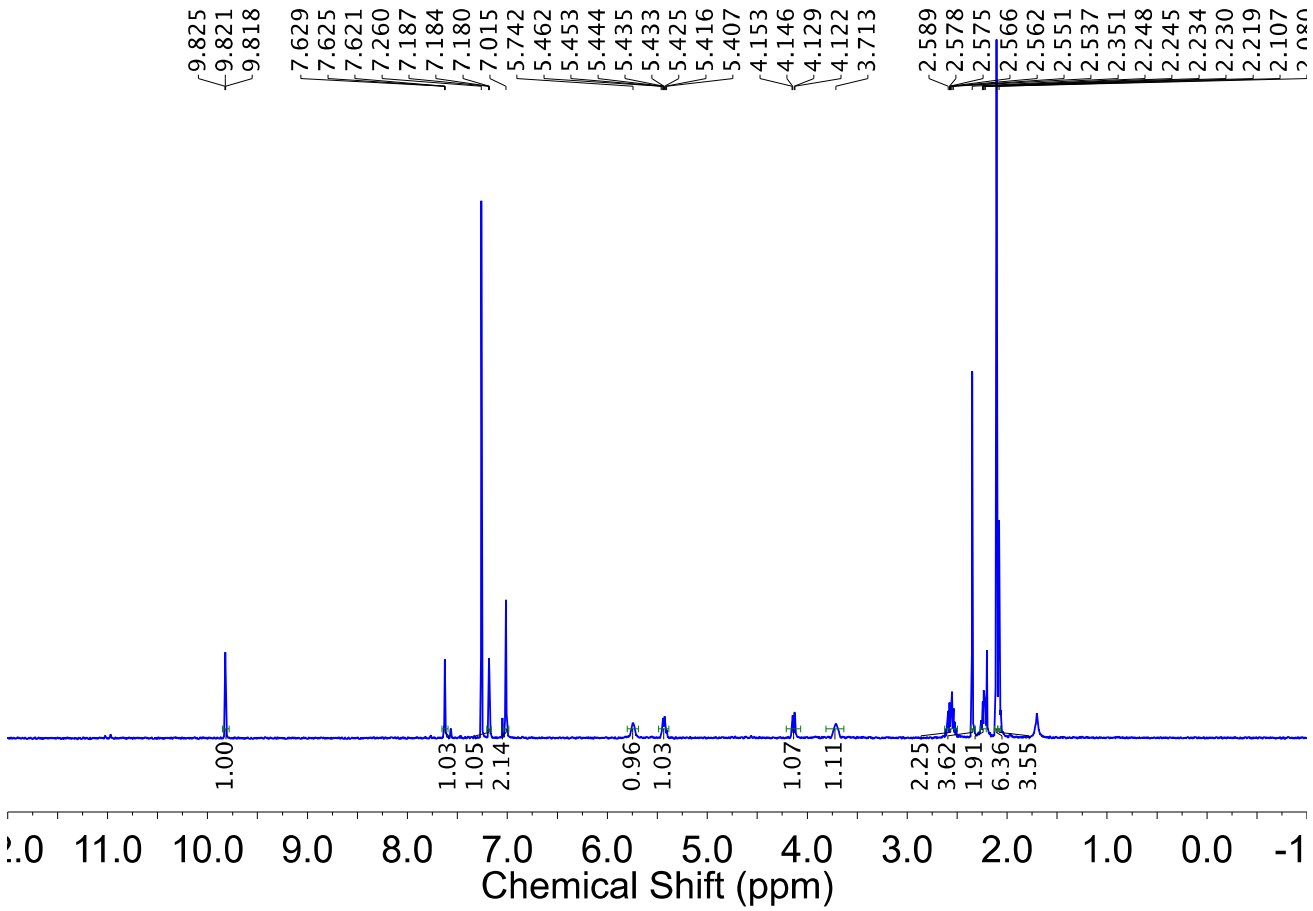

Figure S13. ^{1}H NMR (500 MHz, $CDCl_3$, 23 °C) spectrum of partially purified (S)-3-(1-hydroxy-4-(methylthio)butan-2-yl)-1-mesityl-1H-imidazol-3-ium chloride **IS5**. Resonances attributable to **IS5** are labeled and integrated.

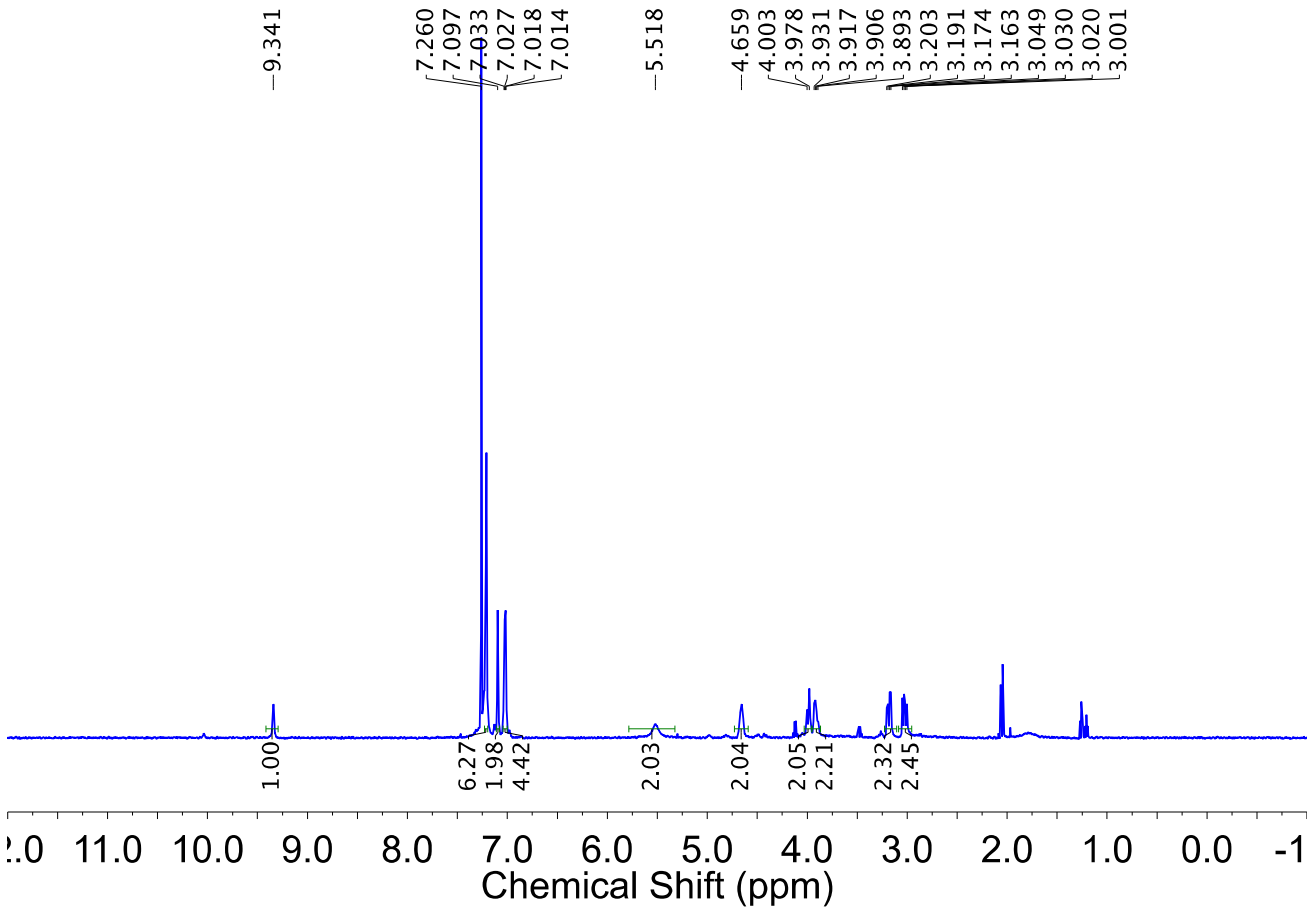

Figure S14. ^{1}H NMR (500 MHz, $CDCl_3$, 23 °C) spectrum of partially purified 1,3-bis((S)-1-hydroxy-3-phenylpropan-2-yl)-1H-imidazol-3-ium chloride **IS7**. Resonances attributable to **IS7** are labeled and integrated.

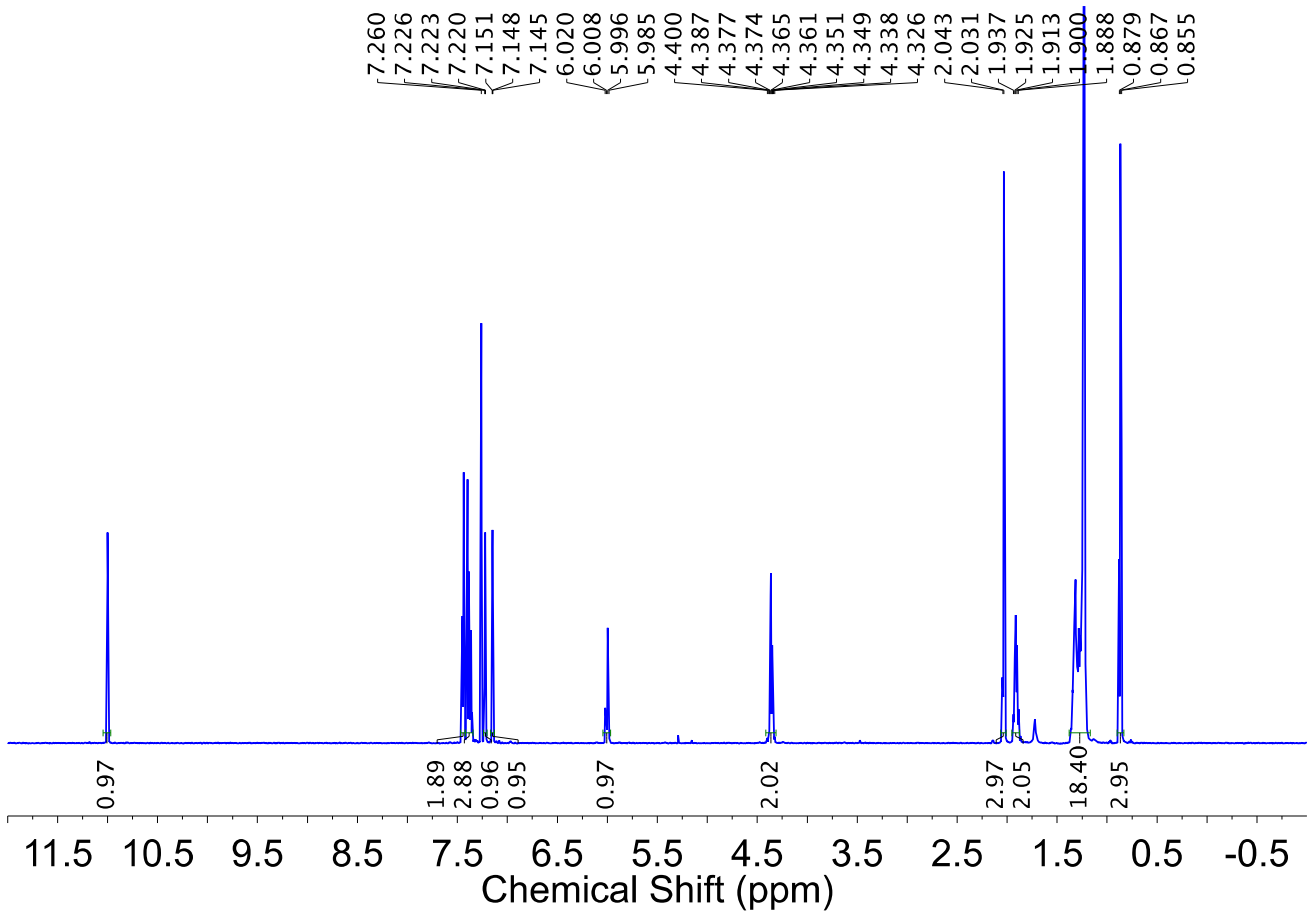

Figure S15. ^{1}H NMR (600 MHz, $CDCl_3$, 23 °C) spectrum of (R)-3-dodecyl-1-(1-phenylethyl)-1H-imidazol-3-ium chloride **IS10**.

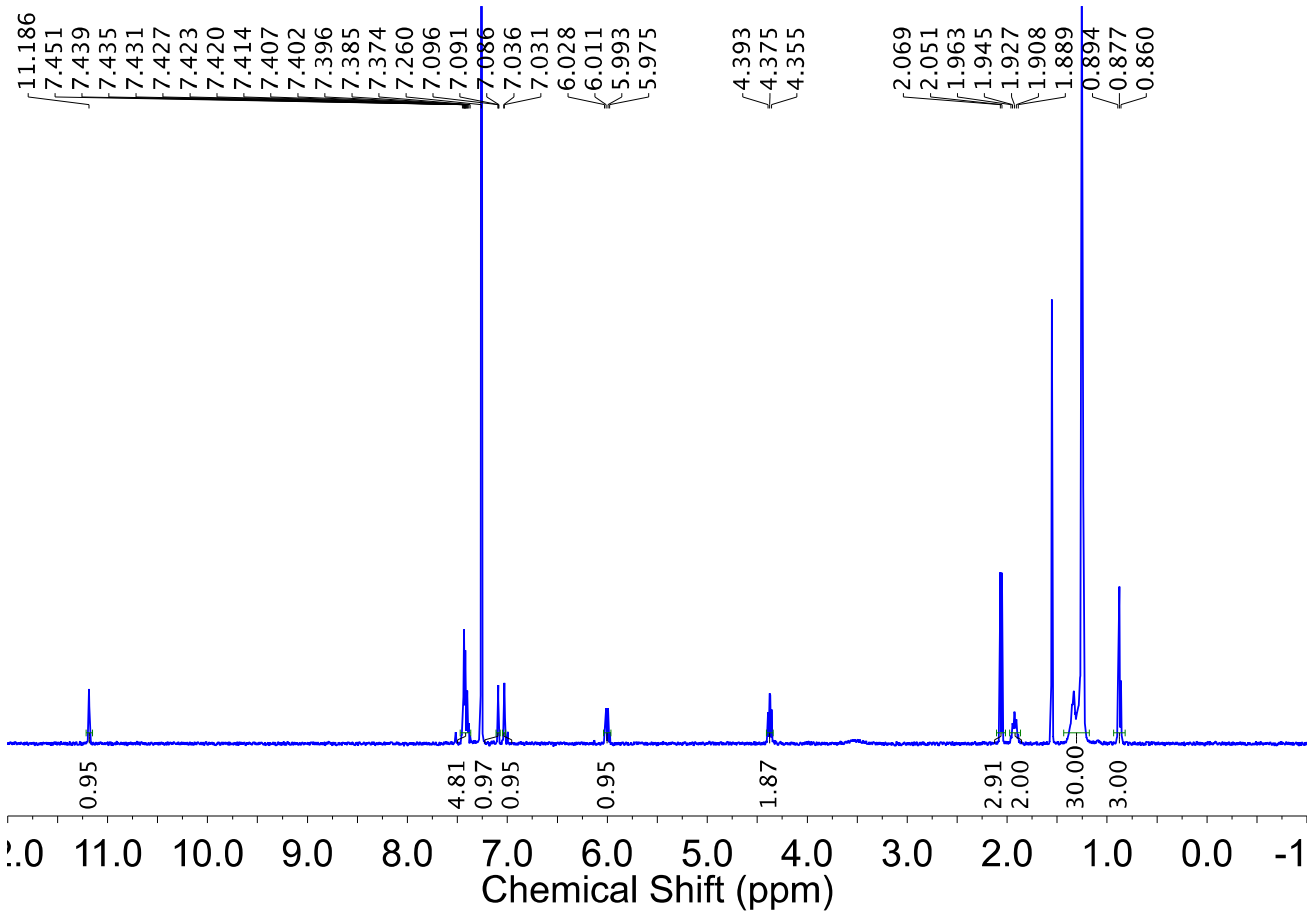

Figure S16. ^{1}H NMR (400 MHz, $CDCl_3$, 23 °C) spectrum of (R)-3-octadecyl-1-(1-phenylethyl)-1H-imidazol-3-ium chloride **IS11**.

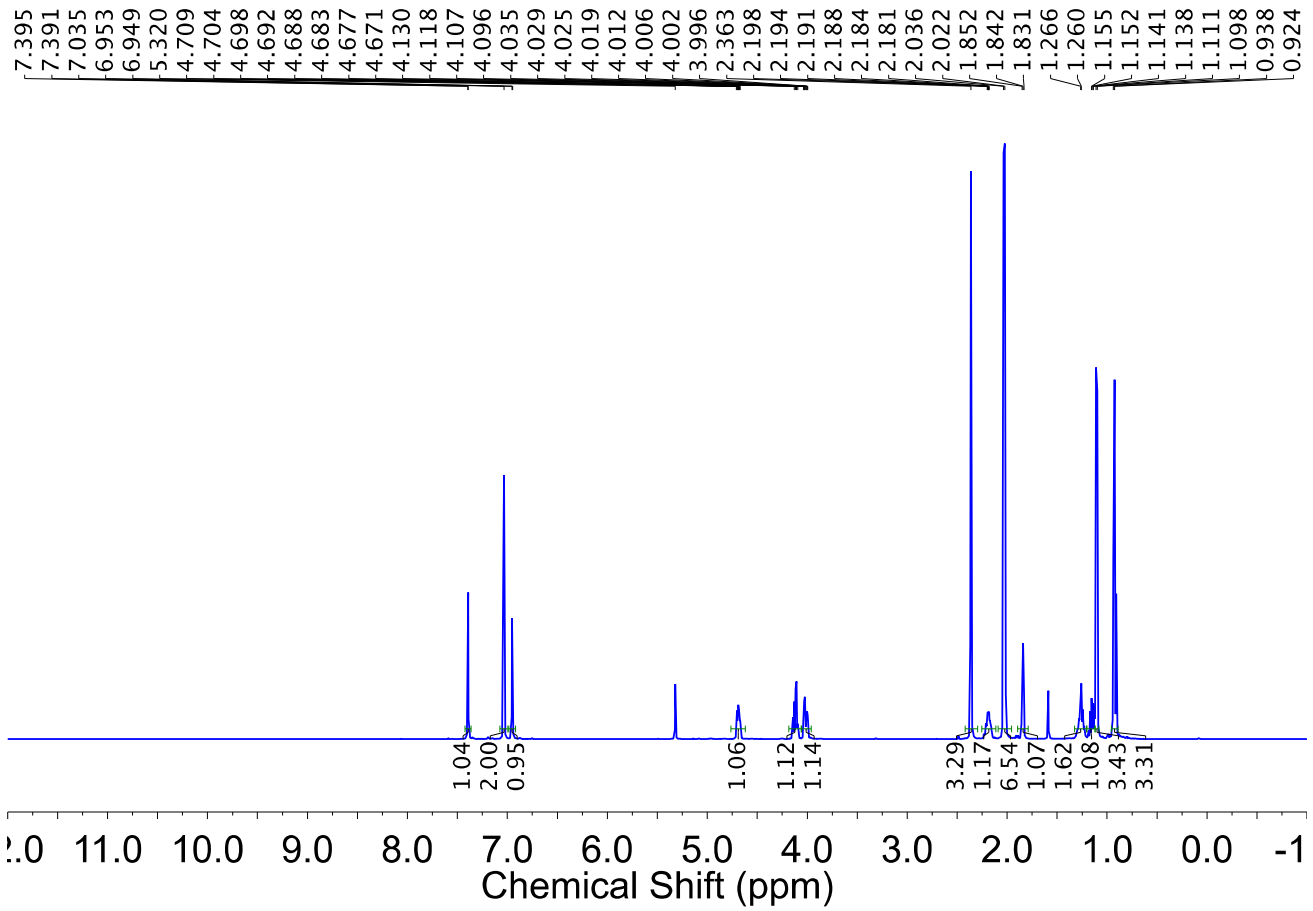

Figure S17. ^{1}H NMR (500 MHz, CD_2Cl_2, 23 °C) spectrum of (1-((2S,3S)-1-hydroxy-3-methylpentan-2-yl)-3-mesityl-1,3-dihydro-2H-imidazol-2-ylidene)gold(I) chloride **2**.

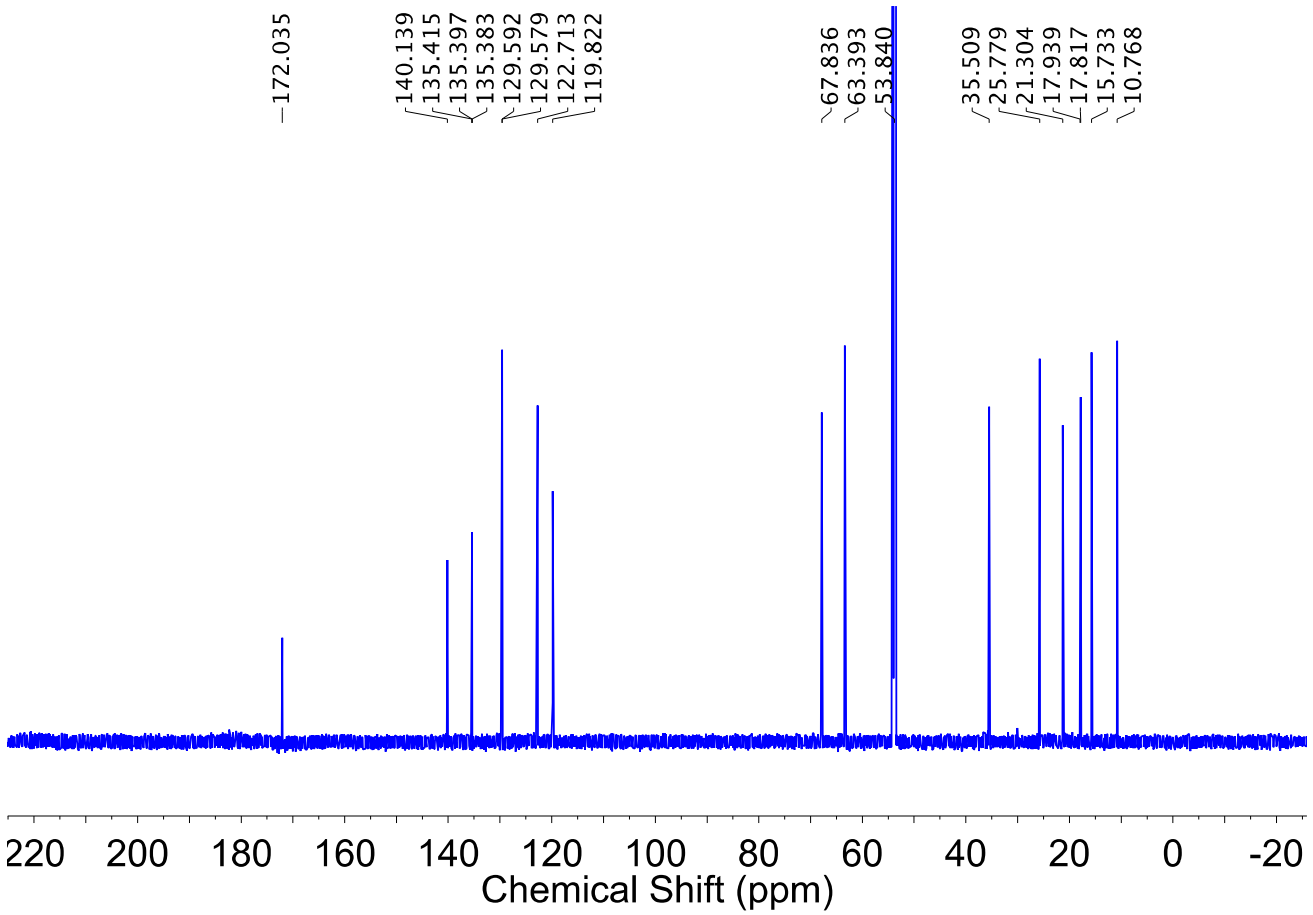

Figure S18. ^{13}C NMR (225 MHz, CD_2Cl_2, 23 °C) spectrum of (1-((2S,3S)-1-hydroxy-3-methylpentan-2-yl)-3-mesityl-1,3-dihydro-2H-imidazol-2-ylidene)gold(I) chloride **2**.

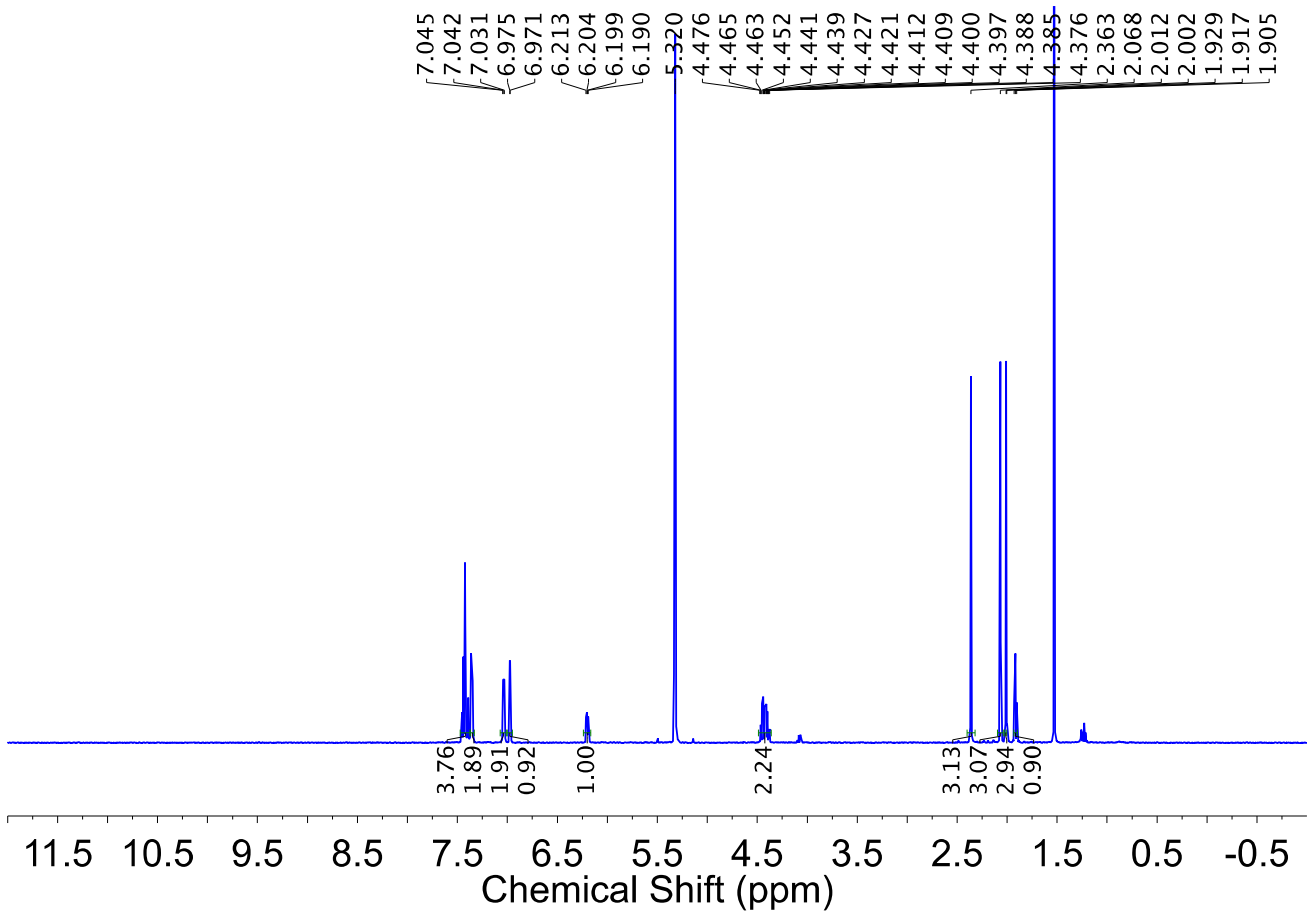

Figure S19. ^{1}H NMR (500 MHz, CD_2Cl_2, 23 °C) spectrum of (S)-(1-(2-hydroxy-1-phenylethyl)-3-mesityl-1,3-dihydro-2H-imidazol-2-ylidene)gold(I) chloride **3**.

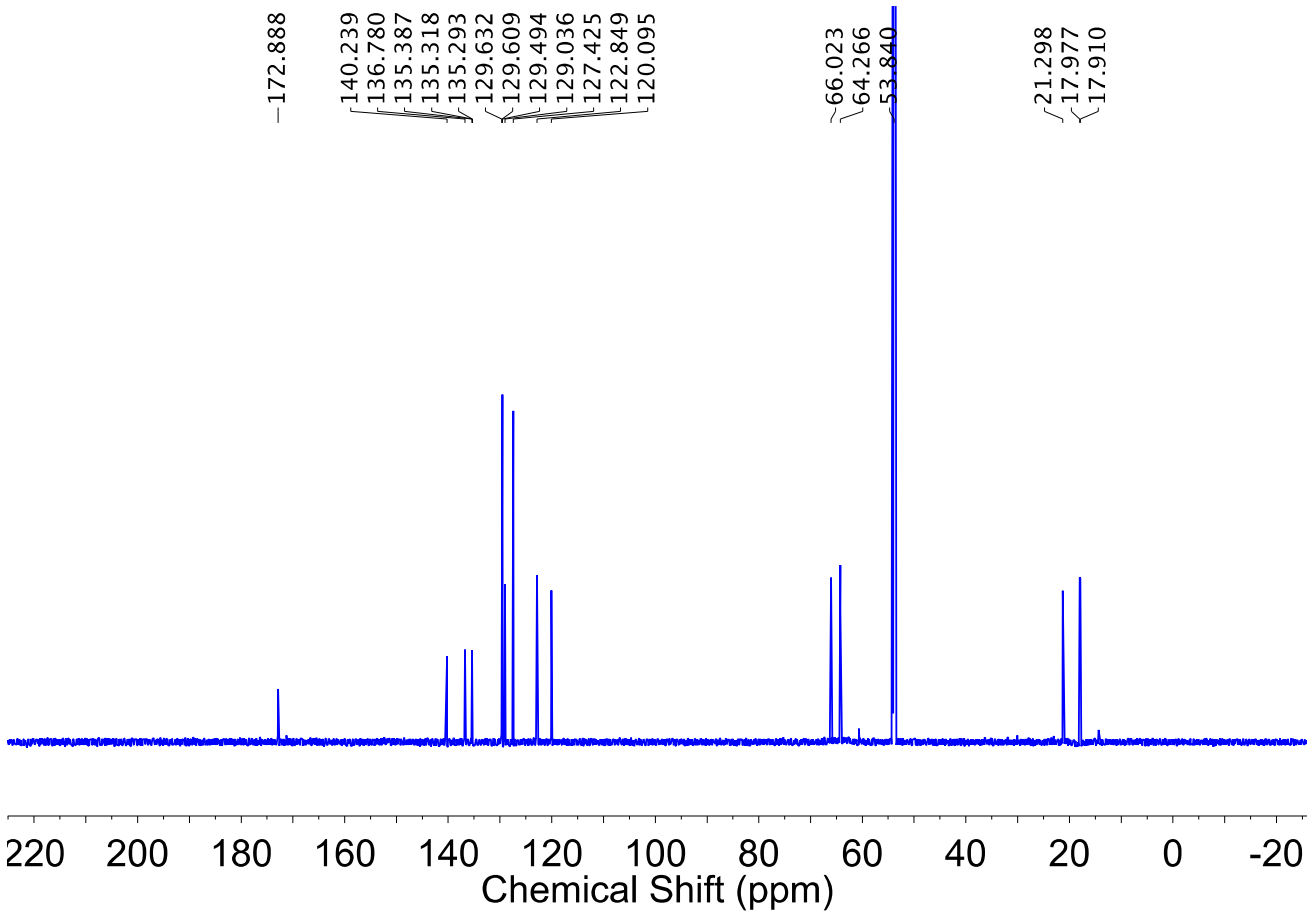

Figure S20. ^{13}C NMR (225 MHz, CD_2Cl_2, 23 °C) spectrum of (S)-(1-(2-hydroxy-1-phenylethyl)-3-mesityl-1,3-dihydro-2H-imidazol-2-ylidene)gold(I) chloride **3**.

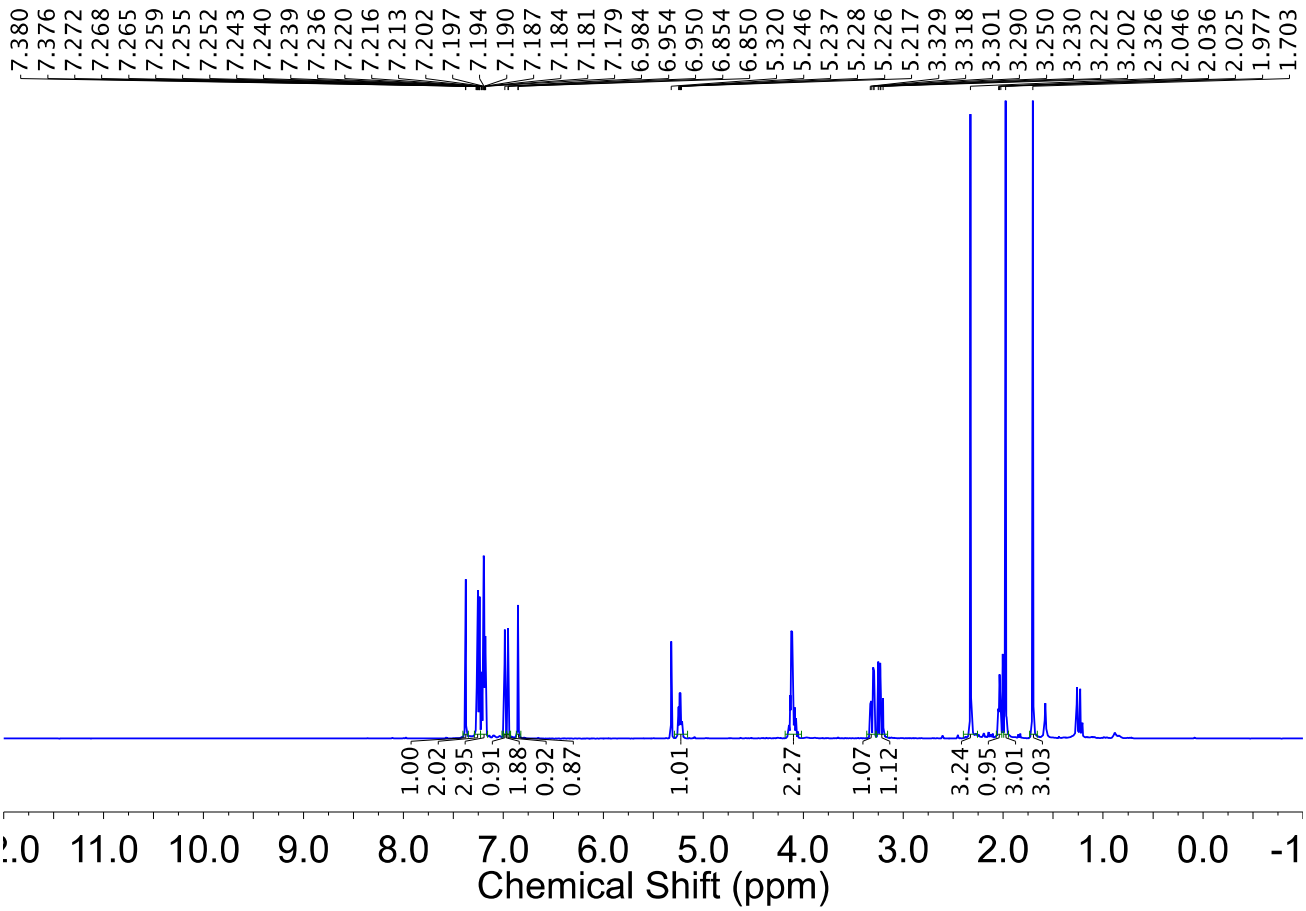

Figure S21. ^{1}H NMR (500 MHz, CD_2Cl_2, 23 °C) spectrum of (S)-(1-(1-hydroxy-3-phenylpropan-2-yl)-3-mesityl-1,3-dihydro-2H-imidazol-2-ylidene)gold(I) chloride **4**.

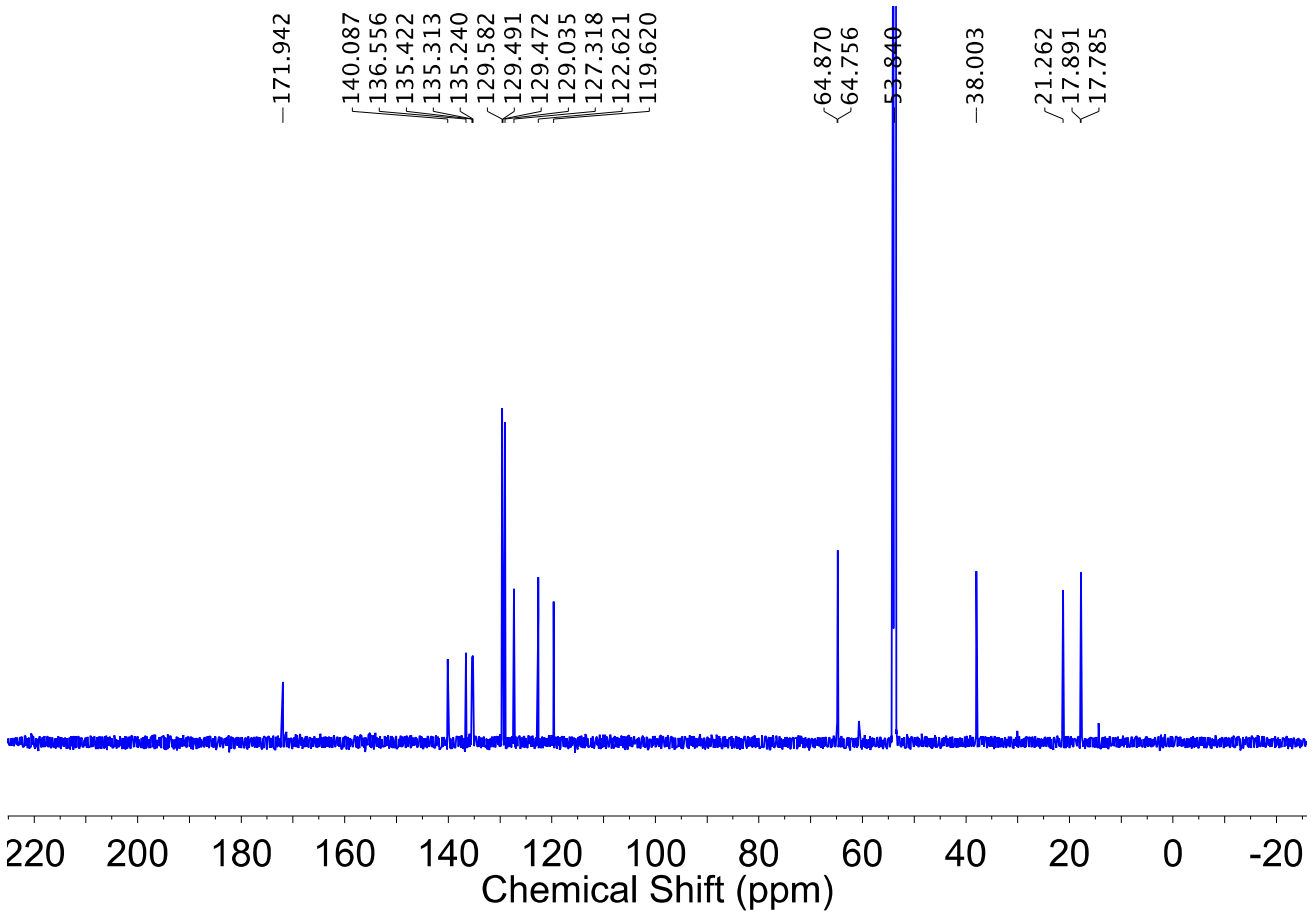

Figure S22. ^{13}C NMR (225 MHz, CD_2Cl_2, 23 °C) spectrum of (S)-(1-(1-hydroxy-3-phenylpropan-2-yl)-3-mesityl-1,3-dihydro-2H-imidazol-2-ylidene)gold(I) chloride **4**.

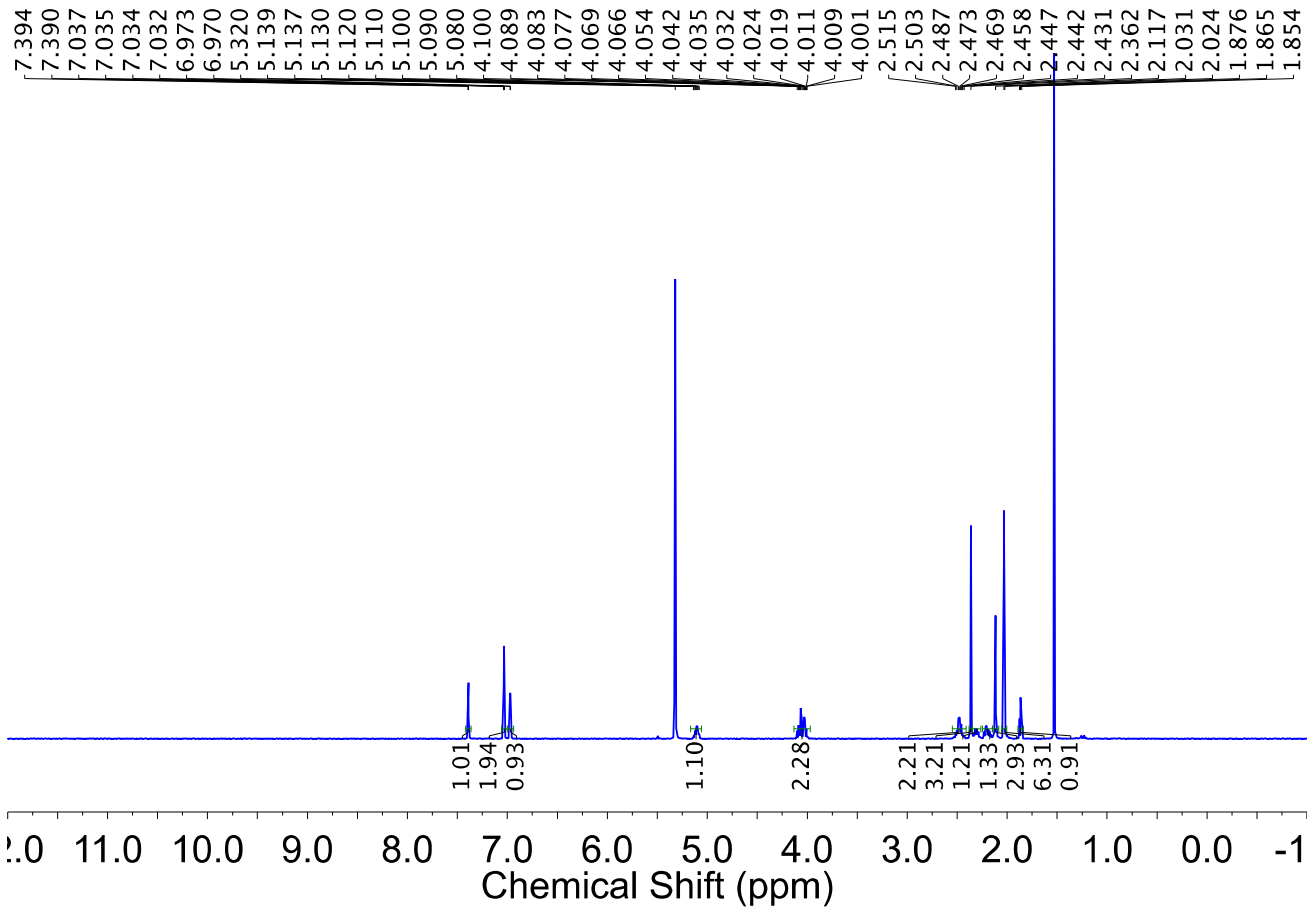

Figure S23. ^{1}H NMR (500 MHz, CD_2Cl_2, 23 °C) spectrum of (S)-(1-(1-hydroxy-4-(methylthio)butan-2-yl)-3-mesityl-1,3-dihydro-2H-imidazol-2-ylidene)gold(I) chloride **5**.

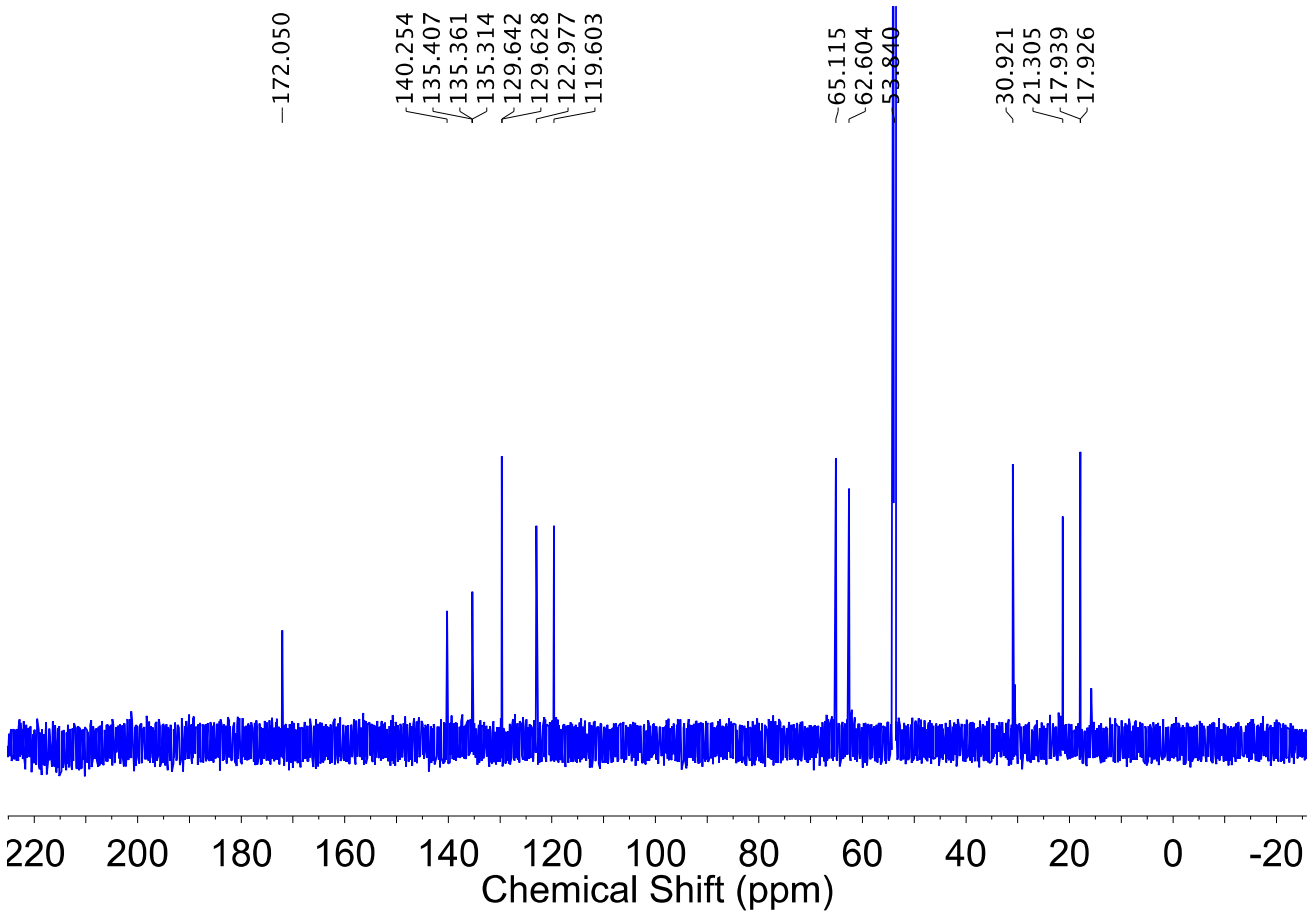

Figure S24. ^{13}C NMR (225 MHz, CD_2Cl_2, 23 °C) spectrum of (S)-(1-(1-hydroxy-4-(methylthio)butan-2-yl)-3-mesityl-1,3-dihydro-2H-imidazol-2-ylidene)gold(I) chloride **5**.

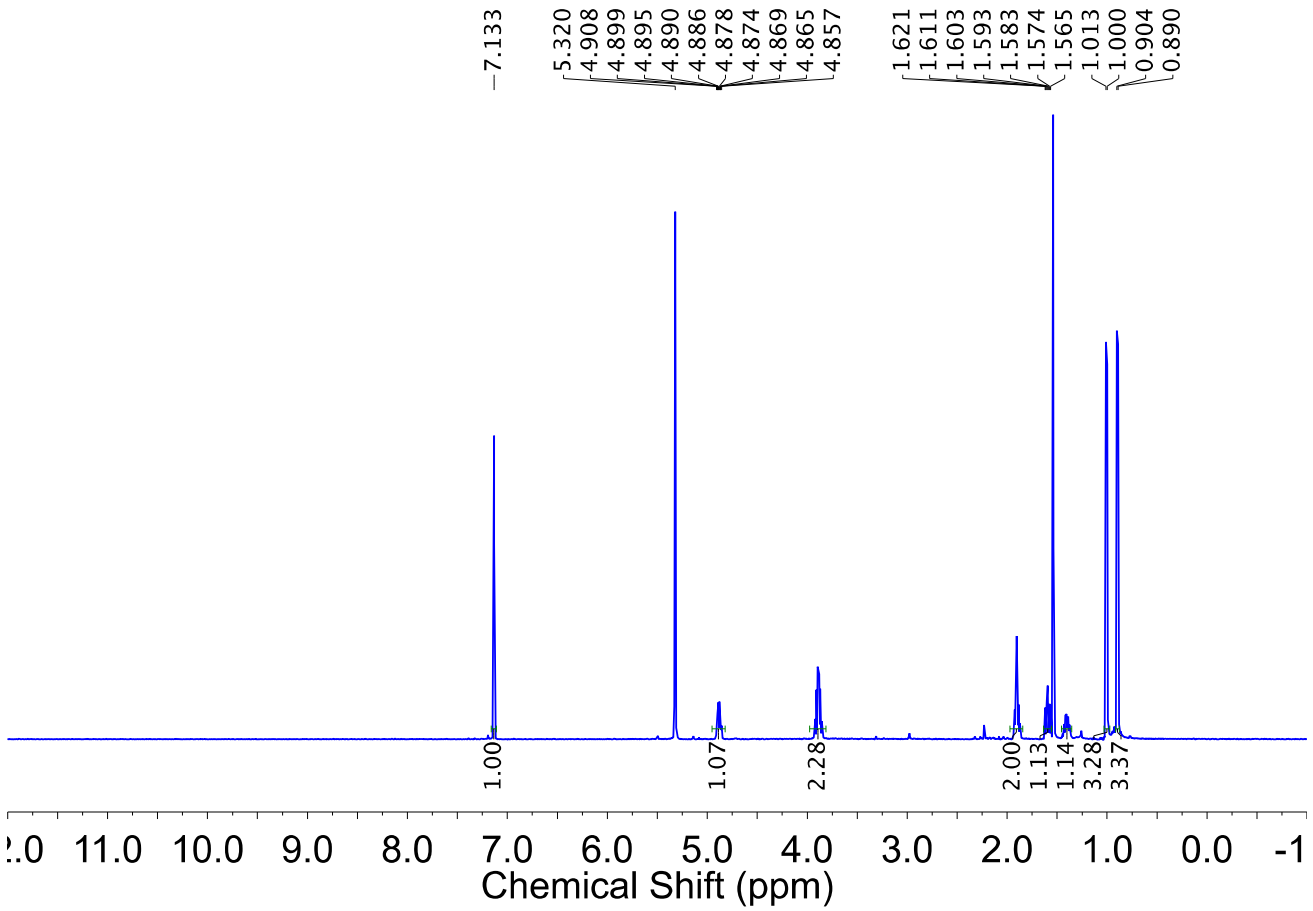

Figure S25. ^{1}H NMR (500 MHz, CD_2Cl_2, 23 °C) spectrum of (1,3-bis((S)-1-hydroxy-4-methylpentan-2-yl)-1,3-dihydro-2H-imidazol-2-ylidene)gold(I) chloride **6**.

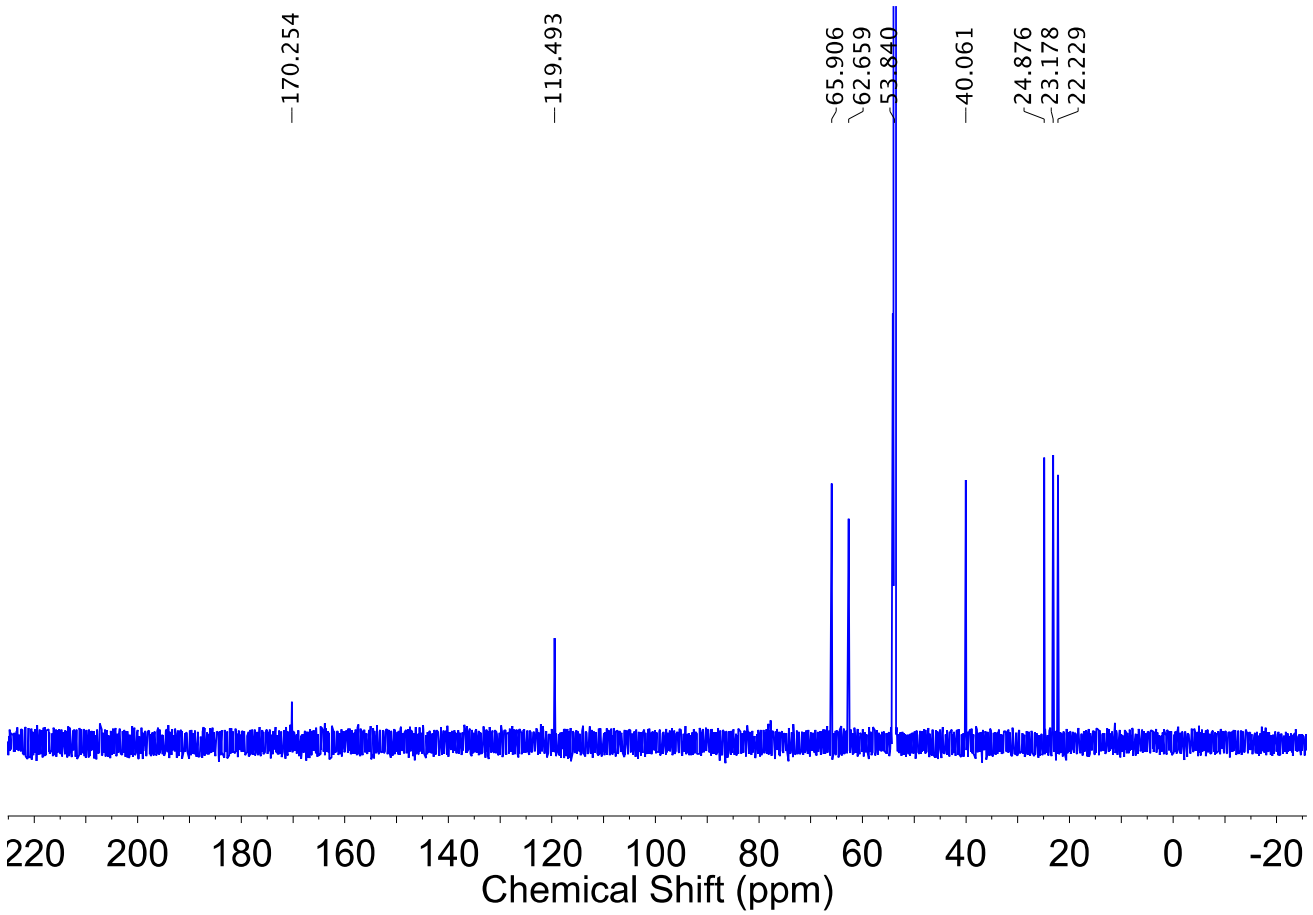

Figure S26. ^{13}C NMR (225 MHz, CD_2Cl_2, 23 °C) spectrum of (1,3-bis((S)-1-hydroxy-4-methylpentan-2-yl)-1,3-dihydro-2H-imidazol-2-ylidene)gold(I) chloride **6**.

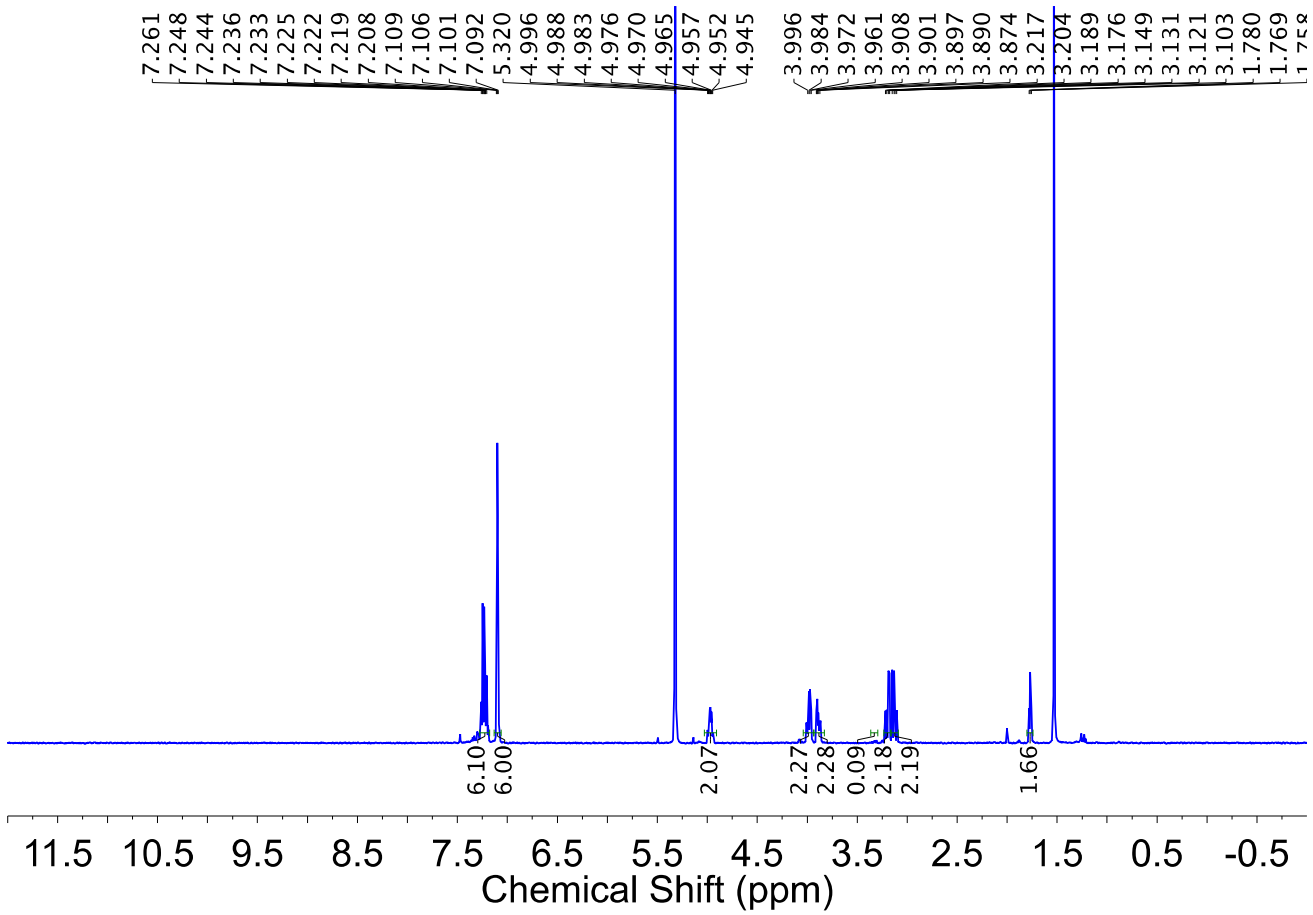

Figure S27. ^{1}H NMR (500 MHz, CD_2Cl_2, 23 °C) spectrum of (1,3-bis((S)-1-hydroxy-3-phenylpropan-2-yl)-1,3-dihydro-2H-imidazol-2-ylidene)gold(I) chloride **7**.

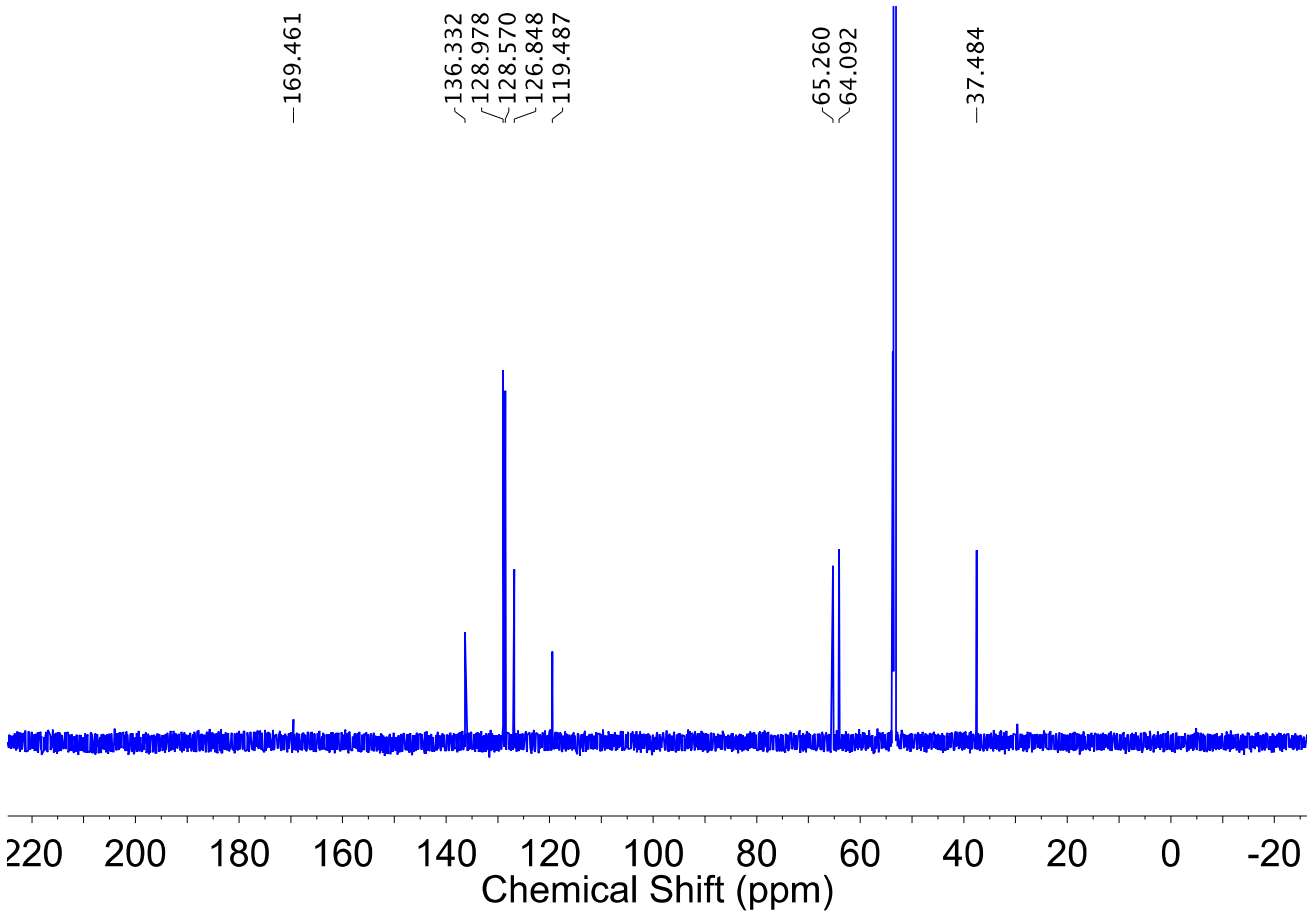

Figure S28. ^{13}C NMR (225 MHz, CD_2Cl_2, 23 °C) spectrum of (1,3-bis((S)-1-hydroxy-3-phenylpropan-2-yl)-1,3-dihydro-2H-imidazol-2-ylidene)gold(I) chloride **7**.

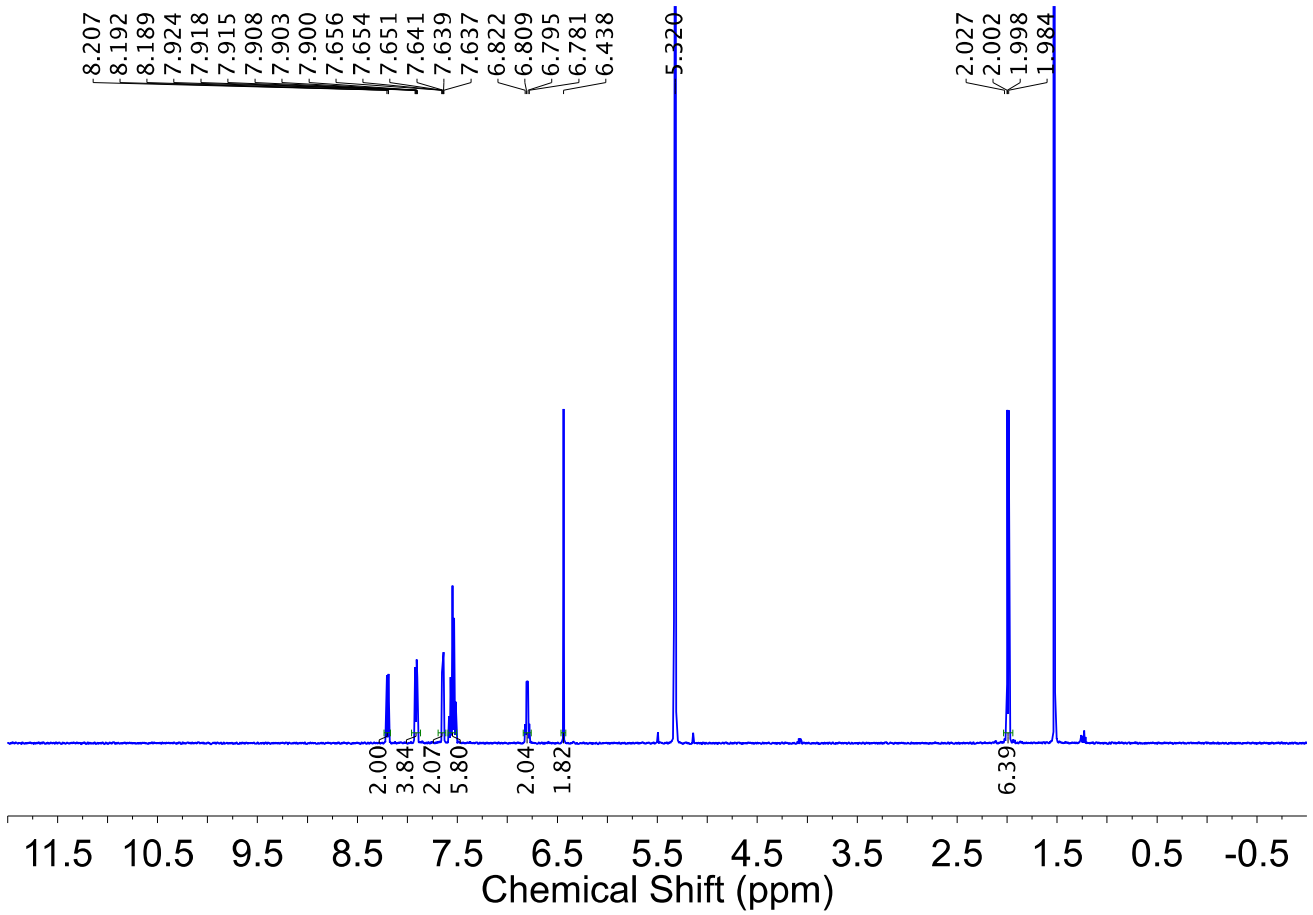

Figure S29. ^{1}H NMR (500 MHz, CD_2Cl_2, 23 °C) spectrum of (1,3-bis((R)-1-(naphthalen-1-yl)ethyl)-1,3-dihydro-2H-imidazol-2-ylidene)gold(I) chloride **8**.

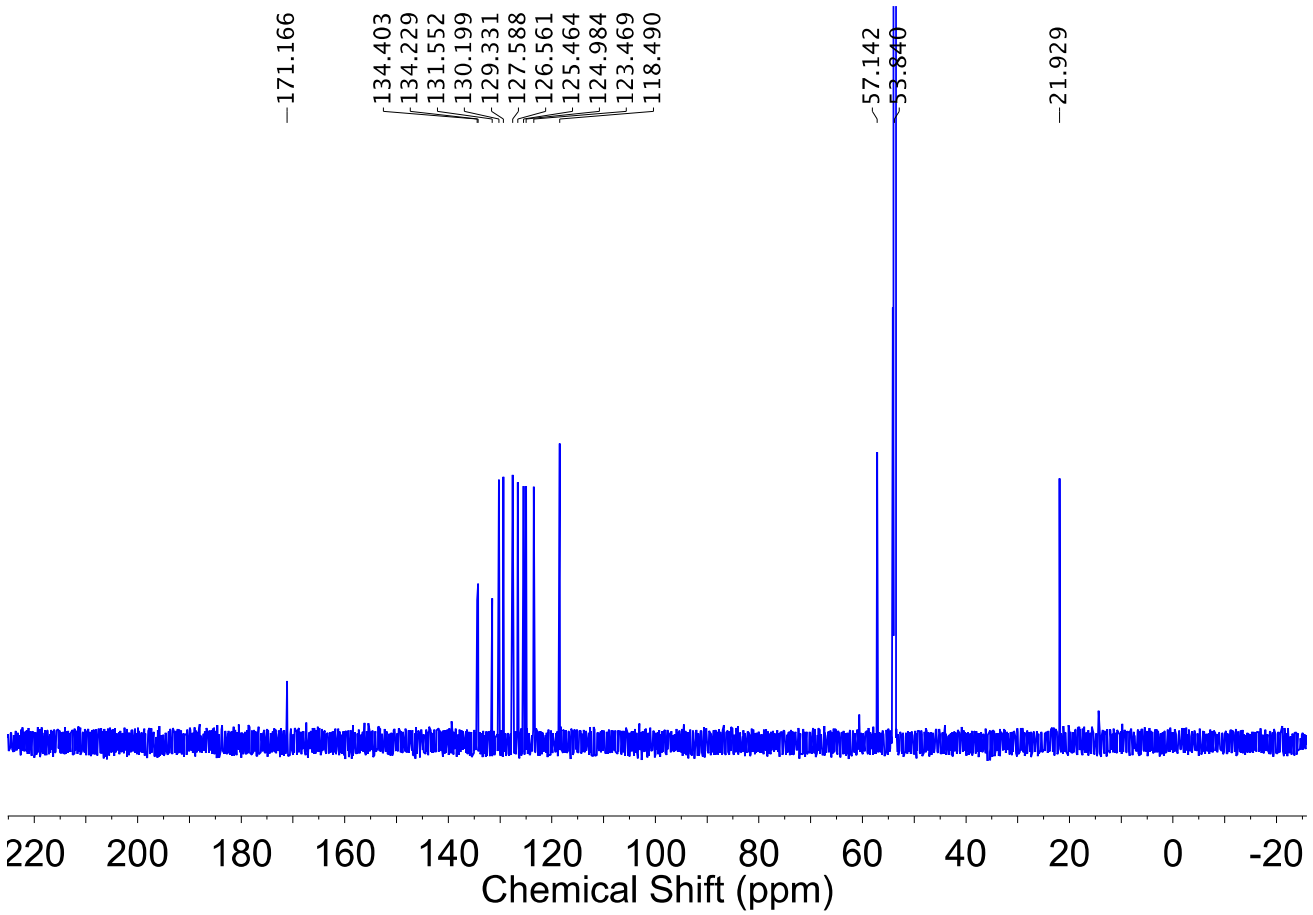

Figure S30. ^{13}C NMR (225 MHz, CD_2Cl_2, 23 °C) spectrum of (1,3-bis((R)-1-(naphthalen-1-yl)ethyl)-1,3-dihydro-2H-imidazol-2-ylidene)gold(I) chloride **8**.

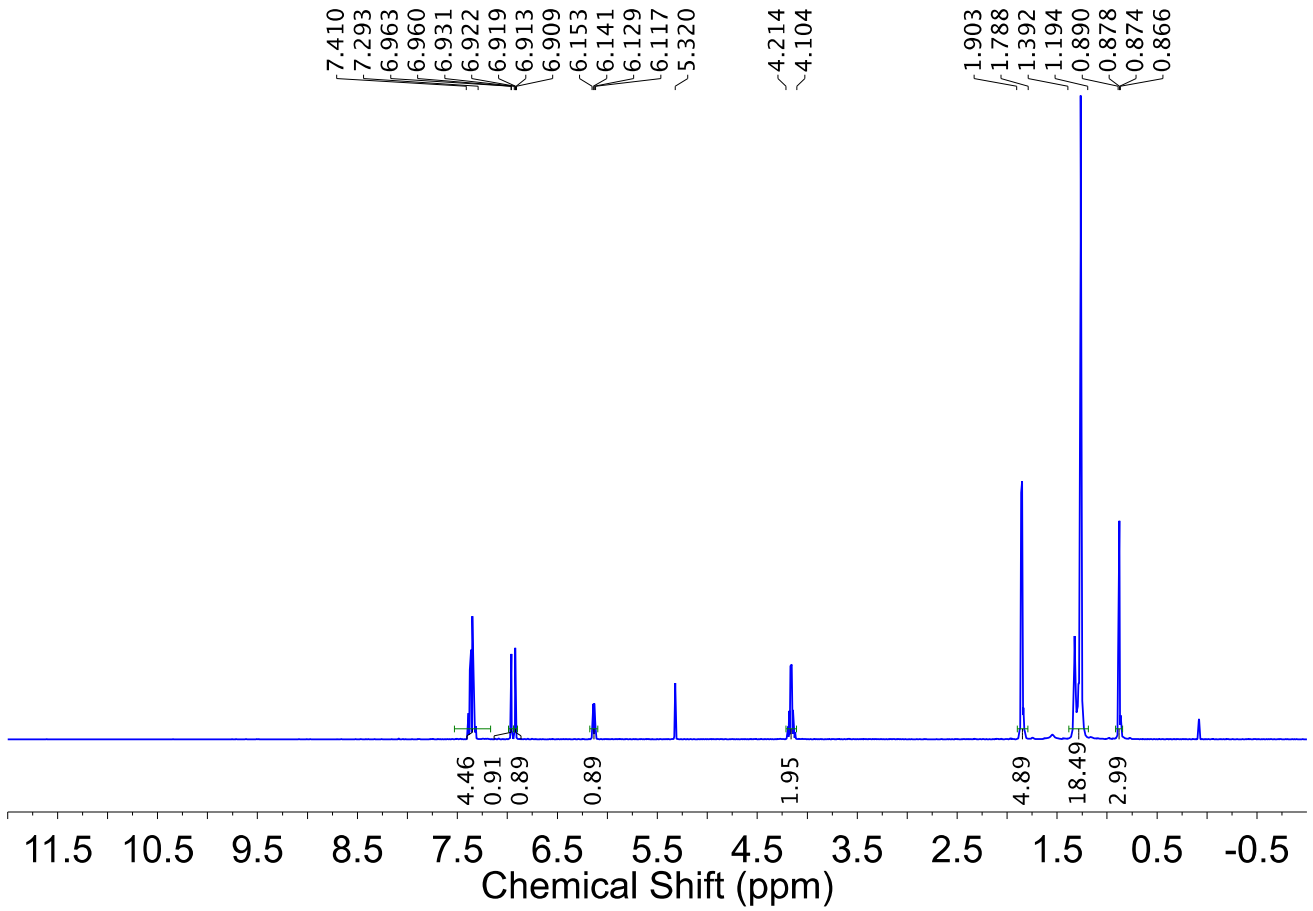

Figure S31. ^{1}H NMR (600 MHz, CD_2Cl_2, 23 °C) spectrum of (R)-(1-dodecyl-3-(1-phenylethyl)-1,3-dihydro-2H-imidazol-2-ylidene)gold(I) bromide **10**.

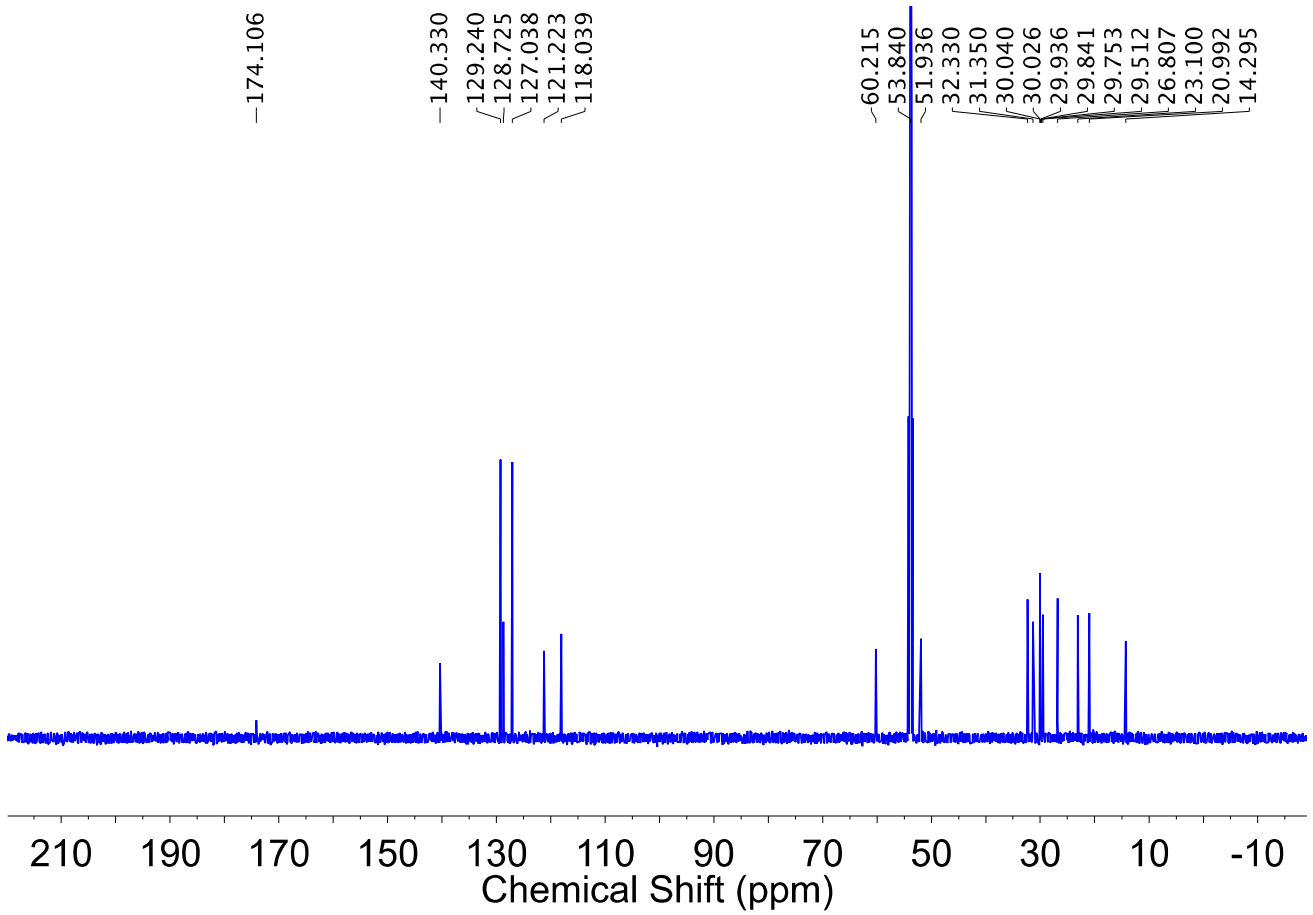

Figure S32. ^{13}C NMR (150 MHz, CD_2Cl_2, 23 °C) spectrum of (R)-(1-dodecyl-3-(1-phenylethyl)-1,3-dihydro-2H-imidazol-2-ylidene)gold(I) bromide **10**.

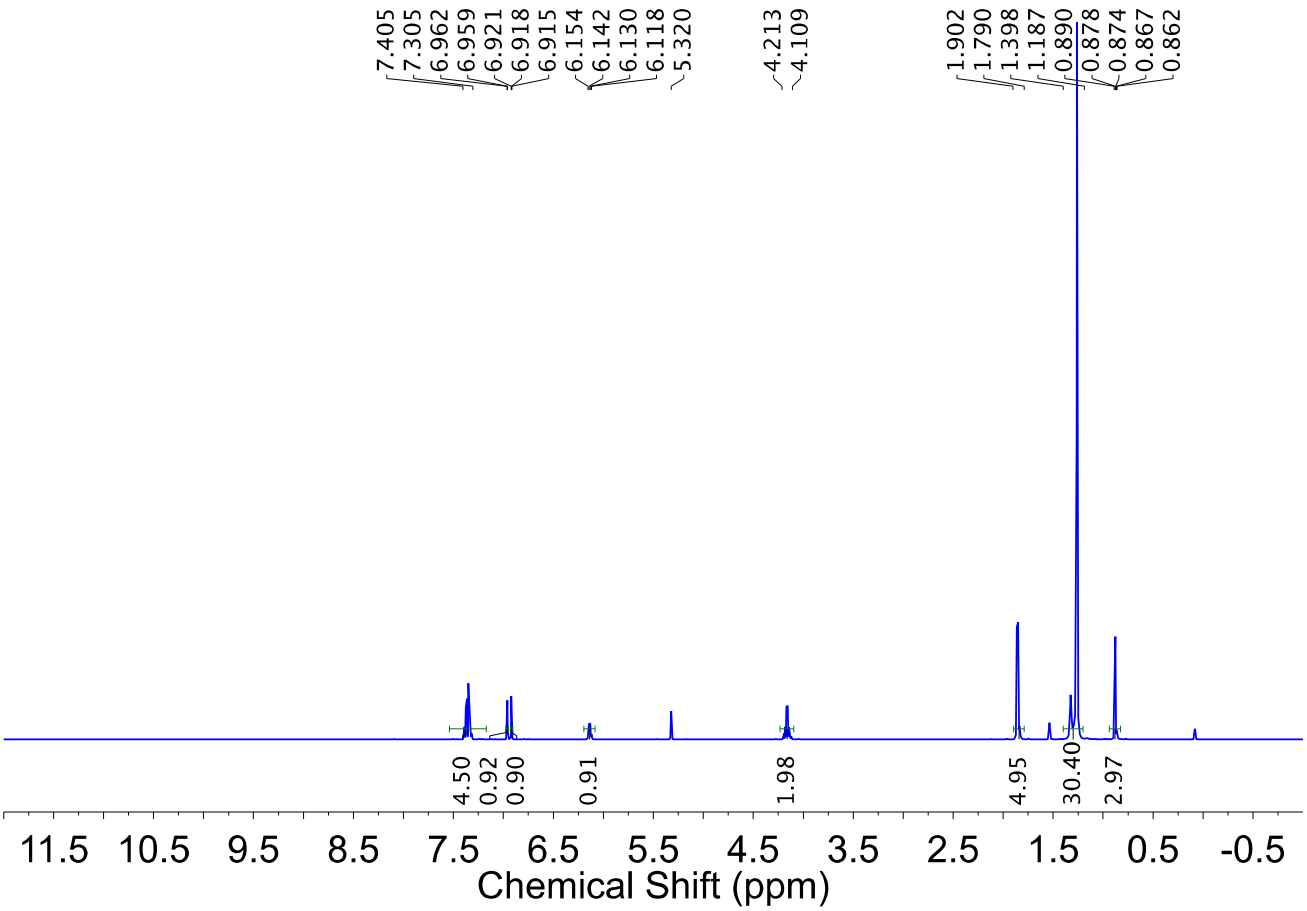

Figure S33. ^{1}H NMR (600 MHz, CD_2Cl_2, 23 °C) spectrum of (R)-(1-octadecyl-3-(1-phenylethyl)-1,3-dihydro-2H-imidazol-2-ylidene)gold(I) bromide **11**.

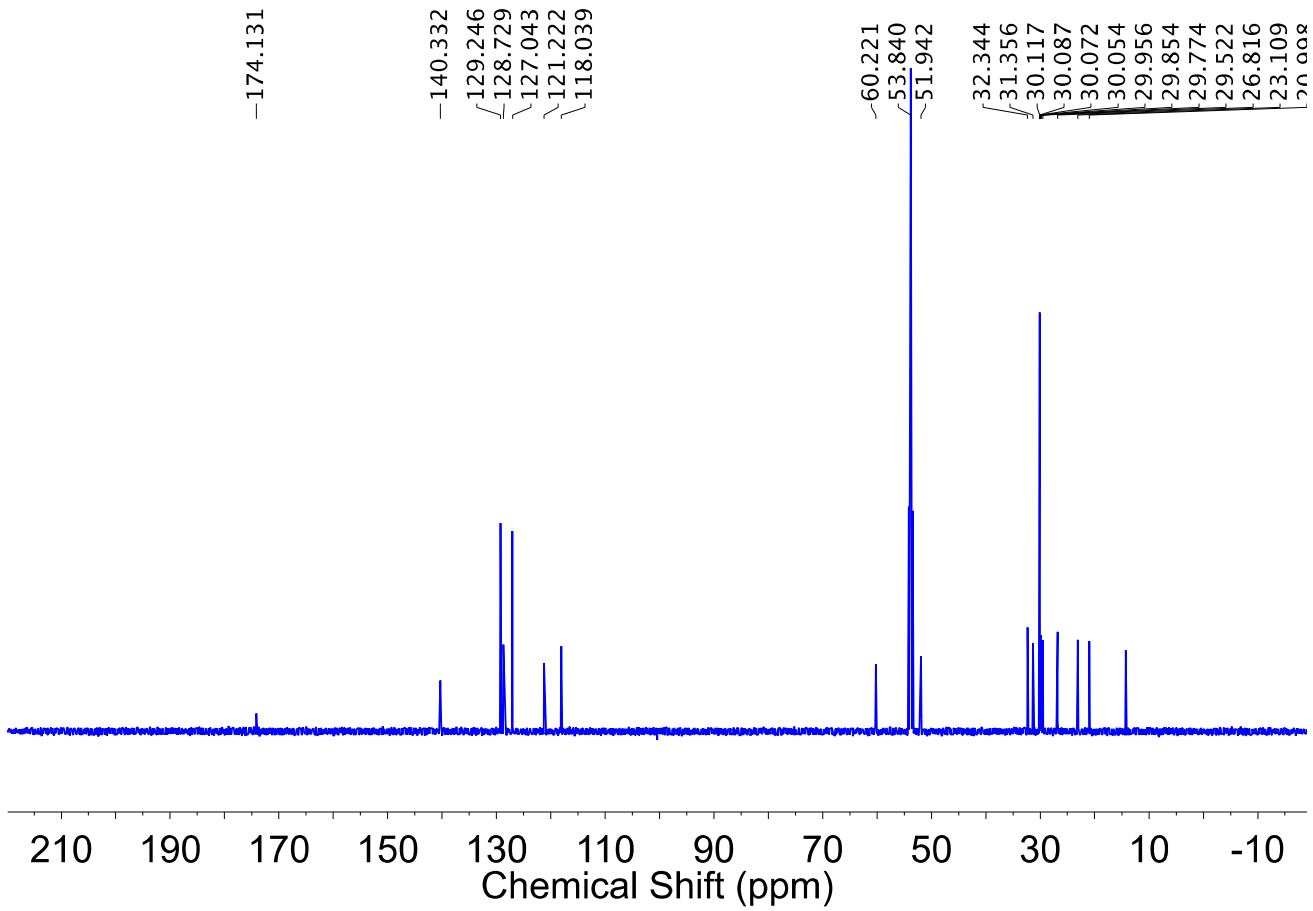

Figure S34. ^{13}C NMR (150 MHz, CD_2Cl_2, 23 °C) spectrum of (R)-(1-octadecyl-3-(1-phenylethyl)-1,3-dihydro-2H-imidazol-2-ylidene)gold(I) bromide **11**.

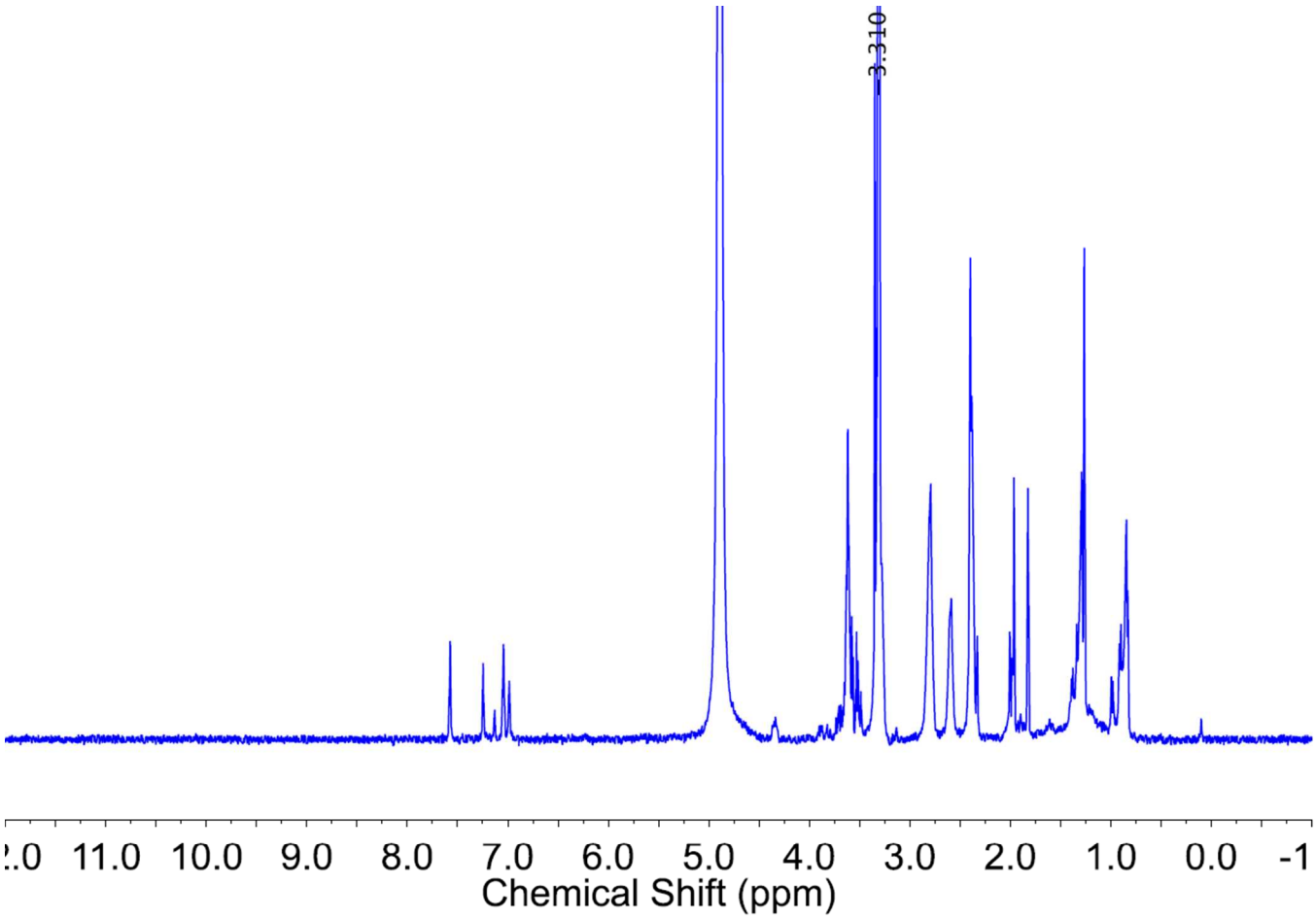

Figure S35. ^{1}H NMR (400 MHz, CD_3OD, 23 °C) spectrum of **Au/G4OH-NP-1** after dialysis againt MeOH, dried, and redispersed in CD_3OD.

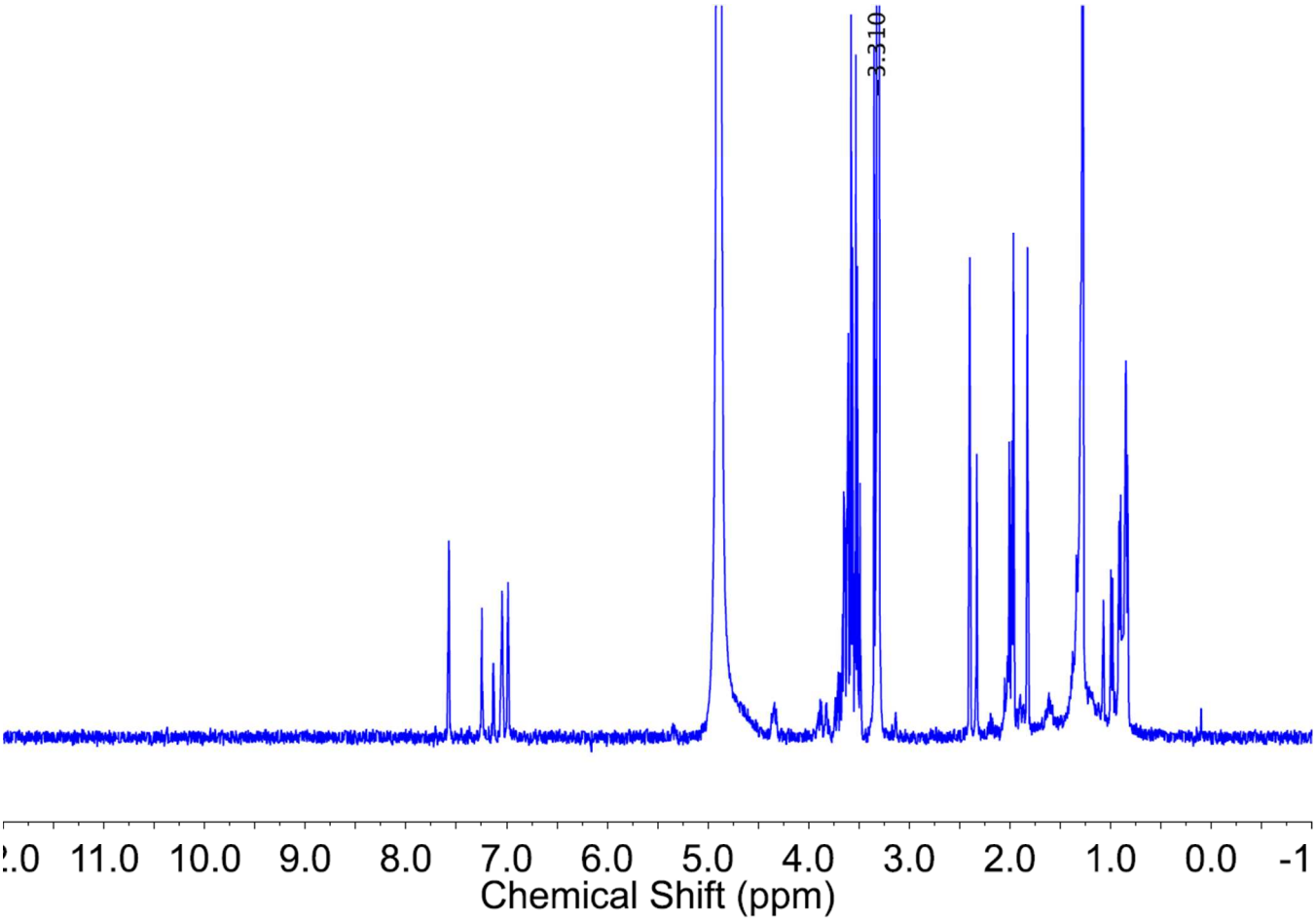

Figure S36. ^{1}H NMR (400 MHz, CD_3OD, 23 °C) spectrum of **AuNP-1** after dialysis againt MeOH, dried, and redispersed in CD_3OD.

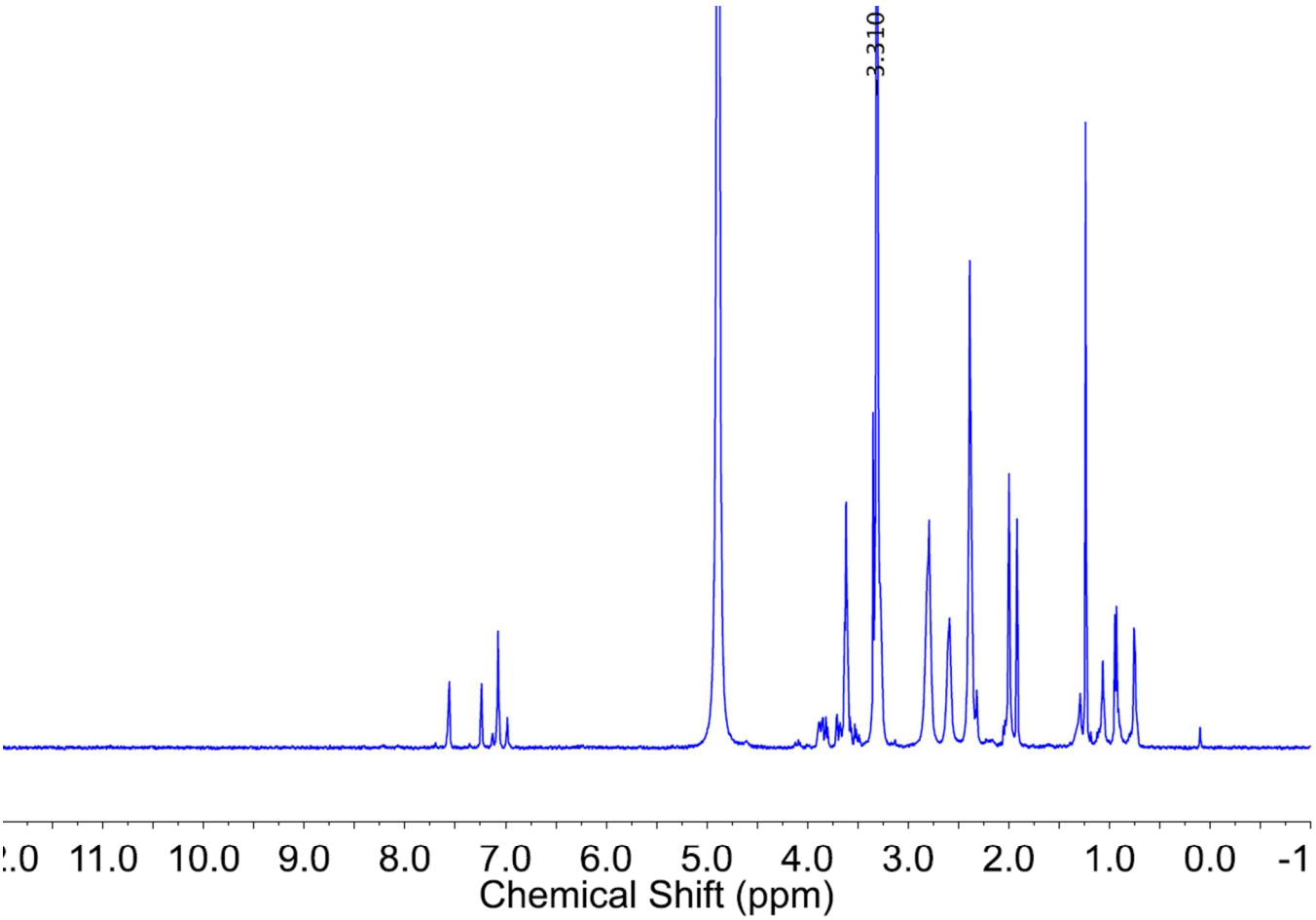

Figure S37. ^{1}H NMR (400 MHz, CD_3OD, 23 °C) spectrum of **Au/G4OH-NP-2** after dialysis againt MeOH, dried, and redispersed in CD_3OD.

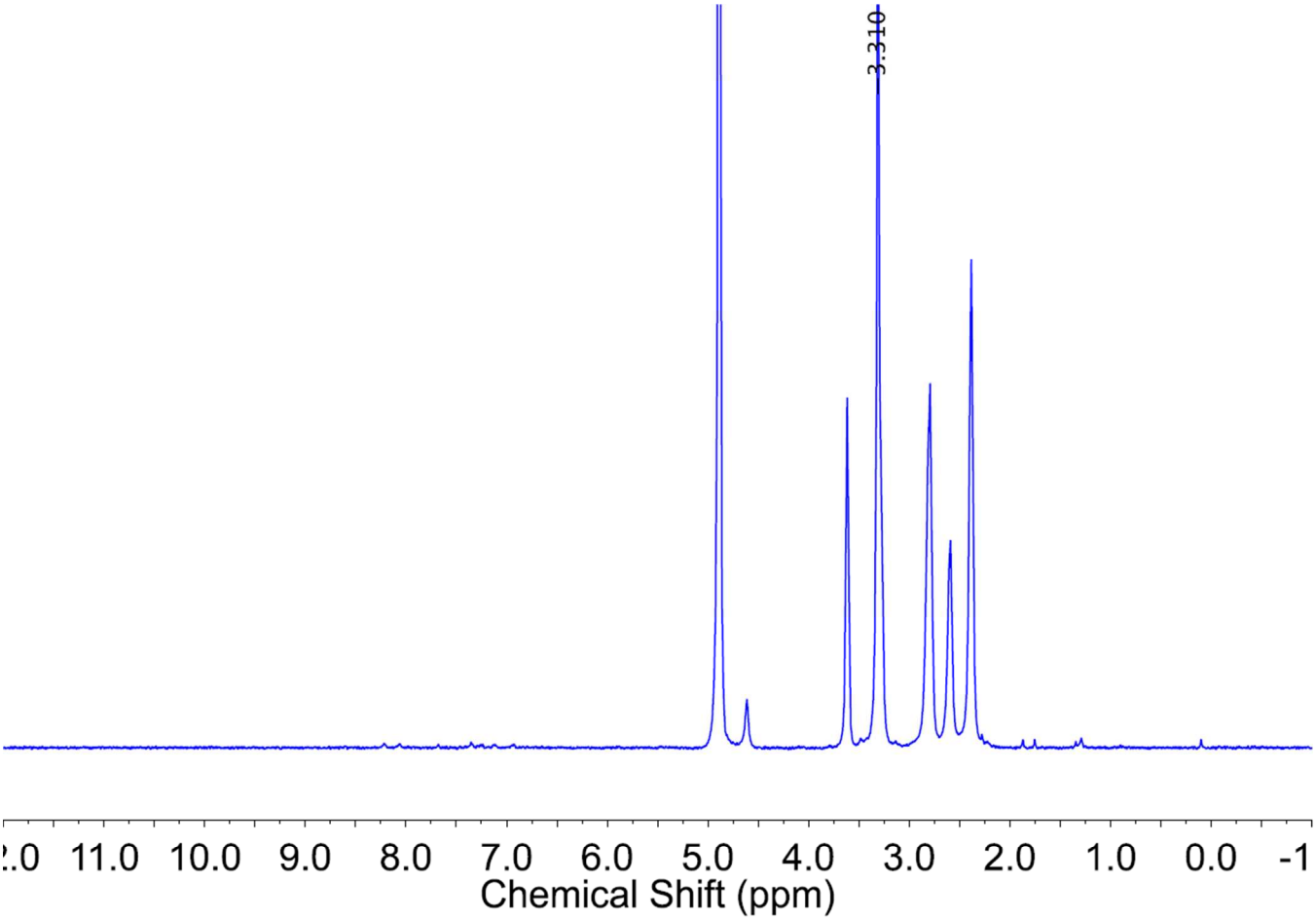

Figure S38. ^{1}H NMR (400 MHz, CD_3OD, 23 °C) spectrum of **Au/G4OH-NP-3** after dialysis againt MeOH, dried, and redispersed in CD_3OD.

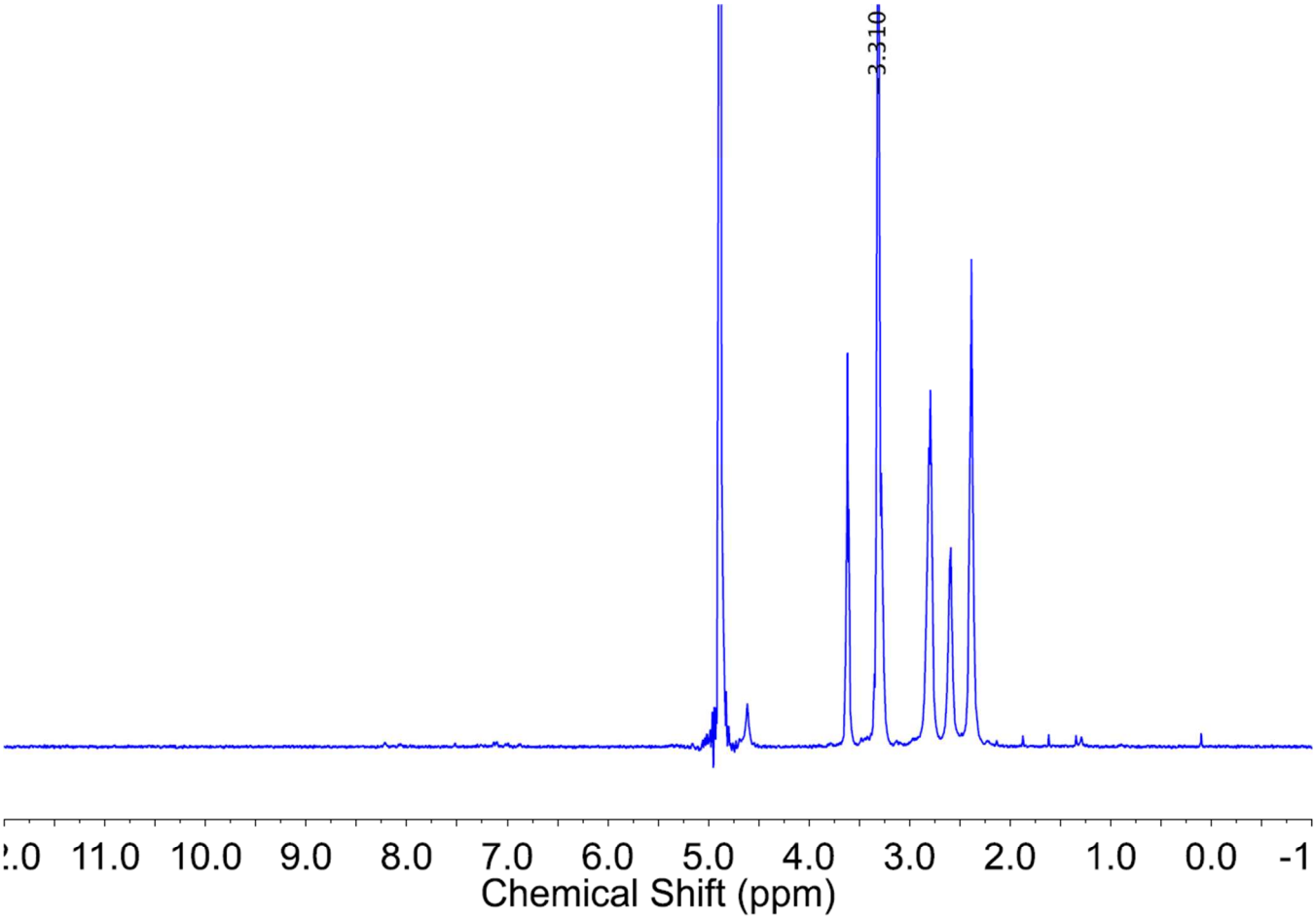

Figure S39. ^{1}H NMR (400 MHz, CD_3OD, 23 °C) spectrum of **Au/G4OH-NP-4** after dialysis againt MeOH, dried, and redispersed in CD_3OD.

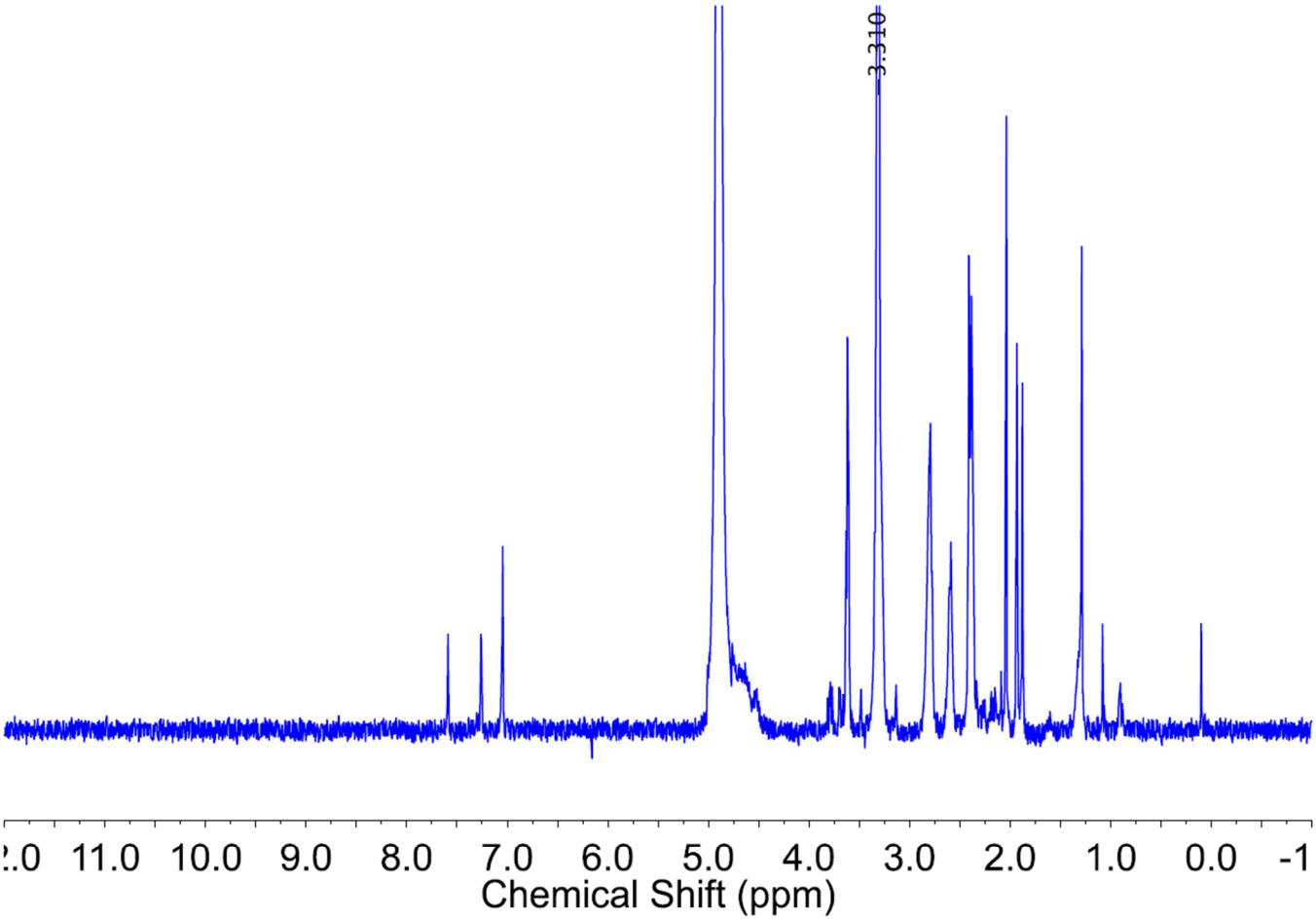

Figure S40. ^{1}H NMR (400 MHz, CD_3OD, 23 °C) spectrum of **Au/G4OH-NP-5** after dialysis againt MeOH, dried, and redispersed in CD_3OD.

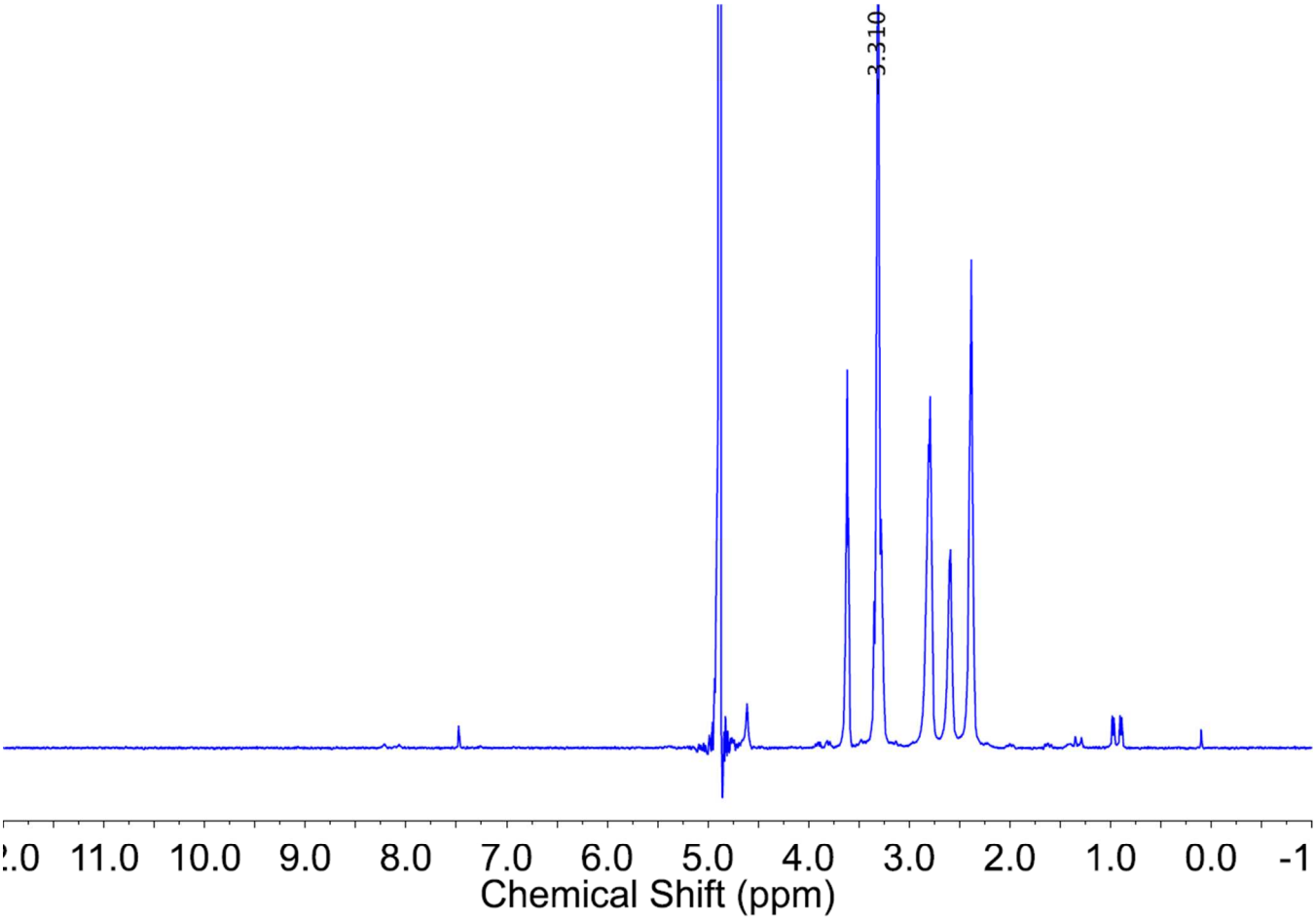

Figure S41. ^{1}H NMR (400 MHz, CD_3OD, 23 °C) spectrum of **Au/G4OH-NP-6** after dialysis againt MeOH, dried, and redispersed in CD_3OD.

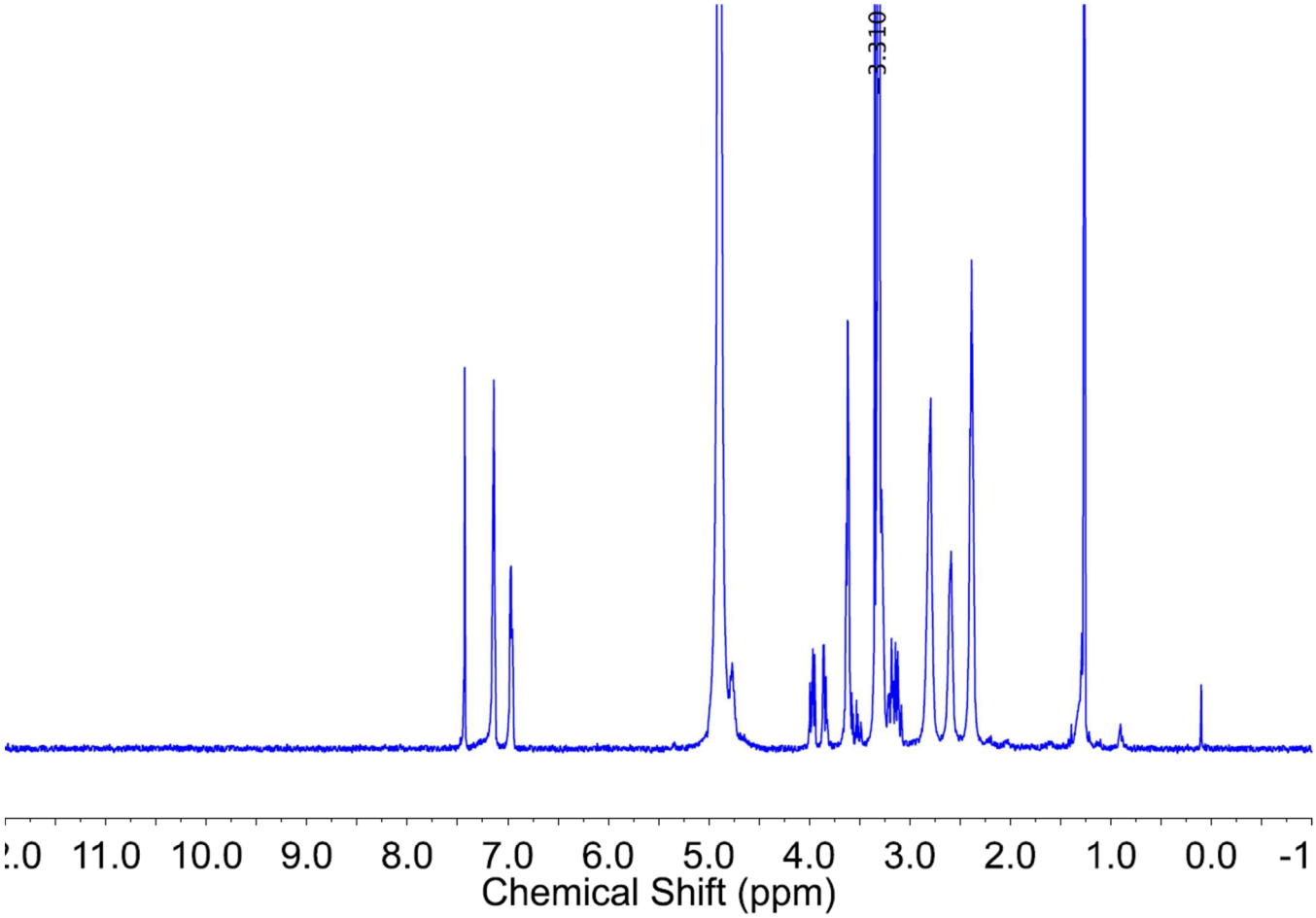

Figure S42. ^{1}H NMR (400 MHz, CD_3OD, 23 °C) spectrum of **Au/G4OH-NP-7** after dialysis againt MeOH, dried, and redispersed in CD_3OD.

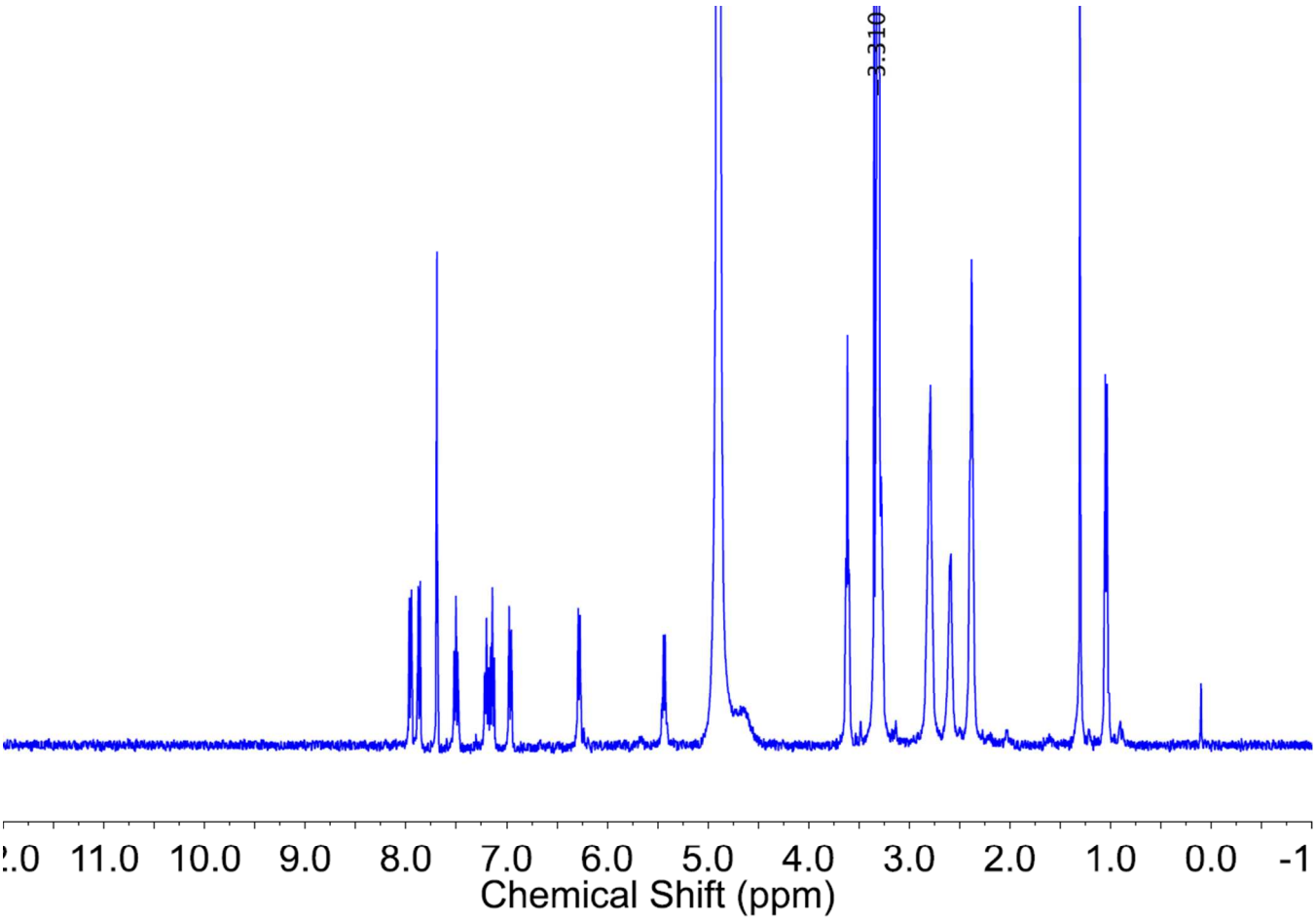

Figure S43. ^{1}H NMR (400 MHz, CD_3OD, 23 °C) spectrum of **Au/G4OH-NP-8** after dialysis againt MeOH, dried, and redispersed in CD_3OD.

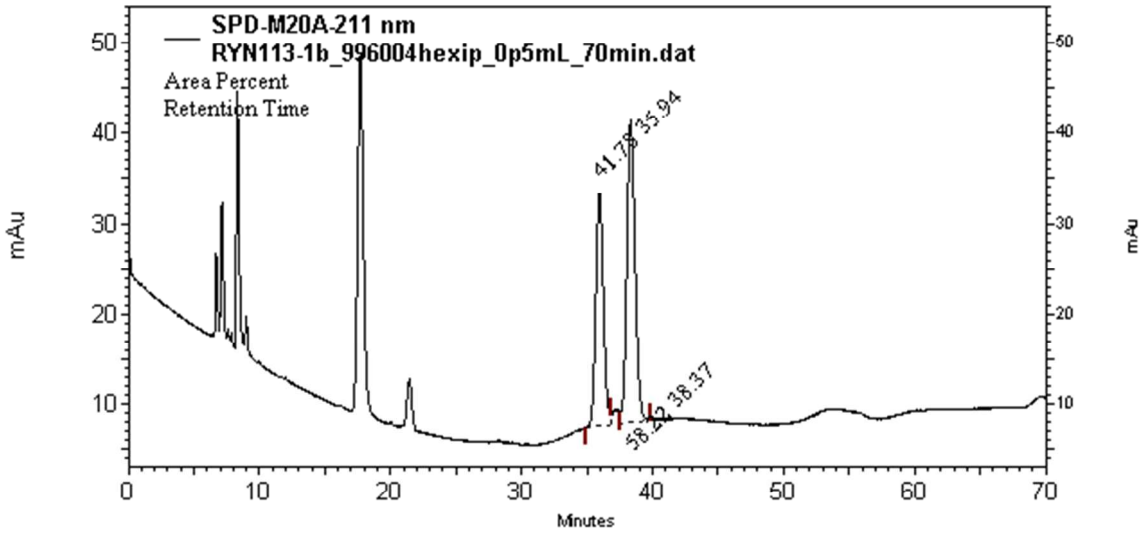

Figure S44. Chiral HPLC analysis of the product from the full conversion of **A** catalyzed by **Cat-1** in CD_2Cl_2 at room temperature.

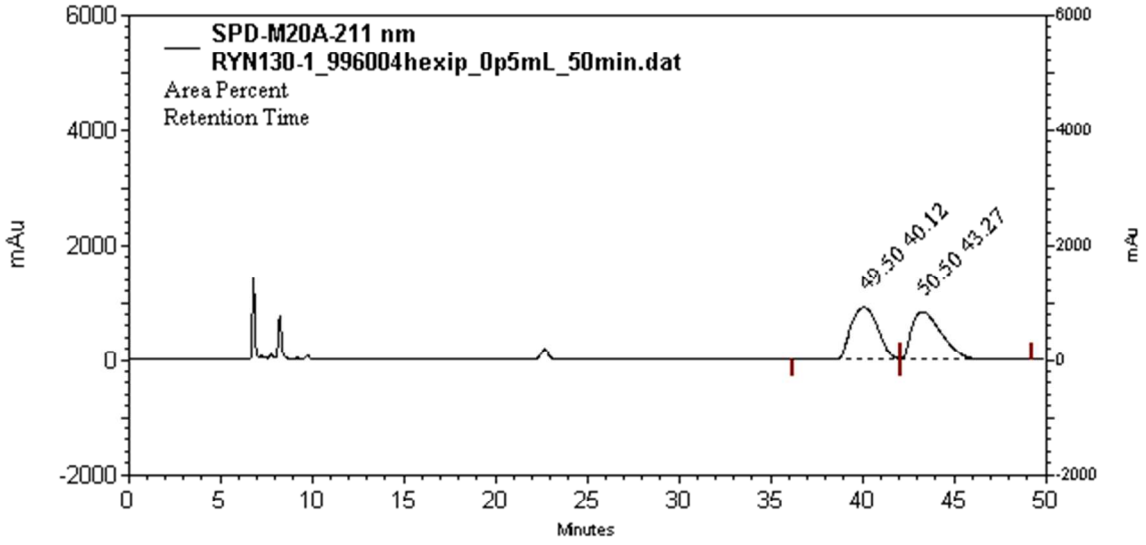

Figure S45. Chiral HPLC analysis of the product from the full conversion of **A** catalyzed by **Cat-2** in CD_2Cl_2 at room temperature.

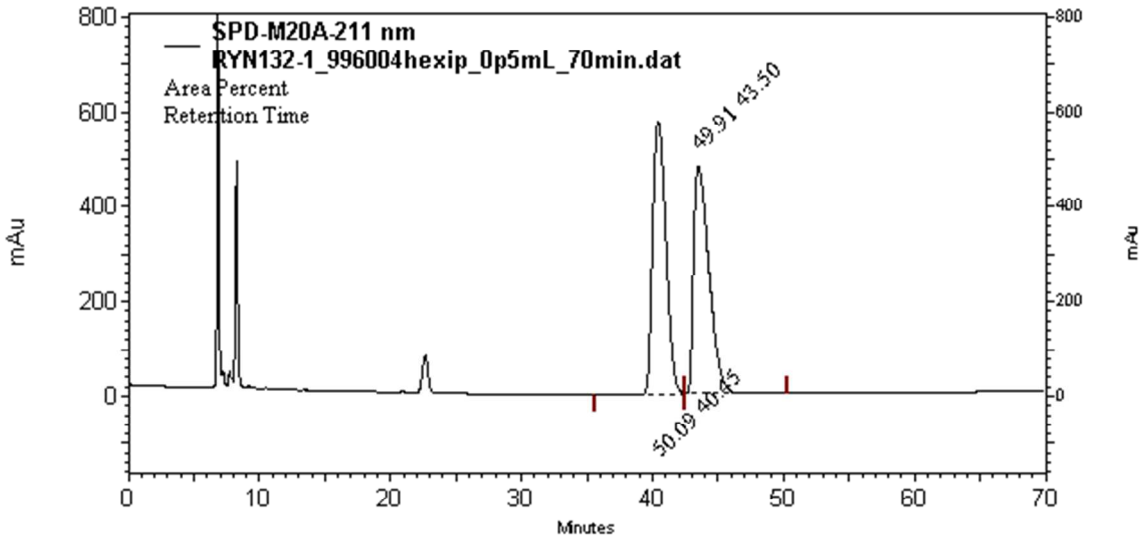

Figure S46. Chiral HPLC analysis of the product from the full conversion of **A** catalyzed by **Cat-3** in CD_2Cl_2 at room temperature.

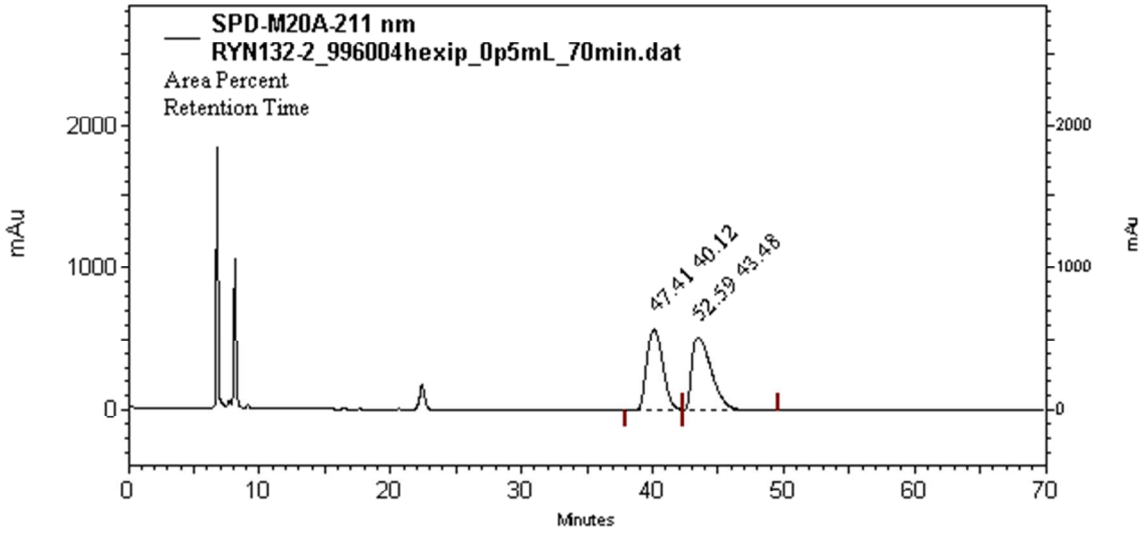

Figure S47. Chiral HPLC analysis of the product from the full conversion of **A** catalyzed by **Cat-4** in CD_2Cl_2 at room temperature.

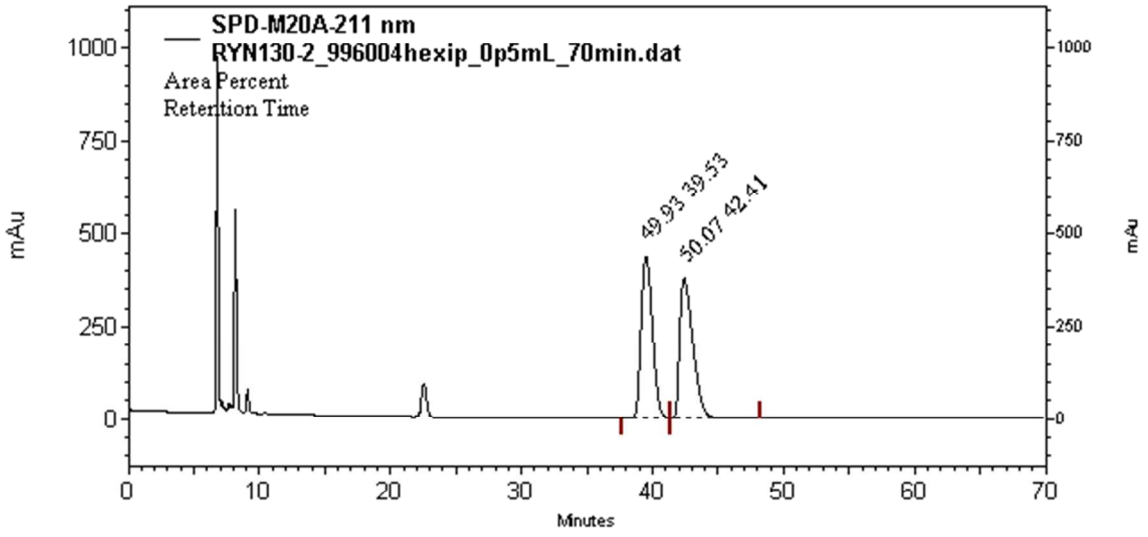

Figure S48. Chiral HPLC analysis of the product from the full conversion of **A** catalyzed by **Cat-5** in CD_2Cl_2 at room temperature.

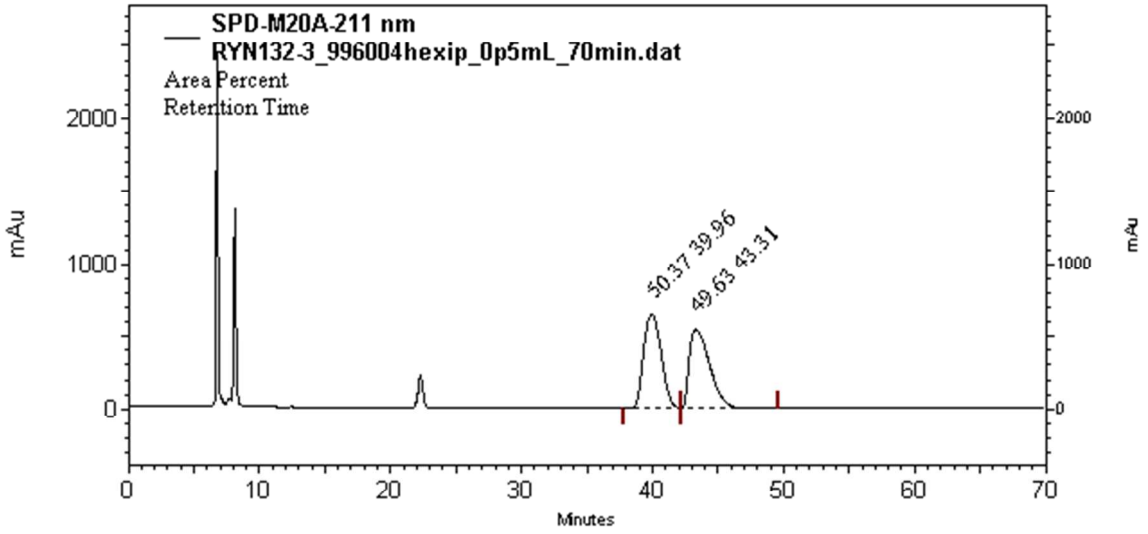

Figure S49. Chiral HPLC analysis of the product from the full conversion of **A** catalyzed by **Cat-6** in CD_2Cl_2 at room temperature.

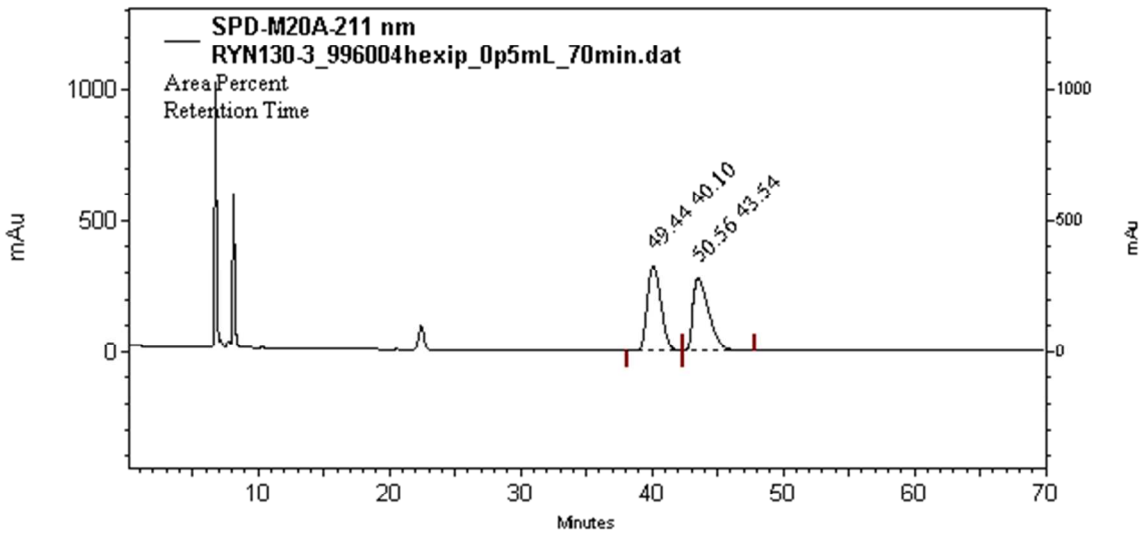

Figure S50. Chiral HPLC analysis of the product from the full conversion of **A** catalyzed by **Cat-7** in CD_2Cl_2 at room temperature.

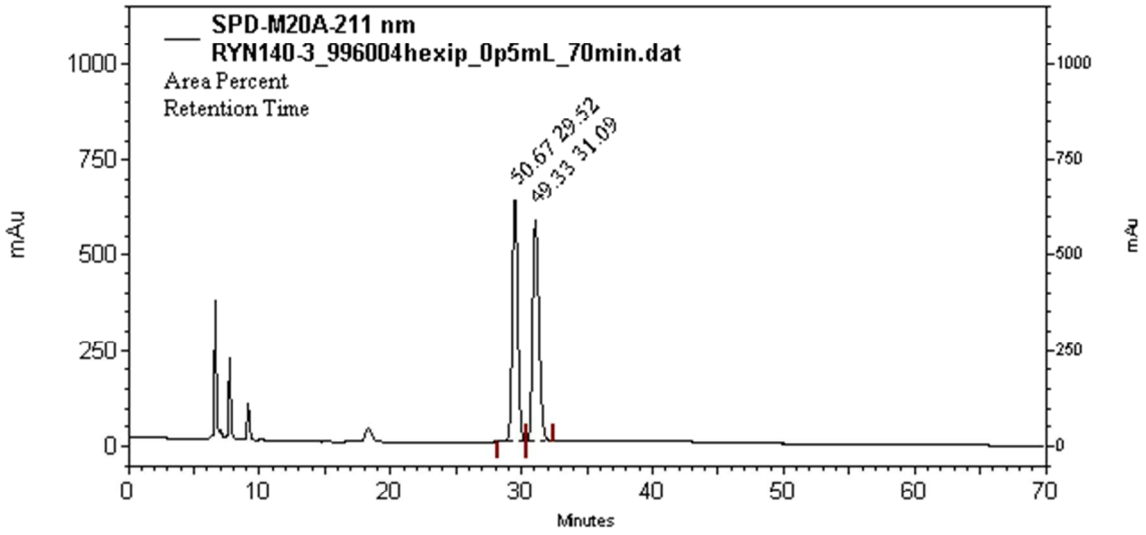

Figure S51. Chiral HPLC analysis of the product from the conversion of **A** catalyzed by **Cat-8** in CD_2Cl_2 at room temperature.

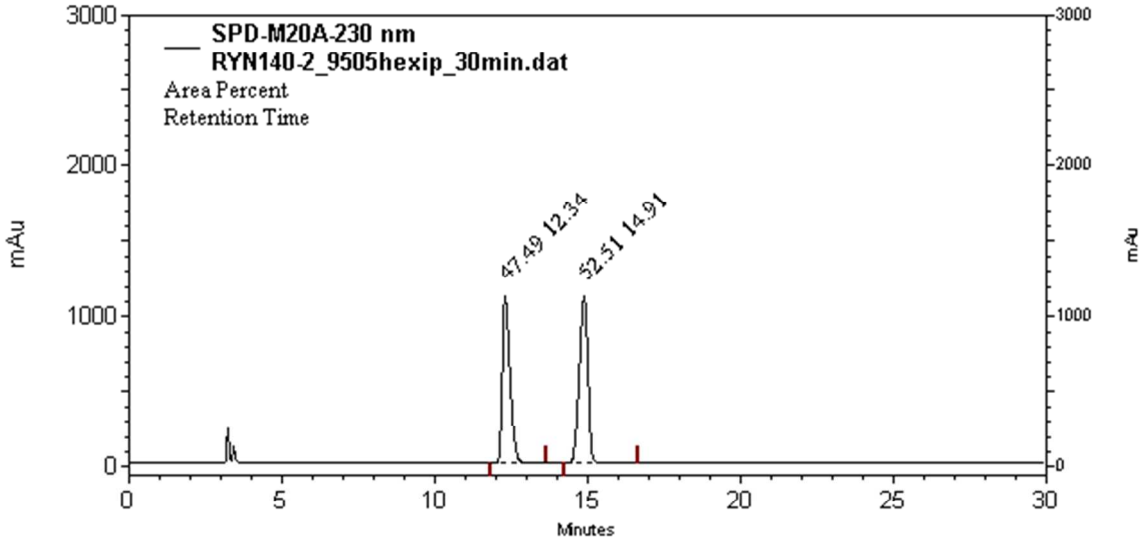

Figure S52. Chiral HPLC analysis of the product from the full conversion of **A'** catalyzed by **Cat-1** in CD_2Cl_2 at room temperature.

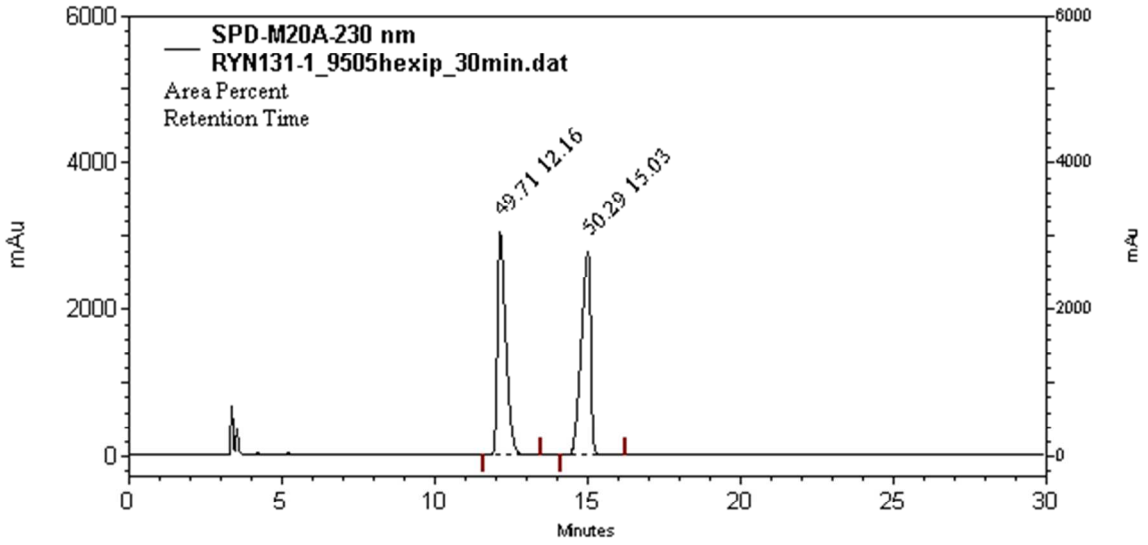

Figure S53. Chiral HPLC analysis of the product from the full conversion of **A'** catalyzed by **Cat-2** in CD_2Cl_2 at room temperature.

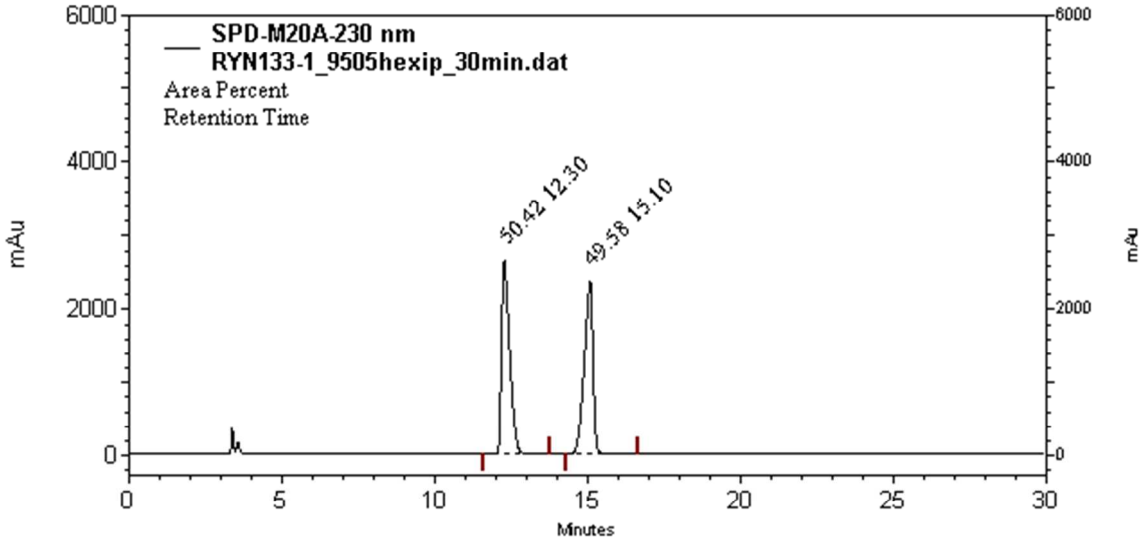

Figure S54. Chiral HPLC analysis of the product from the full conversion of **A'** catalyzed by **Cat-3** in CD_2Cl_2 at room temperature.

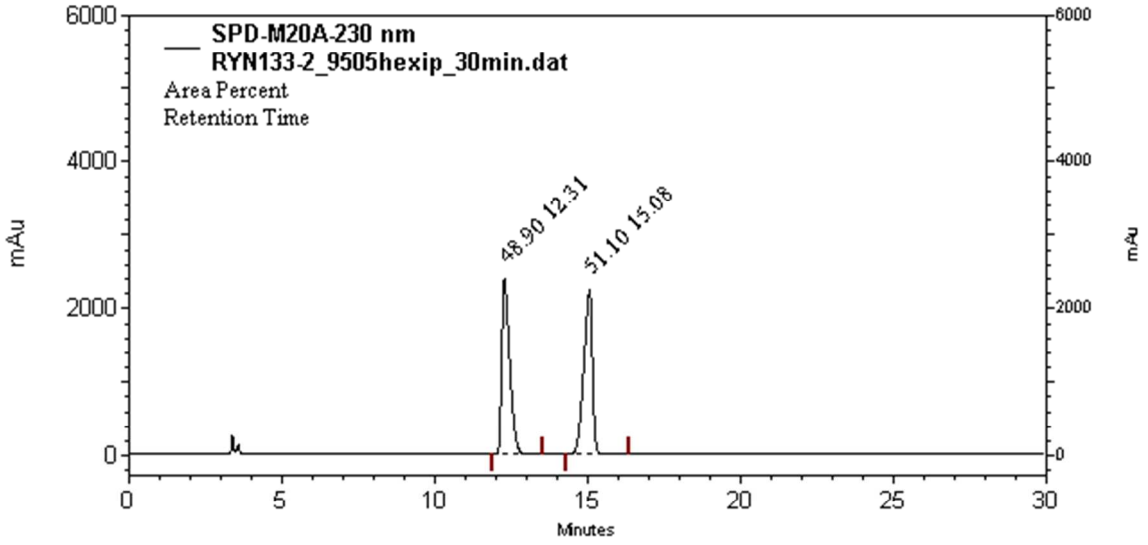

Figure S55. Chiral HPLC analysis of the product from the full conversion of **A'** catalyzed by **Cat-4** in CD_2Cl_2 at room temperature.

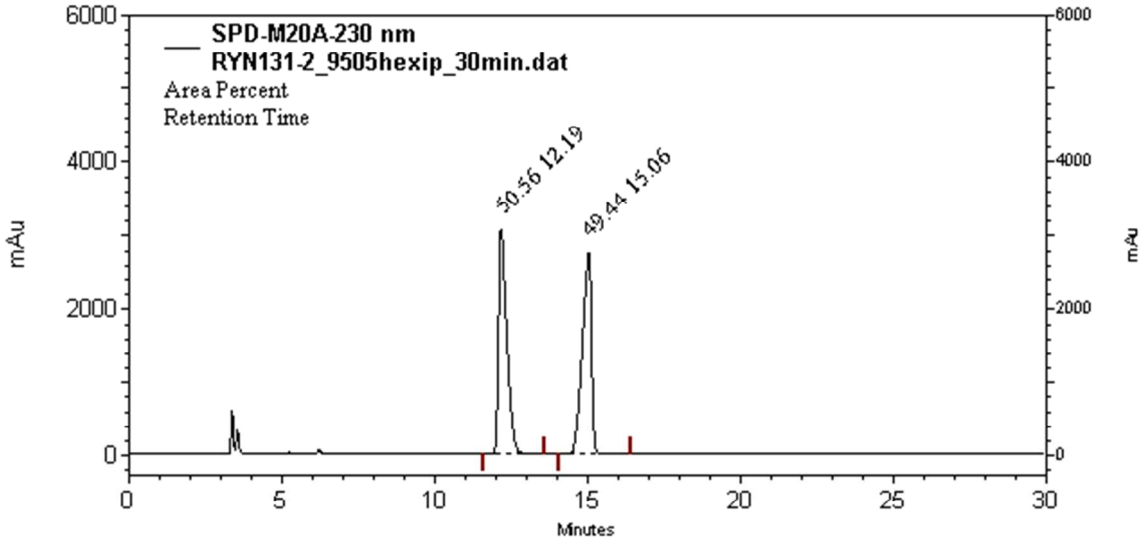

Figure S56. Chiral HPLC analysis of the product from the full conversion of **A'** catalyzed by **Cat-5** in CD_2Cl_2 at room temperature.

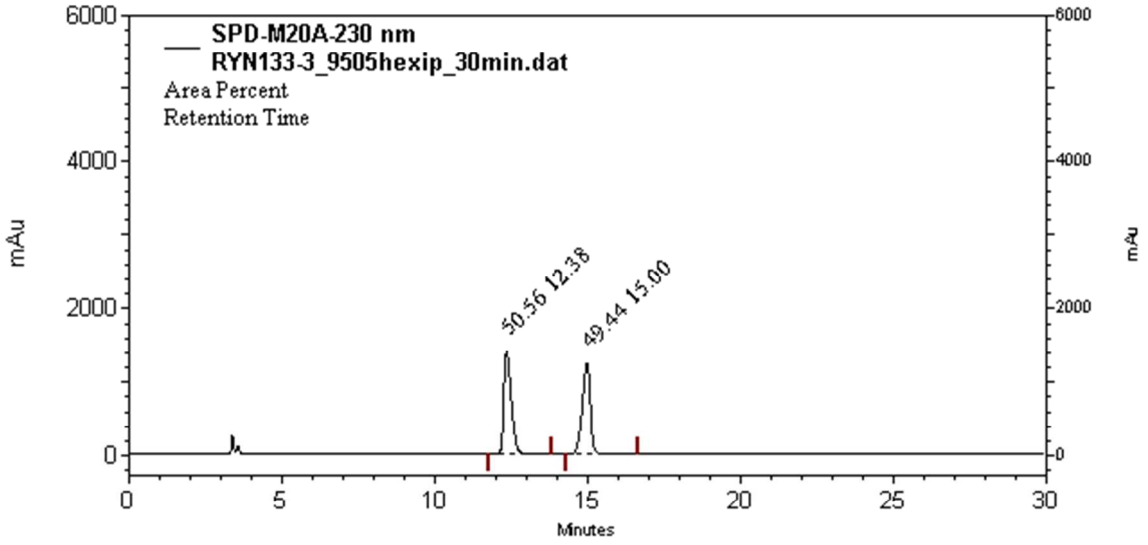

Figure S57. Chiral HPLC analysis of the product from the full conversion of **A'** catalyzed by **Cat-6** in CD_2Cl_2 at room temperature.

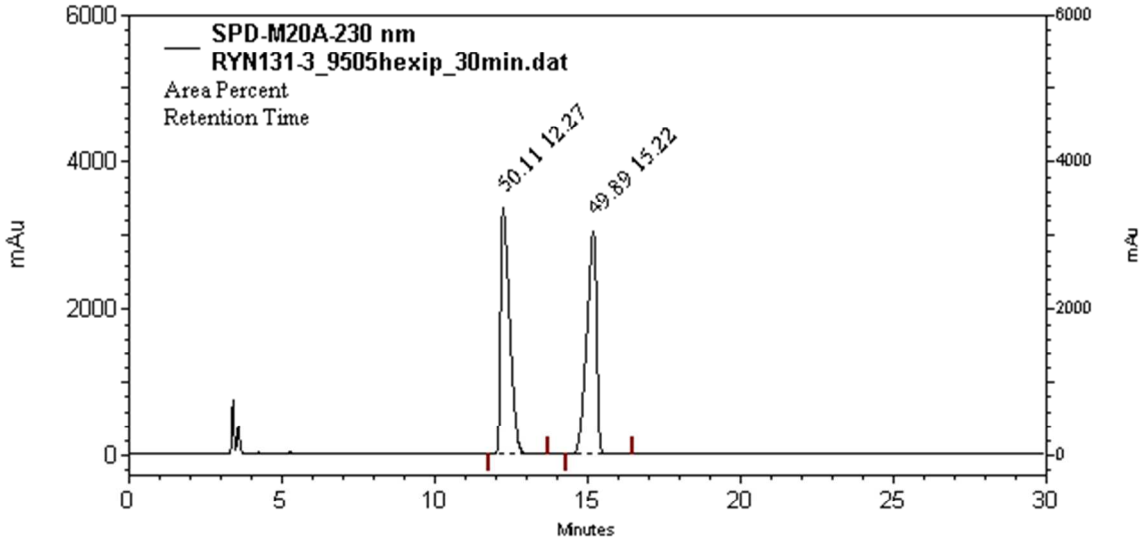

Figure S58. Chiral HPLC analysis of the product from the full conversion of **A'** catalyzed by **Cat-7** in CD_2Cl_2 at room temperature.

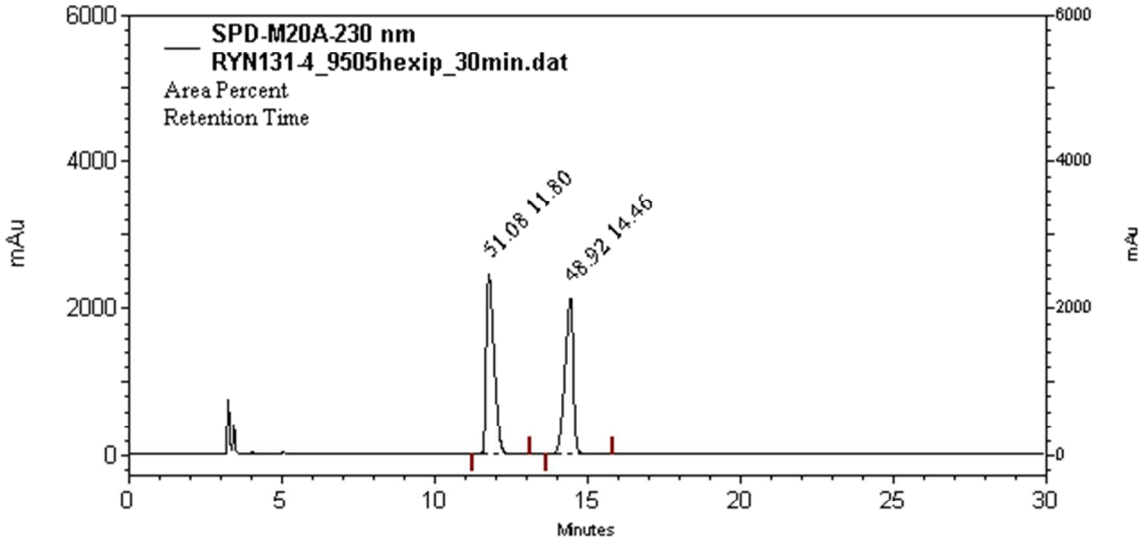

Figure S59. Chiral HPLC analysis of the product from the full conversion of **A'** catalyzed by **Cat-8** in CD_2Cl_2 at room temperature.

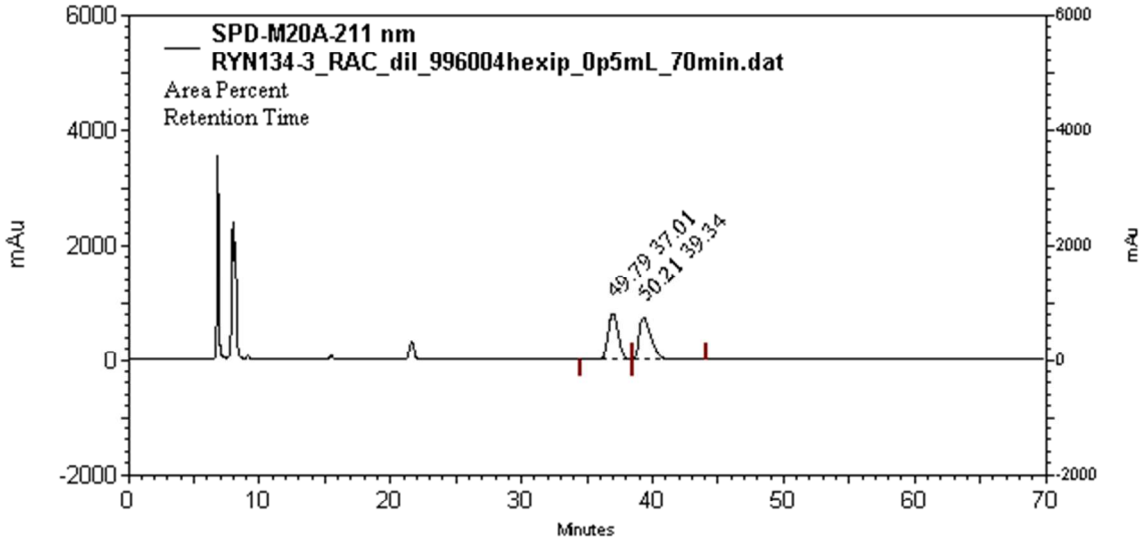

Figure S60. Chiral HPLC analysis of the product from the full conversion of **A** catalyzed by **Cat-0** in toluene at 373 K.

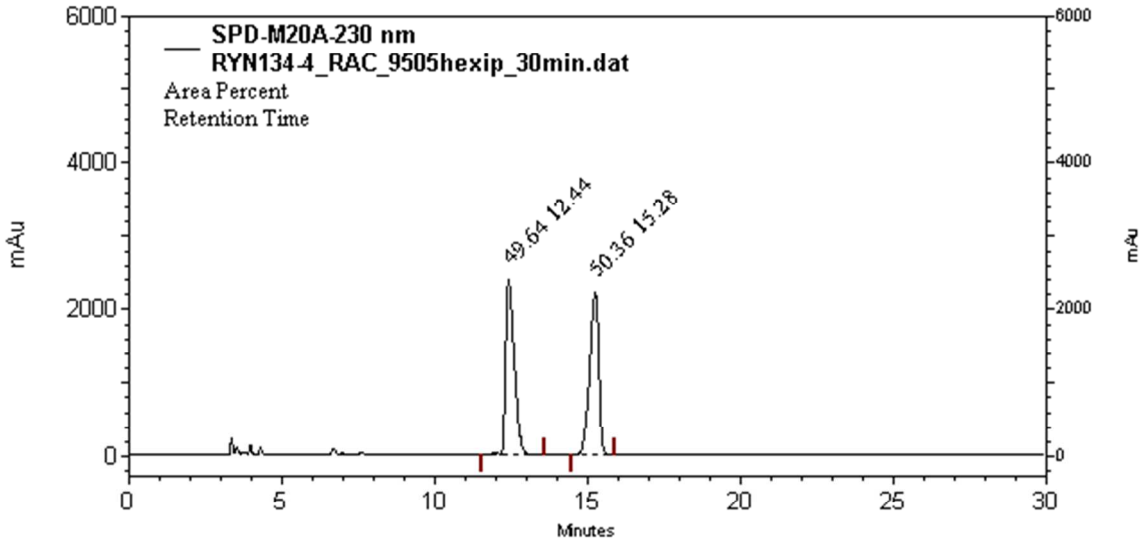

Figure S61. Chiral HPLC analysis of the product from the full conversion of **A'** catalyzed by **Cat-0** in toluene at 373 K.

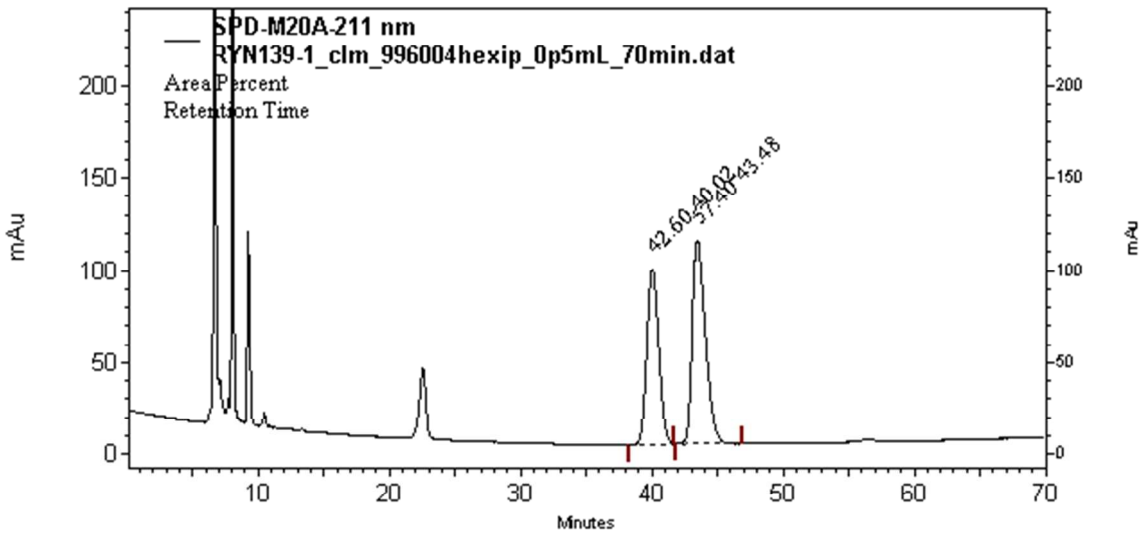

Figure S62. Chiral HPLC analysis of the product from the conversion of **A** catalyzed by **Cat-1** in CD_2Cl_2 at 273 K.

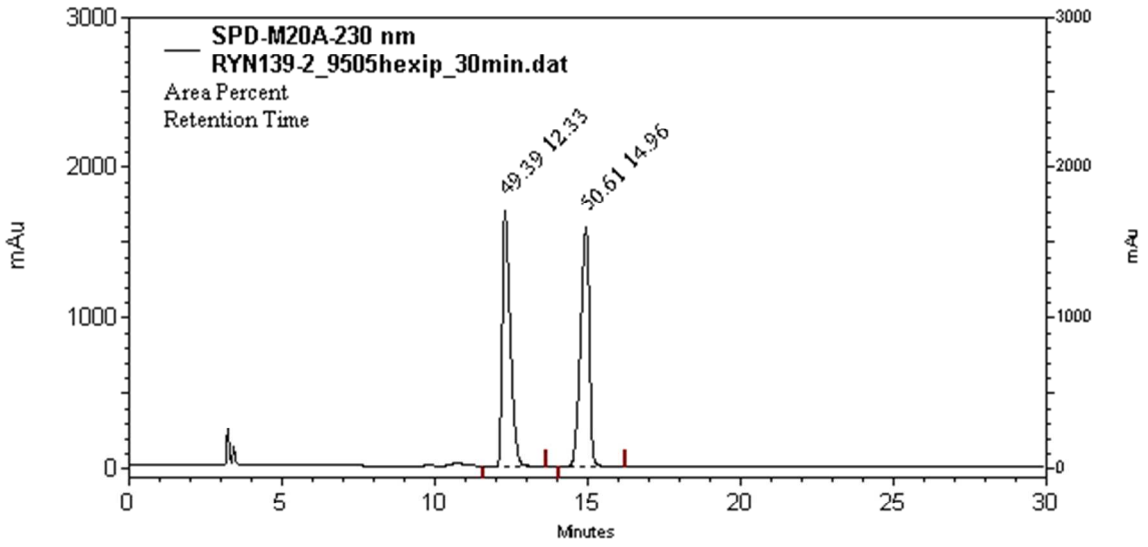

Figure S63. Chiral HPLC analysis of the product from the conversion of **A'** catalyzed by **Cat-1** in CD_2Cl_2 at 273 K.

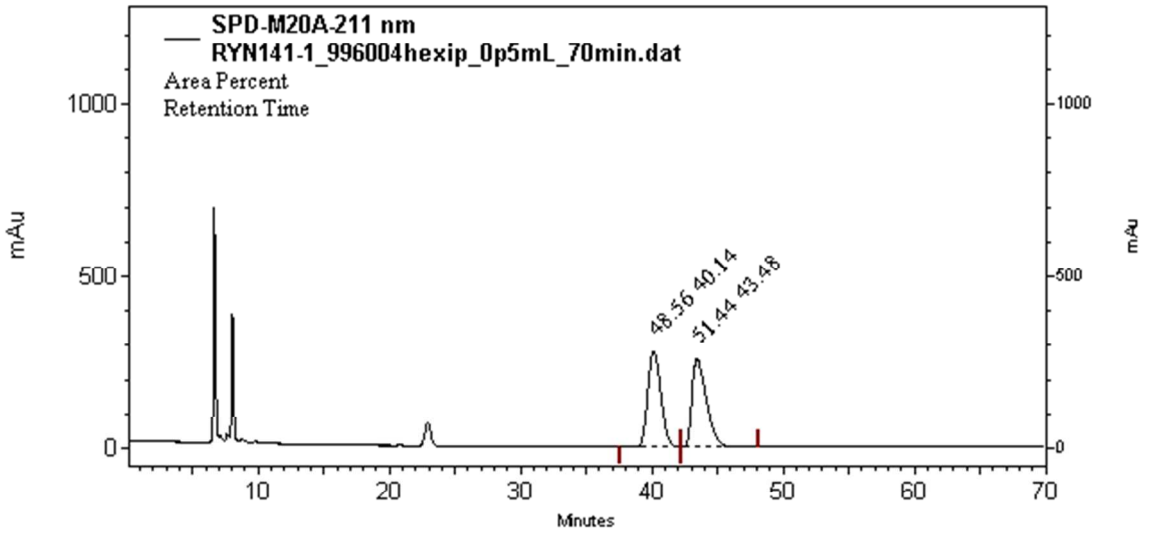

Figure S64. Chiral HPLC analysis of the product from the conversion of **A** catalyzed by **Cat-1** in C_6F_6 at room temperature.

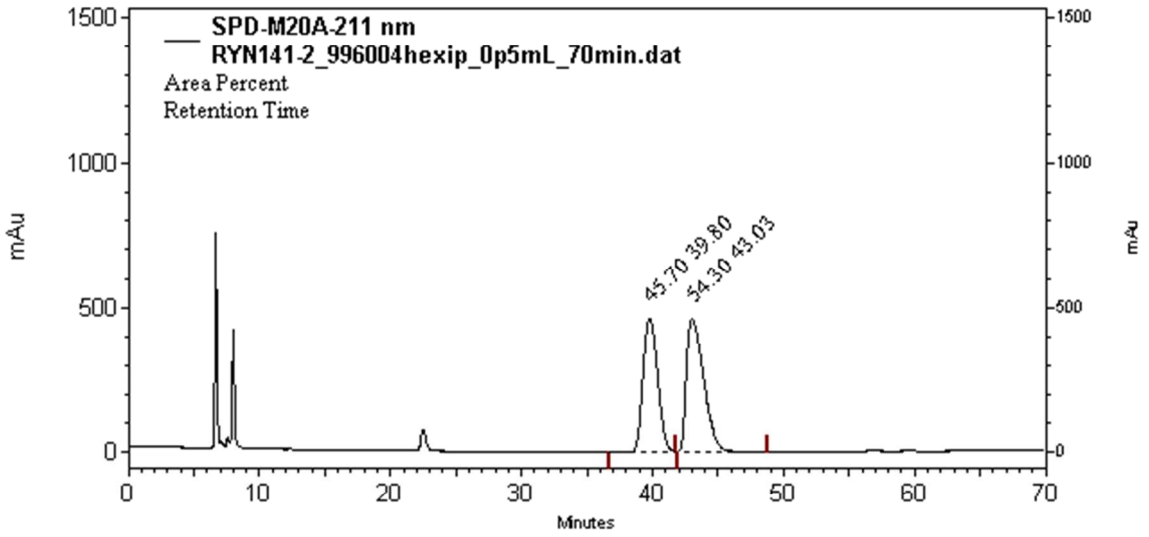

Figure S65. Chiral HPLC analysis of the product from the conversion of **A** catalyzed by **Cat-1** in C_6D_6 at room temperature.

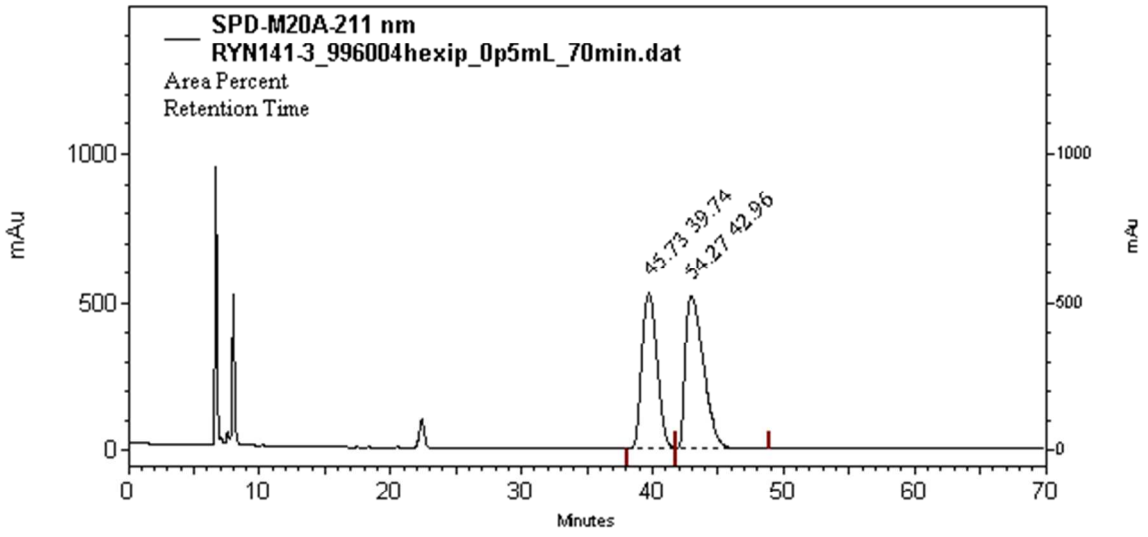

Figure S66. Chiral HPLC analysis of the product from the conversion of **A** catalyzed by **Cat-1** in Tol-d_8 at room temperature.

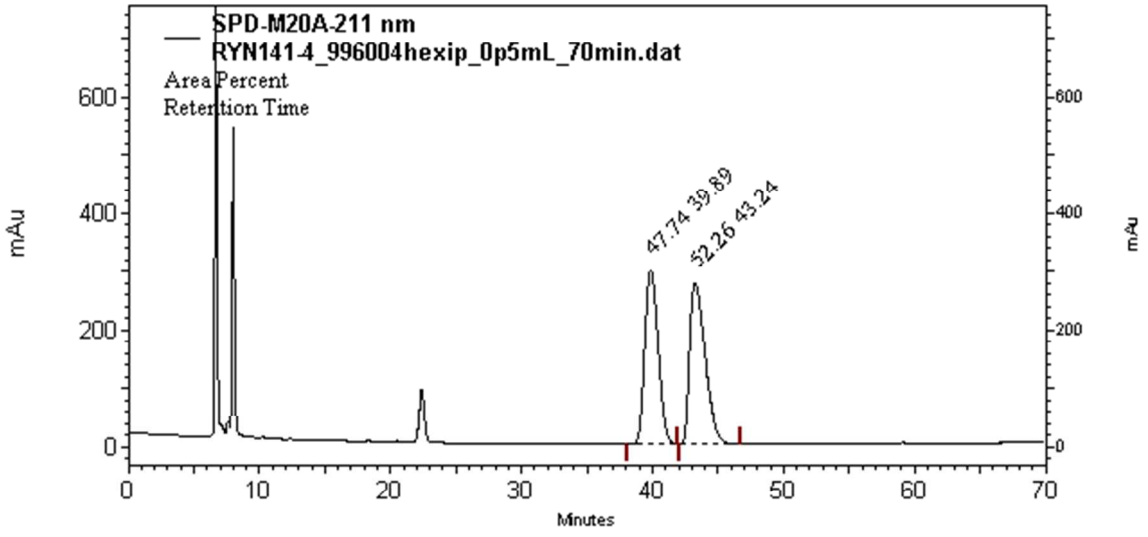

Figure S67. Chiral HPLC analysis of the product from the conversion of **A** catalyzed by **Cat-1** in cyclohexane at room temperature.

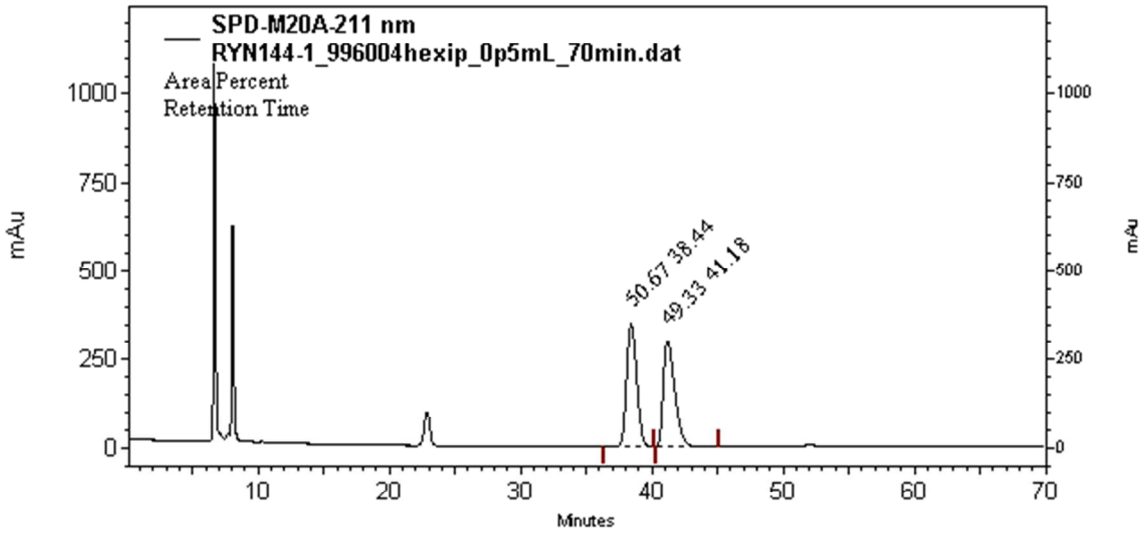

Figure S68. Chiral HPLC analysis of the product from the conversion of **A** catalyzed by **AuNP-1/SBA-15** in CD_2Cl_2 at room temperature.

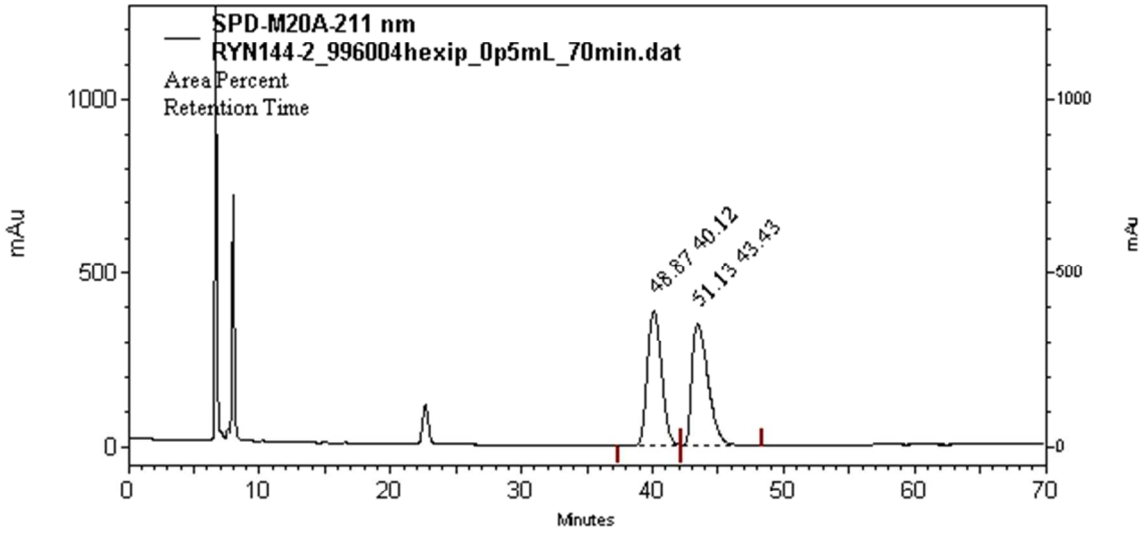

Figure S69. Chiral HPLC analysis of the product from the conversion of **A** catalyzed by **Cat-1'** in CD_2Cl_2 at room temperature.

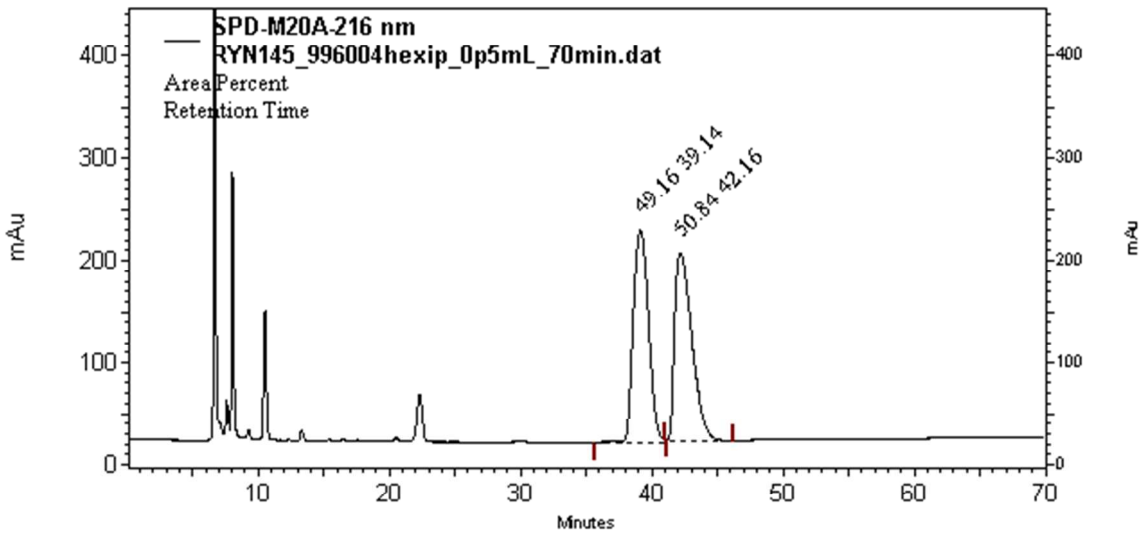

Figure S70. Chiral HPLC analysis of the product from the conversion of **A** catalyzed by **1(cation)** in CD_2Cl_2 at room temperature.

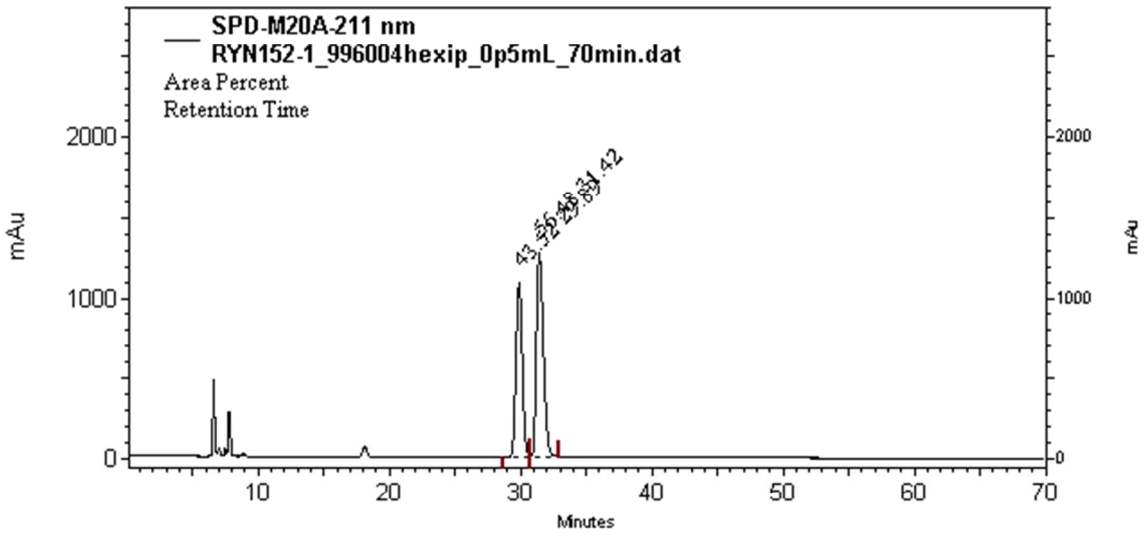

Figure S71. Chiral HPLC analysis of the product from the conversion of **A** catalyzed by **1**/G2OH/SBA-15 in CD_2Cl_2 at room temperature.

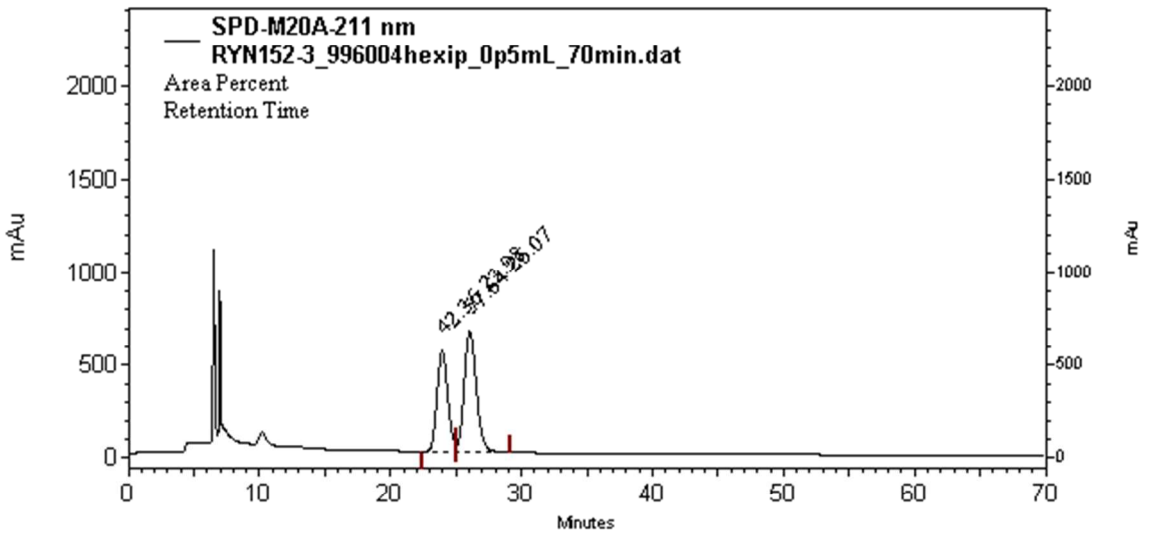

Figure S72. Chiral HPLC analysis of the product from the conversion of **A** catalyzed by **1**/G5OH/SBA-15 in CD_2Cl_2 at room temperature.

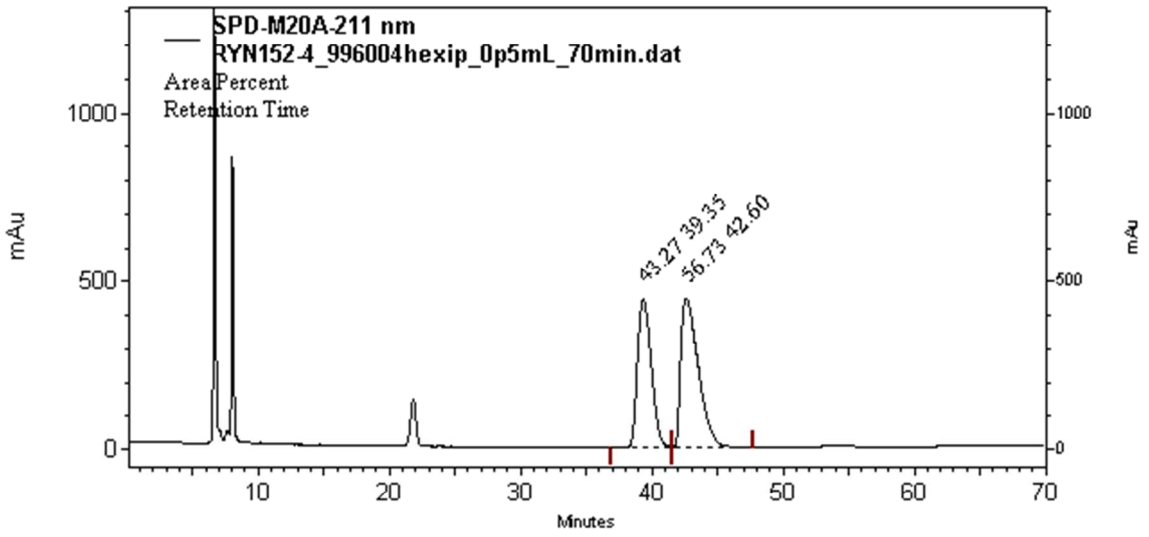

Figure S73. Chiral HPLC analysis of the product from the conversion of **A** catalyzed by **1**/G6OH/SBA-15 in CD_2Cl_2 at room temperature.

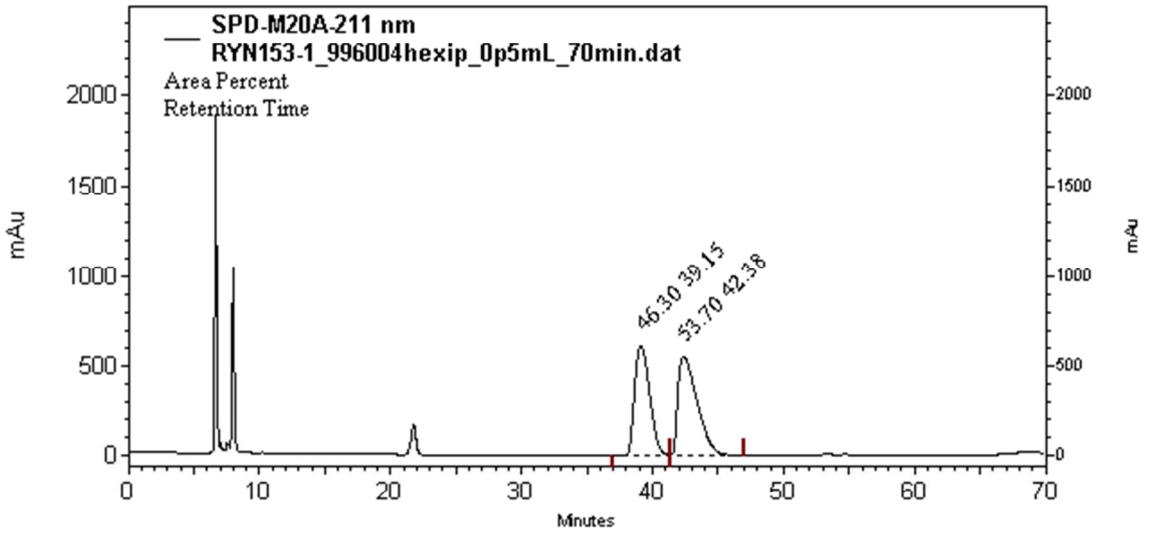

Figure S74. Chiral HPLC analysis of the product from the conversion of **A** catalyzed by $\mathbf{(1)_{40}}$/G4OH/SBA-15 in CD_2Cl_2 at room temperature.

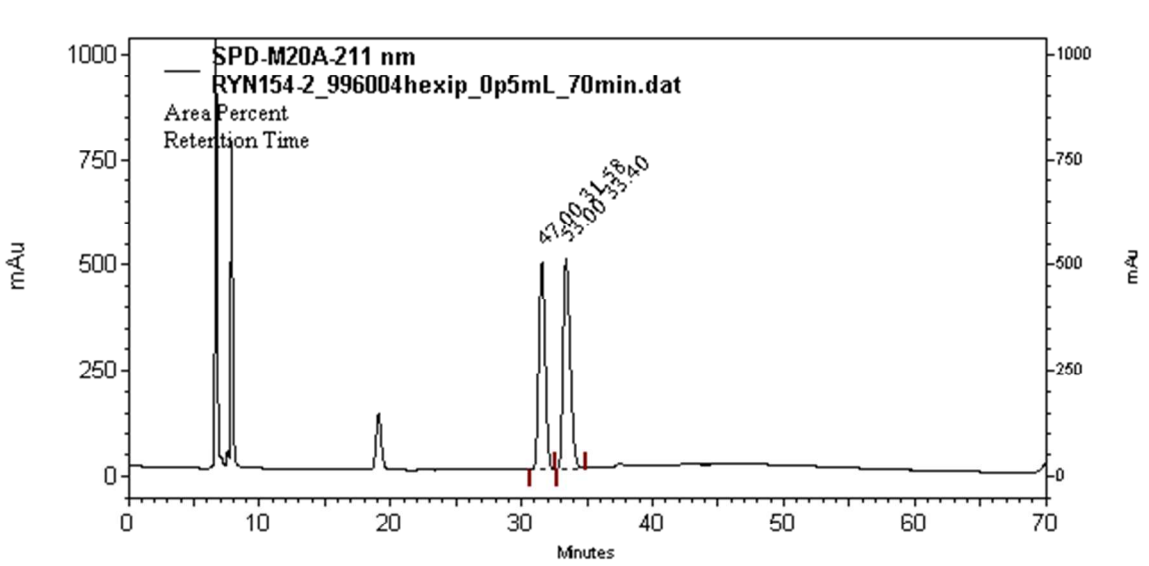

Figure S75. Chiral HPLC analysis of the product from the conversion of **A** catalyzed by $\mathbf{(1)_{60}}$/G4OH/SBA-15 in CD_2Cl_2 at room temperature.

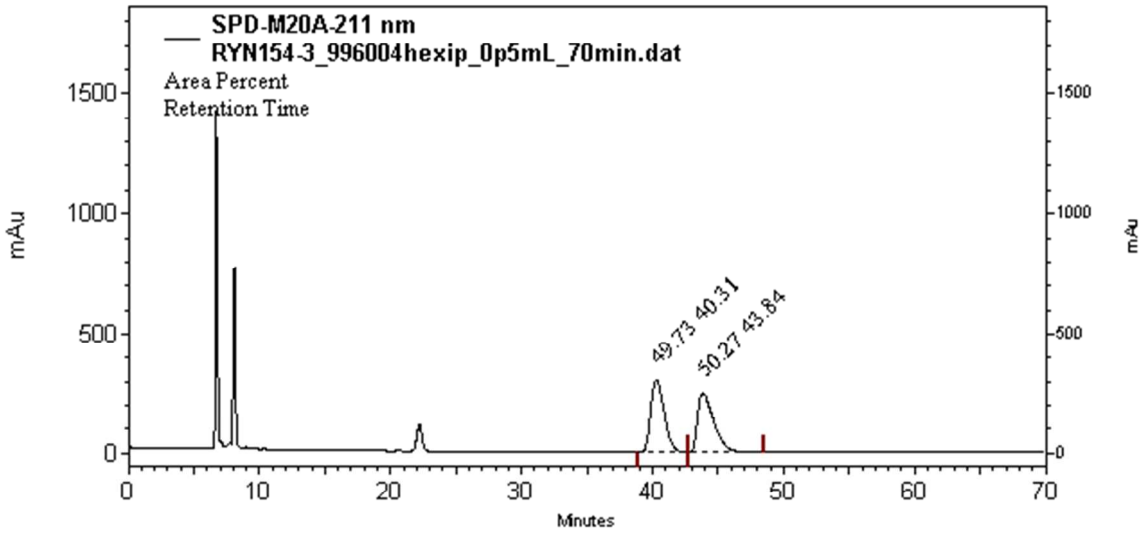

Figure S76. Chiral HPLC analysis of the product from the conversion of **A** catalyzed by **AuNP-1**/SBA-15 in CD_2Cl_2 at room temperature.

References

1. Pangborn, A. B.; Giardello, M. A.; Grubbs, R. H.; Rosen, R. K.; Timmers, F. J., *Organometallics* **1996,** 15, 1518-1520.
2. Borrmann, T.; Lim, T. H.; Cope, H.; Lucas, K.; Lorden, M., *Gold Bull.* **2013,** 46, 13-18.
3. Shu, X.-Z.; Nguyen, S. C.; He, Y.; Oba, F.; Zhang, Q.; Canlas, C.; Somorjai, G. A.; Alivisatos, A. P.; Toste, F. D., *J. Am. Chem. Soc.* **2015,** 137, 7083-7086.
4. Winn, C. L.; Guillen, F.; Pytkowicz, J.; Roland, S.; Mangeney, P.; Alexakis, A., *J. Organomet. Chem.* **2005,** 690, 5672-5695.
5. Arduengo, A. J. Preparation of 1,3-disubstituted imidazolium salts. US5077414A, 1991.
6. Tudose, A.; Demonceau, A.; Delaude, L., *J. Organomet. Chem.* **2006,** 691, 5356-5365.
7. Still, W. C.; Kahn, M.; Mitra, A., *J. Org. Chem.* **1978,** 43, 2923-2925.
8. Fulmer, G. R.; Miller, A. J. M.; Sherden, N. H.; Gottlieb, H. E.; Nudelman, A.; Stoltz, B. M.; Bercaw, J. E.; Goldberg, K. I., *Organometallics* **2010,** 29, 2176-2179.
9. Brillson, L. J. In *An Essential Guide to Electronic Material Surfaces and Interfaces*, John Wiley & Sons, Ltd: West Sussex, UK, 2016; pp 76-117.
10. (a) Fairley, N., *Casaxps Manual 2.3. 15, Rev. 1.3, Orange Book; CasaXPS Software Ltd.* **2009**; (b) *http://www.casaxps.com/help_manual/manual_updates/peak_fitting_in_xps.pdf*. **2006**.
11. Chenakin, S. P.; Kruse, N., *Phys. Chem. Chem. Phys.* **2016,** 18, 22778-22782.
12. Mauduit, M.; BASLE, O.; Queval, P.; Jahier, C.; Artur, I. Metal alkylidene complexes comprising an unsymmetrical unsaturated NHC ligand. EP2821409A1, 2015.
13. Price, G. A.; Brisdon, A. K.; Flower, K. R.; Pritchard, R. G.; Quayle, P., *Tetrahedron Lett.* **2014,** 55, 151-154.
14. Collado, A.; Gomez-Suarez, A.; Martin, A. R.; Slawin, A. M. Z.; Nolan, S. P., *Chem. Commun.* **2013,** 49, 5541-5543.